

# Exploring the function of IGFN1 and MLTK in skeletal muscle

Xiang Li

PhD

University of York  
Biology

September 2016

## Abstract:

Kyphoscoliosis peptidase (KY) is a Z-disc protein essential for muscle maintenance and its absence underlies a unique type of muscular dystrophy in humans and mice <sup>1-3</sup>. The function of KY remains uncharacterised, thus there is limited understanding about the mechanisms underlying the muscle pathology observed due to KY deficiency. Immunoglobulin-like and fibronectin type III domain containing 1 (IGFN1) was identified as a KY interaction partner which in turn interacts with MLK-like mitogen-activated protein triple kinase (MLTK) <sup>4</sup>. This thesis aimed to develop further understanding of these interaction partners to gain novel insights into mechanisms of muscle maintenance.

In this thesis, the specific interactions between IGFN1\_V1 and MLTK isoforms were confirmed for the first time via immunoprecipitation and pull down assays. In addition, MLTK $\beta$  is confirmed as the primary isoform in skeletal muscle.

The effects of ectopic expression of IGFN1\_V1 and MTLK isoforms in mouse skeletal muscle are examined. The Z-disc localisation of these proteins is confirmed, along with nuclear localisation for IGFN1\_V1. In addition, expression of IGFN1\_V1 drives both ectopically and endogenously expressed MLTK $\beta$  to the nucleus. This data shows that the z-disc is the likely site for IGFN1-MLTK interactions, and suggests a function for IGFN1\_V1 in the shuttling of MLTK $\beta$  to the nucleus.

Overexpression of recombinant MLTK $\beta$  results in skeletal muscle fibre cross sectional area increases, and some overexpressing fibres showed disorganized myofibrils. Together with the previous finding that overexpression <sup>5</sup> or reduction <sup>6</sup> of MLTK $\beta$  causes myofibril disorganization in either cardiac or skeletal muscles, this indicates that a certain expression level of MLTK $\beta$  is important for maintaining muscle health.

This thesis also describes the generation of IGFN1-deficient mouse myoblasts, which show abnormal differentiation patterns, including short myotube formation and globular differentiation bodies, indicating that IGFN1 is important for regulation of muscle myogenesis.

# Contents

Abstract:.....	ii
Contents.....	iii
Tables:.....	viii
Figures:.....	ix
Acknowledgement:.....	xi
Declaration:.....	xii
1. INTRODUCTION.....	1
1.1 Skeletal muscle: .....	2
1.2 Muscular dystrophy: .....	5
1.2.1 Signalling in muscle Hypertrophy and Atrophy: .....	7
1.3 THE KY MUTANT:.....	11
1.3.1 The <i>ky</i> mutant mouse: .....	11
1.3.2 The <i>ky</i> mutant human:.....	14
1.4 IGFN1: .....	16
1.4.1 Identification of the <i>Igfn1</i> locus:.....	16
1.4.2 Tissue distribution of <i>Igfn1</i> mRNA transcripts:.....	16
1.4.3 Identification of <i>Igfn1</i> cDNAs in skeletal muscle: .....	17
1.4.4 Subcellular localization of IGFN1: .....	18
1.4.5 IGFN1 interaction partners: .....	21
1.4.6 <i>Igfn1</i> transcription levels in hypertrophic or atrophic muscle:.....	22
1.5 MLTK: .....	23
1.5.1 The genomic and proteomic features of MLTK: .....	23
1.5.2 Tissue distribution of <i>mltk</i> mRNA transcripts: .....	24
1.5.3 MLTK induces hypertrophic responses <i>in vitro</i> and <i>in vivo</i> : .....	25
1.5.4 MLTK mutation: .....	26
1.5.5 More functions of MLTK: .....	27
1.6 Aim of this thesis:.....	28
2. Materials and methods.....	31
2.1 MATERIALS.....	32
2.1.1 General buffers .....	32
2.2 CELL STRAINS AND CULTURE .....	33
2.2.1 Bacterial strains:.....	33
2.2.2 Bacterial culture:.....	34

2.2.3 Mammalian cell lines: .....	35
2.2.4 Mammalian cell culture: .....	35
2.2.5 C2C12 myotube differentiation: .....	36
2.2.6 Cell transfection: .....	36
2.2.7 Cell fixation: .....	37
2.2.8 Immunofluorescence on cells: .....	38
2.2.9 Establishment of stable cell lines constitutively producing IGFN1-tdTomato or IGFN1_V1-tdTomato .....	39
2.3 Establishment of IGFN1 knockout cell lines.....	39
2.3.1 Mismatch cleavage assay.....	39
2.3.2 Establishment of IGFN1 knockout C2C12 cell lines.....	40
2.4 RT-PCR.....	41
2.4.1 RT-PCR testing MLTK $\alpha$ and MLTK $\beta$ endogenous expression levels in skeletal muscle.....	41
2.4.2 RT-PCR confirm <i>Igfn1</i> gene knocking out in C2C12 cells .....	42
2.5 ELECTROPORATION AND MUSCLE SAMPLE PREPARATION.....	42
2.5.1 Transfection into skeletal muscle using <i>in vivo</i> electroporation .....	42
2.5.2 Skeletal muscle sample preparation and fixation.....	43
2.5.3 Embedding tissues into Wax.....	44
2.5.4 Hematoxylin and eosin stain (H & E).....	45
2.6 MOLECULAR TECHNIQUES.....	46
2.6.1 Polymerase chain reaction (PCR).....	46
2.6.2 Purification of PCR products .....	48
2.6.3 Agarose gel electrophoresis.....	48
2.6.4 Gel extraction of DNA .....	49
2.6.5 Sequencing of DNA .....	49
2.6.6 Preparation of DNA from mammalian cells .....	49
2.6.7 Preparation of DNA from muscle.....	50
2.7 CLONING .....	50
2.7.1 Ligations into pENTR/D-TOPO Entry Gateway vector (Invitrogen).....	50
2.7.2 TdTomato replacement of cycle 3 GFP in pcDNA™-DEST47 Vector .....	50
2.7.3 Gateway cloning.....	51
2.7.4 Transformation of chemically competent cells.....	51
2.7.5 Plasmid preparation from bacterial cultures .....	52
2.7.6 DNA quantification.....	52
2.7.7 Restriction digests.....	53
2.8 PROTEIN ANALYSIS:.....	53

2.8.1 Protein sample preparation from cells: .....	53
2.8.2 Protein sample preparation from muscle.....	53
2.8.3 Bradford assay .....	54
2.8.4 SDS-PAGE .....	54
2.8.5 Western blotting.....	55
2.8.6 Primary antibodies.....	56
2.8.7 Secondary antibodies.....	57
2.8.8 Stripping of western blot membrane using restore plus reagent .....	57
2.9 Identification of interactions between IGFN1 and MLTK .....	58
2.9.1 Immunoprecipitation .....	58
2.9.2 Pull down of COS7-produced MLTK-GFP by <i>E.coli</i> -produced IGFN1-His (from Matthew Winder, placement student).....	59
2.10 Statistics .....	60
2.11 Co-localization analysis .....	60
3. Ectopic expression of IGFN1 and MLTK isoforms <i>in vitro</i> and <i>in vivo</i> : subcellular localizations.....	62
3.1 INTRODUCTION .....	63
3.2 RESULTS.....	65
3.2.1 IGFN1-tdTomato and IGFN1_V1-tdTomato subcellular localization in COS7 .....	65
3.2.2 IGFN1-tdTomato and IGFN1_V1-tdTomato subcellular localization in C2C12 .....	67
3.2.3 IGFN1 and IGFN1_V1 subcellular localization in skeletal muscle .....	71
3.2.4 Subcellular localization of MLTK $\alpha$ and MLTK $\beta$ in COS7 .....	75
3.2.5 MLTK $\alpha$ and MLTK $\beta$ subcellular localization in skeletal muscle.....	77
3.3 CONCLUSION:.....	80
4. Interaction between IGFN1_V1 and MLTKs .....	82
4.1 INTRODUCTION .....	83
4.2 RESULTS.....	83
4.2.1 Pull down using recombinant IGFN1_V1-v5 and MLTK $\alpha$ -GFP or MLTK $\beta$ -GFP from transfected COS7 cells .....	83
4.2.2 Pull down using recombinant IGFN1_V1-his from <i>E.coli</i> and MLTK $\alpha$ -GFP or MLTK $\beta$ -GFP from transfected COS7 (from Matthew Winder, placement student) .....	86
4.2.3 IGFN1_V1-tdTomato co-expression with MLTK $\alpha$ -GFP or MLTK $\beta$ -GFP in skeletal muscle ...	88
4.2.4 Co-expression of IGFN1_V1-tdTomato with MLTK $\alpha$ -GFP or MLTK $\beta$ -GFP causes both proteins to become aggregated around nuclei in skeletal muscle.....	93
4.2.5 Co-expression of IGFN1_V1-tdTomato with MLTK $\alpha$ -GFP or MLTK $\beta$ -GFP in COS7 leads to decreased IGFN1_V1-tdTomato expression .....	96
4.3 CONCLUSION.....	100
5. Quantifications of MLTK isoforms in skeletal muscle .....	102

5.1 INTRODUCTION .....	103
5.2 RESULTS.....	104
5.2.1 Real-time PCR primer selection .....	104
5.2.2 MLTK $\beta$ is the primary isoform in mouse skeletal muscle .....	107
5.3 CONCLUSIONS .....	108
6. Effects of MLTK $\beta$ and IGFN1_V1 overexpression on muscle fibre size and morphology .....	110
6.1 INTRODUCTION .....	111
6.2 RESULTS.....	112
6.2.1 <i>In vivo</i> overexpression of MLTK $\alpha$ -tdTomato or MLTK $\beta$ -tdTomato induces muscle fibre growth.....	112
6.2.2 <i>In vivo</i> overexpression of MLTK $\beta$ -tdTomato causes changes in muscle fibre morphology .....	116
6.2.3 overexpression of IGFN1_V1-tdTomato in mouse skeletal muscle.....	119
6.3 CONCLUSIONS.....	122
7. CRISPR/Cas mediated IGFN1_V1 gene editing <i>in vitro</i> and <i>in vivo</i> .....	124
7.1 INTRODUCTION: .....	125
7.2 RESULTS.....	125
7.2.1 IGFN1 CRISPR/Cas functional characterization.....	125
7.2.2 IGFN1 CRISPR/Cas cell lines generation.....	132
7.2.3 RT-PCR confirms IGFN1 gene knockout in C2C12 cells .....	135
7.2.4 Validation and characterization of IGFN1 knockout cell clones .....	138
7.2.5 Knocking down IGFN1 in mouse skeletal muscle.....	144
7.3 CONCLUSION:.....	149
8. Characterization of an MLTK deficient mouse.....	153
8.1 INTRODUCTION .....	154
8.2 RESULTS.....	154
8.2.1 H&E staining analysis indicates MLTK deficiency causes phenotypic changes in mouse skeletal muscles .....	154
8.2.2 Fibre typing analysis in soleus of MLTK deficient mice.....	158
8.2.3 RT-PCR analysis of MLTK expression in mouse skeletal muscle .....	160
8.2.4 Western blot analysis of MLTK expression in mouse skeletal muscle.....	161
8.3 CONCLUSIONS .....	163
9. DISCUSSION.....	165
9.1 Introduction and aims:.....	166
9.2 Subcellular localization of IGFN1 and MLTK: .....	166
9.3 The interactions between IGFN1_V1 and MLTK $\beta$ :.....	171

9.4 Muscle hypertrophy induced by MLTK overexpression:.....	172
9.5 Knocking out/down IGFN1 <i>in vivo</i> and <i>in vitro</i> : .....	173
Abbreviations: .....	178
BIBLIOGRAPHY: .....	180

## Tables:

Table 7.1: Cell size measurement of IGFN1 knockout clones.....	140
Table 8.1: MLTK deficient mice contain more nuclei in soleus fibres than control mice. ....	155

## Figures:

Figure 1.1 A schematic of the structure of skeletal muscle, a muscle cell and the contractile, sarcomeric unit. ....	4
Figure 1.2: Phenotypic analyses of the ky mutant mouse. ....	12
Figure 1.3: A diagram of the predicted domain composition of IGFN1. ....	16
Figure 1.4: Northern blot analysis of Igfn1 mRNA transcripts in mouse tissues. ....	17
Figure 1.5: A diagram of the genomic structure of IGFN1 and domain composition of IGFN1. ....	18
Figure 1.6: Subcellular localization of IGFN1 in adult mouse skeletal muscle and primary mouse neonatal cardiomyocytes. ....	20
Figure 1.7: A diagram of the domain composition of MLTK $\alpha$ and MLTK $\beta$ . ....	24
Figure 1.8: Signalling pathways possibly relate to MLTK, IGFN1 or KY. ....	30
Figure 3.1: IGFN1-tdTomato and IGFN1_V1-tdTomato subcellular localization in COS7 cells. ....	66
Figure 3.2: IGFN1-tdTomato and IGFN1_V1-tdTomato subcellular localization in C2C12. ....	70
Figure 3.3: IGFN1-tdTomato and IGFN1_V1-tdTomato subcellular localization in mouse skeletal muscle. ....	74
Figure 3.4: MLTK $\alpha$ -GFP and MLTK $\beta$ -GFP subcellular localization in COS7 cells. ....	76
Figure 3.5: MLTK $\alpha$ -tdTomato and MLTK $\beta$ -tdTomato subcellular localization in skeletal muscle. ....	79
Figure 4.1: Pull down assays analysis the interactions between specific isoform of IGFN1 and MLTK. ....	85
Figure 4.2: Pull-down assays analyze MLTK interaction sites on IGFN1_V1. ....	87
Figure 4.3: Electroporation of IGFN1_V1-tdTomato and MLTK $\alpha$ -GFP or MLTK $\beta$ -GFP in EDL/TA muscle in vivo. ....	92
Figure 4.4: Co-expression in vivo of IGFN1_V1-tdTomato with MLTK $\alpha$ -GFP or MLTK $\beta$ -GFP causes apparent aggregations of the recombinant proteins. ....	95
Figure:4.5 Co-expression of IGFN1_V1-tdTomato with MLTK $\alpha$ -GFP or MLTK $\beta$ -GFP in COS7 cells. ....	99
Figure 5.1: RT-PCR primer pair design and amplification test. ....	106
Figure 5.2: Real-time PCR quantification of MLTK $\alpha$ and MLTK $\beta$ relative expression levels in mouse skeletal muscle. ....	108
Figure 6.1: Overexpression of MLTK proteins in mouse skeletal muscle increases fibre cross-sectional area. ....	115

Figure 6.2 overexpression of MLTK $\beta$ -tdTomato causes muscle fibre morphology changes in mouse skeletal muscle.....	118
Figure 6.3: Overexpression of IGFN1_V1-tdTomato and GFP in skeletal muscle.....	121
Figure 7.1: IGFN1 CRISPR/Cas functional characterisation by mismatch cleavage assay.....	131
Figure 7.2 PCR screening for IGFN1 knockout cell lines. ....	134
Figure 7.3: Real-time PCR quantification of <i>Igfn1</i> expression in <i>Igfn1</i> knockout cell lines.....	137
Figure 7.4: Characterization of morphological changes to IGFN1 knockout myoblasts.....	139
Figure 7.5: Characterization of morphological changes in IGFN1 knockout clones during cell differentiation. ....	143
Figure 7.6: Attempt at <i>In vivo</i> knockout of IGFN1 by electroporation of IGFN1 CRISPR/Cas plasmid in mouse EDL/TA muscle. ....	148
Figure 8.1: characterisation of MLTK deficient mice by H&E staining and cross sectional area measurement.....	157
Figure 8.2: Data showing the proportion of type I and type IIA fibres in soleus muscle in MLTK deficient mice and a control mouse. ....	159
Figure 8.3: Real-time PCR quantification of MLTK $\beta$ expression in MLTK deficient mice and control mouse.....	161
Figure 8.4 Western blot analysis of MLTK expression in mouse skeletal muscle.....	163
Figure 9.1: Sequence chromatograms of PCR products from <i>Igfn1</i> in targeted samples. ....	175

## Acknowledgement:

Firstly, I would like to express my sincere gratitude to my advisor Dr Gonzalo Blanco for the continuous support of my Ph.D study and related research, for his patience, motivation, and immense knowledge. His guidance helped me throughout my research and the writing of this thesis. I could not have imagined having a better advisor and mentor for my Ph.D study.

Besides my advisor, I would like to thank the rest of my Thesis Advisory Panel: Dr Nathalie Signoret, and Dr Gareth J O Evans, for their insightful comments and encouragement, but also for the hard questions which incentivised me to widen my research from various perspectives.

I would like to thank the Radhika V. Sreedhar Scholarship. My sincere thanks also goes to Professor Norman J Maitland, who provided me an opportunity of lab assistant experience and thus partly funded me during my studies.

I thank my fellow labmates, Elliot Jokl and Tobias Cracknell, in for the stimulating discussions, for bearing with my not so good English, for the days we were working together, and for all the fun we have had in the last four years.

Last but not the least, I would like to thank my family: my parents and to my grandparents for supporting me throughout all my studies and my life in general.

## Declaration:

This thesis is a presentation of my original research work. Wherever contributions of others are involved, every effort is made to indicate this clearly, with due reference to the literature, and acknowledgement of collaborative research and discussions. This work has not previously been presented for an award at this, or any other, University. The work was done under the guidance of Dr. Gonzalo Blanco, at biology department of the University of York. Part of the work was presented at the 44th European Muscle Conference, Warsaw, Poland September, 21-25, 2015.

The work in chapter 4 section 4.2.2 describes joint work with Matthew Winder, placement student.

# Chapter 1

## 1. INTRODUCTION

## 1.1 Skeletal muscle:

Muscle is an important tissue found in most animals. Its primary function relates to force production and controlling movement. There are three principal types of muscle, skeletal muscle, cardiac muscle and smooth muscle. Both smooth muscle and cardiac muscle are involuntary muscles controlled by the autonomic nervous system <sup>7</sup>, which are necessary for sustaining contractions in the heart and blood vessels, as well as in other organs such as the bladder, uterus, gastrointestinal tract and the respiratory tract. In contrast, skeletal muscle is a voluntary muscle controlled by the somatic nervous system <sup>8</sup> and the skeletal muscles are important for maintaining posture and controlling locomotion.

Skeletal muscle cells (myofibers) are formed from the fusion of myoblasts during myogenesis. Muscle fibres generated in this process are cylindrical and multinucleated. Bundles of myofibers are bound together to make up a fascicle, and many fascicles group together to form a muscle (figure 1.1). Each myofiber is composed of a series of contractile units termed myofibrils, which contain repeating functional units called sarcomeres along the length of the fibre. Under a light microscope, sarcomeres appear as light and dark bands, therefore skeletal muscle is termed as striated muscle. The sarcomeric structures are composed of myofilaments including thin and thick filaments. The thick filaments are comprised of myosin, which appears as a dark band under the light microscope, defined as the A-band. In the middle of the A-band is a paler region termed the H-zone, where the thick filaments and thin filaments are not superimposed. Within the H-zone, the middle of the sarcomere, is the M-line which is composed of elements which crosslink the thick filaments. The thin filaments are comprised of actin, which extends from the Z-disc into the A-band. The Z-disc is defined as the outer boundary of the sarcomere (i.e., the sarcomeric unit runs between adjacent Z-discs).

It is located in the middle of the A-band and appears as a dark, fine and dense line (figure 1.1). The Z-disc is important for intracellular signalling, mechanosensation and mechanotransduction. Molecules at the Z-disc also have important roles in protein turnover, autophagy, regulation of muscle development and degradation<sup>9</sup>. The Z-disc also functions to link muscle sarcomeres to membrane systems<sup>10,11</sup>.

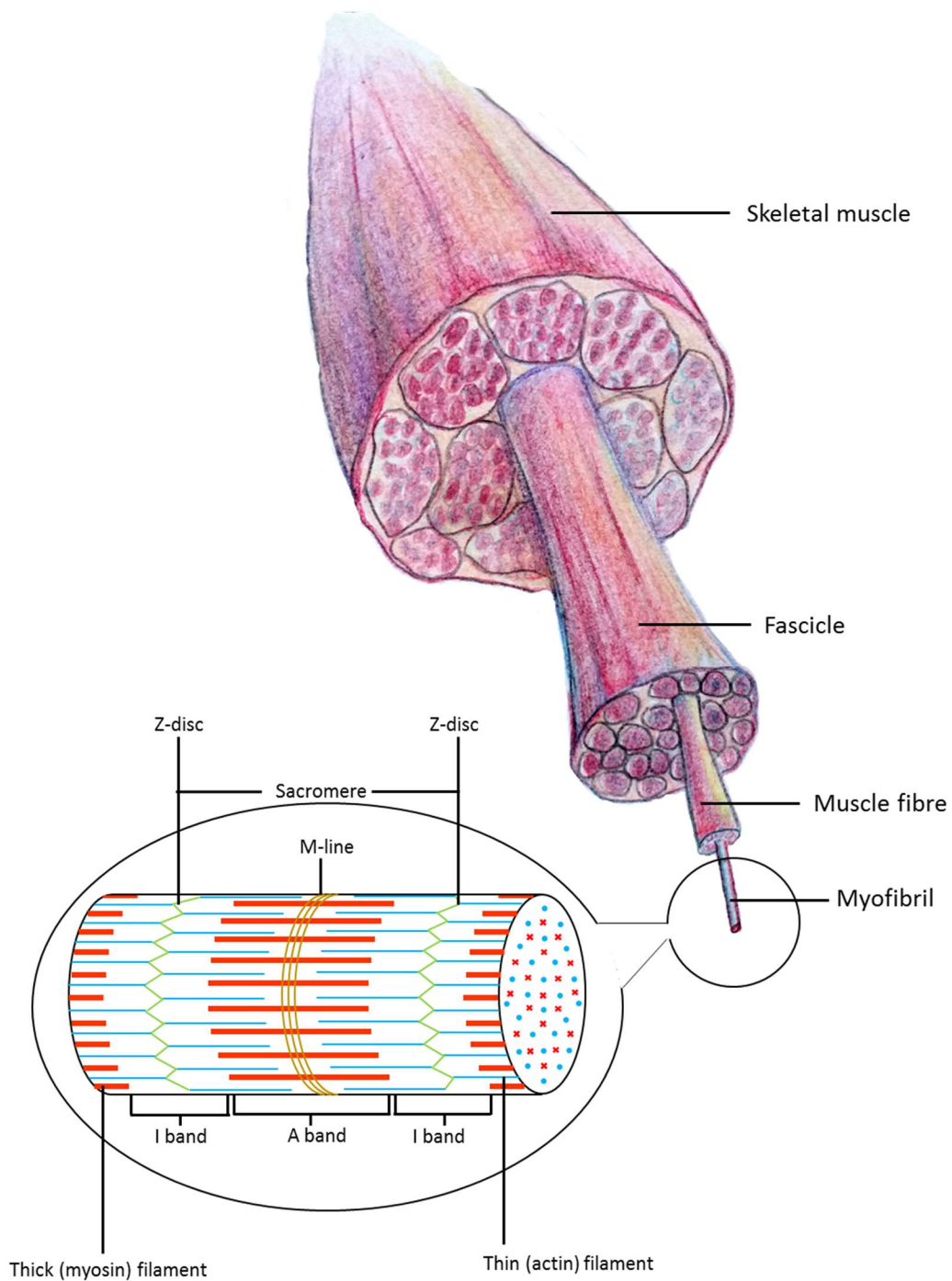


Figure 1.1 A schematic of the structure of skeletal muscle, a muscle cell and the contractile, sarcomeric unit.

The muscle is formed by numbers of fascicles and surrounded by epimysium. Individual fascicles are made up of muscle cells, each cells surrounded by a sarcolemma membrane. Muscle cells are in turn formed by bundles of parallel myofibrils, which contain thick and thin filaments.

## 1.2 Muscular dystrophy:

Myopathy is a collective term for muscular diseases that cause muscle fibre dysfunction and lead to muscular weakness. Many factors can lead to myopathies, such as injury, cramps/sprains from overuse, muscular dystrophy, inflammation, infections or other causes.

Muscle wastage (cachexia) is also associated with ageing and diseases such as cancer.

Muscular dystrophies are a group of muscle diseases caused by mutations in genes encoding muscle proteins. The mutations can be inherited from parents or occur during early development. Dystrophic muscles show significant size variations in muscle fibres, fibre necrosis, small regenerating fibres, centralised nuclei and some infiltration of connective tissue <sup>12</sup>.

Muscular dystrophy can be sub-divided into groups based on the distribution of muscle weakness, severity of symptoms, mode of inheritance and age of onset. There are nine main groups of muscular dystrophy including Becker muscular dystrophy, Congenital muscular dystrophy, Duchenne muscular dystrophy, Distal muscular dystrophy, Emery–Dreifuss muscular dystrophy, Facioscapulohumeral muscular dystrophy, Limb-girdle muscular dystrophy, Myotonic muscular dystrophy and Oculopharyngeal muscular dystrophy. Some of these muscular dystrophies are discussed in further detail below:

- Duchenne muscular dystrophy (DMD) is the most common type, which typically affects approximately 1 in 3,500 males. The symptoms begin at 3 to 5 years of age with muscle weakness. Usually patients are reliant on wheelchairs by the age of 11 due to the progression of muscle weakness, and the disease results in early death because of respiratory failure <sup>13</sup>. The gene responsible for this disease is located on

the X chromosome encoding a 427kDa protein named dystrophin. Mutation of this gene causes absence of dystrophin protein in muscle. Dystrophin is a cytoplasmic protein linking the actin cytoskeleton to the extracellular matrix of skeletal muscle through the dystrophin-glycoprotein complex<sup>14</sup>.

- Becker muscular dystrophy (BMD) is also caused by a dystrophin gene mutation, which leads to the expression of a truncated protein with partial functionality. Compared to DMD, BMD has less severe symptoms. The patients generally retain walking ability until 16 years age, and some of them can lead near-normal lives until age 40 to 50<sup>15</sup>.
- Congenital muscular dystrophies (CMD) are a group of autosomal, recessively-inherited diseases with muscle weakness from birth. CMDs ascribe to mutations from a variety of different genes including genes encoding protein laminin $\alpha$ 2, fukutin, integrin $\alpha$ 7, collagen 6 etc. Different mutations result in a variety of different clinical symptoms.<sup>16</sup>
- Distal muscular dystrophies are a group of muscle disorders with progressive muscle weakness in the forearm, hand, lower-limb or feet. The genes responsible for distal muscular dystrophies are various, including *Desmin*, *Dysferlin*, *GNE*, *Titin*, *MYH7*, *ZASP*, *Myotilin*, *Nebulin* and *Matrin3*.<sup>17</sup>

At present, there is no cure for muscular dystrophies. Current treatments, including physical therapy, corrective surgery and some medications, can only slow the progress of muscle weakness. Study of muscular dystrophy on animal models containing the same mutations that

underlie human muscle diseases could help to broaden knowledge about the mechanisms governing skeletal muscle function and maintenance. Such models will provide a remarkable tool to develop new therapeutic approaches to tackling myopathies.

### 1.2.1 Signalling in muscle Hypertrophy and Atrophy:

Whether a muscle undergoes hypertrophy or atrophy is determined by the balance between the synthesis of new proteins and protein degradation. In conditions where the rate of protein synthesis exceeds the rate of degradation, muscle undergoes hypertrophic growth. In the reverse case, muscle becomes atrophic. Many causes, such as mechanical stress, nutrient availability, physical activity and levels of certain growth factors can affect the balance of protein volume in muscle. These causes are sensed and regulated by a variety of signalling pathways. The following will introduce some well-known pathways that are responsible for muscle hypertrophy or atrophy.

Muscle growth:

There are two major pathways controlling skeletal muscle growth: IGF1-PI3K-Akt/PKB-mTOR pathway and myostatin-Smad3 pathway

- IGF1-PI3K-Akt/PKB-mTOR pathway: positive regulation of muscle growth. insulin-like growth factor 1 (IGF1) can induce muscle hypertrophy by muscle specific overexpression<sup>18</sup>. Two downstream pathways can be activated by IGF1, namely phosphoinositide-3-kinase-Akt (PI3K-Akt) and mitogen-activated protein

kinase/extracellular signal-regulated kinase (MAPK/ERK). Expression of constitutively activated Akt leads to significant fibre hypertrophy<sup>19,20</sup>. Akt is known to stimulate protein synthesis by activation of mammalian target of rapamycin (mTOR) and its downstream effectors. There are two known complexes composed by mTOR and its interaction partners, which are mTOR complex 1 (mTORC1) and mTOR complex 2 (mTORC2). Muscle-specific knockout of mTOR reduces the size of fast muscle fibres during postnatal growth and severe myopathy<sup>21</sup>. mTOR not only responds to Akt but also responds to multiple upstream signals. Likewise, protein synthesis is not the cellular processes which mTOR controls, others include autophagy. Rapamycin is a specific mTOR inhibitor, mainly affecting mTORC1, although it can affect mTORC2 during chronic treatment<sup>22</sup>. Two major downstream effectors of mTORC1 are S6 kinase 1 and factor 4E-binding protein 1 (4E-BP1), which feed into elevated synthesis of new proteins, for example by ribosome activation. Deletion of S6 kinase 1 results in muscle atrophy and the response to constitutive activation of Akt was partially prevented<sup>23</sup>.

- myostatin–Smad3 pathway: negative regulation of muscle growth. Myostatin belongs to the transforming growth factor  $\beta$  (TGF $\beta$ ) superfamily. Disruptive mutations in myostatin cause muscle hypertrophy in a variety of mammalian species<sup>24</sup>. Treating differentiated myotubes with purified myostatin causes reduction of myotube size and inhibition of protein synthesis<sup>25</sup>. Furthermore, systemically administered myostatin causes muscle atrophy in mice<sup>24</sup>. Activin A is another member of TGF $\beta$  family. It interacts with myostatin and they activate a heterodimeric receptor complex composed of a type II receptor (activin receptor II, abbreviation as ACVR II and ACXR

IIB) and a type I receptor (activin receptor-like kinase 4 and 5, abbreviation as ALK4 and ALK5). In myofibers, myostatin-activin A signalling is mediated by phosphorylation of Smad2 or Smad3 transcription factors, which in turns stimulate FoxO signalling and induces protein degradation through the ubiquitin-proteasome system and autophagy-lysosome pathway. Activation of FoxO was found to induce transcription of *atrogen-1* and *MuRF1*, which are important E3 ubiquitin ligases for protein degradation via the ubiquitin-proteasome system. The activation of Smad suppresses Akt signalling and results to inhibition of protein synthesis.<sup>26-28</sup>.

#### Muscle atrophy:

Muscle atrophy results in myofibre shrinkage, including a net loss of proteins, cytoplasm and organelles due to elevated activation of protein degradation pathways. A variety of triggers can induce skeletal muscle atrophy, including denervation, limb suspension and starvation. These triggers lead to the elevated transcription of so-called atrogenes, primarily by releasing the negative regulation of protein degradation pathways by Akt signalling. The Akt is known to negatively regulate both the ubiquitin-proteasome system and autophagy-lysosome pathway via the FoxO transcription factors. Akt phosphorylates all three isoforms of FoxO, FoxO1, FoxO3 and FoxO4, which promotes the translocation of phosphorylated FoxO from the nucleus to the cytoplasm. This prevents the transcription factors from upregulating protein degradation genes, resulting in muscle mass maintenance or hypertrophy. In contrast, inhibition of the Akt pathway activity results in muscle atrophy by allowing the FoxO transcription factors into the nucleus.<sup>28</sup>. There are two main protein degradation pathways: the ubiquitin-proteasome system and the autophagy-lysosome pathway. Both pathways are

thought to be co-ordinately upregulated by FoxO transcription factors in atrophying muscles<sup>29</sup> and their function is described below:

- The ubiquitin-proteasome system is essential to remove sarcomeric proteins in response to damage caused by muscle activity. The pathway depends on the ubiquitination process which adds ubiquitin to a protein substrate. This process consists of three main steps mediated by three types of enzyme, which are ubiquitin-activating enzymes (E1s), ubiquitin-conjugating enzymes (E2s), and ubiquitin ligases (E3s). E1 function to activate ubiquitin by forming a thioester linkage between ubiquitin and the E1<sup>30</sup>. After that, E2 binds to both E1 and activated ubiquitin to transfer ubiquitin from E1 to E2. E3 then generates an isopeptide bond between the target protein and ubiquitin, then more ubiquitin will bind to form a polyubiquitin chain. This signals for the protein to be taken to the proteasome to be degraded<sup>31</sup>. Muscle RING finger 1 (MuRF1) and atrogin-1/MAFbx (muscle atrophy F-box) are two muscle-specific E3 ubiquitin ligases, which are upregulated during muscle atrophy. Deficiency of MuRF1 and atrogin-1/MAFb in mice prevent the muscle atrophy caused by denervation<sup>32</sup>.
- The autophagy-lysosome pathway is an evolutionarily conserved pathway used to degrade and recycle long-lived proteins, cytoplasm and organelles through the degradative lysosome<sup>33,34</sup>. Autophagy can be triggered through stress conditions including starvation of amino acids, viral infection and the unfolded protein response. There are three autophagic routes for delivering material into the lysosome, which are macroautophagy (autophagy), microautophagy and chaperone-mediated autophagy. Macroautophagy operates by enveloping the material to be degraded inside a

autophagosomal membrane and then fusing this with the degradative lysosome <sup>35</sup>. Microautophagy is mediated by lysosome/vacuolar engulfment of cytoplasmic material <sup>35</sup>. Chaperone-mediated autophagy mediates degradation of a chaperone-dependent selection of soluble, cytosolic proteins in lysosomes <sup>36</sup>.

The efficient functioning of these pathways is important for the health of skeletal muscle tissue. If these pathways are disrupted, muscle may not be able to undergo appropriate adaptive responses to physical and metabolic stresses. This may result in skeletal muscle damage and diseases.

### 1.3 THE KY MUTANT:

#### 1.3.1 The *ky* mutant mouse:

The *kyphoscoliosis peptidase (ky)* mutant mouse arose spontaneously in the Bile Duct Ligation (BDL) mouse strain and has become a model of recessive, hereditary kyphoscoliosis. The *ky* gene is located on mouse chromosome 9 and encodes a 72kDa protein, which is expressed in skeletal muscle and heart tissues. The *ky* mutation is a GC deletion near the beginning of the transcript, causing the disruption of amino acid 24 and a frame shift resulting in a premature STOP codon. This leads to the total absence of the Ky protein in the homozygous *ky/ky* mutant mouse <sup>1,4</sup>.

KY contains a putative transglutaminase/protease domain, which has homology to ancestral cysteine proteases in archibacteria <sup>37</sup>. However, protease activity has yet to be found on any of the presumptive substrates. Moreover, aligning the Ky sequence to an alternative protein indicates that the catalytic triad is disrupted, which is essential for enzymatic activity <sup>38</sup>. It is

therefore possible that the transglutaminase-like domain has been co-opted for non-enzymatic molecular interactions.

The *ky/ky* mutant mouse was first reported by Dickinson and Meikle; it suffers from a primary degenerative myopathy which leads to chronic thoraco-lumbar kyphoscoliosis<sup>39,40</sup>. Mutant mice show abnormal curvature of the vertebrae and intervertebral discs from 9 days postpartum, and the mice lack the ability to perform a normal placing reflex as early as 21 days after birth and show distinguishable chronic thoraco-lumbar kyphoscoliosis from about 100 days (figure 1.2A and B)<sup>40,41</sup>.

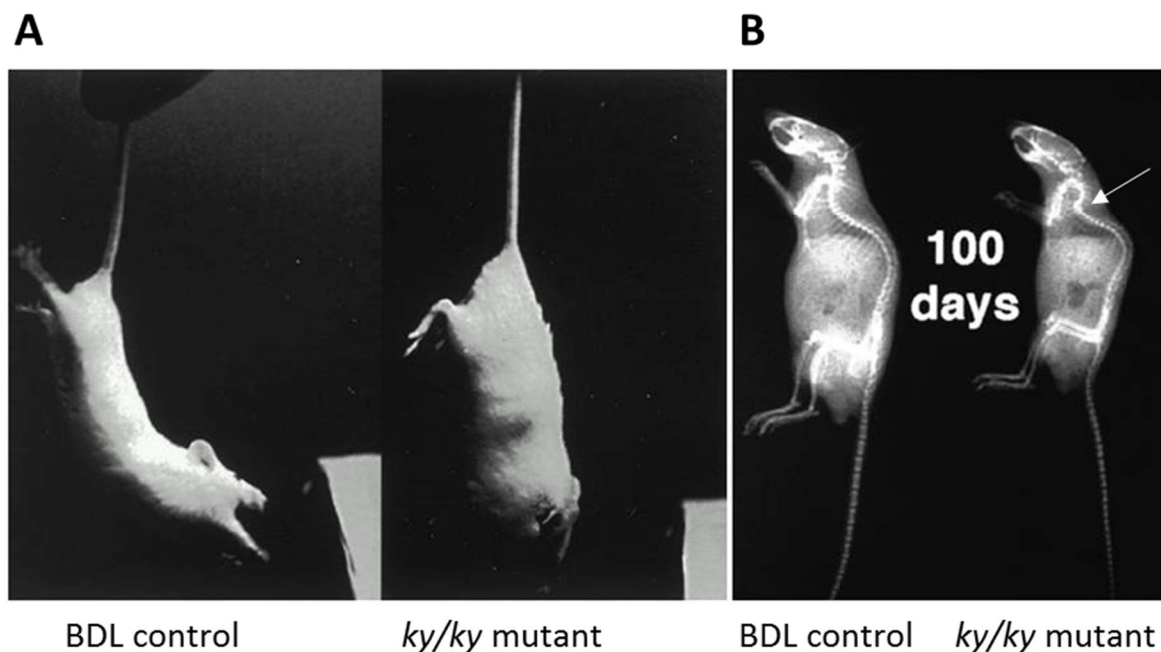


Figure 1.2: Phenotypic analyses of the *ky* mutant mouse.

(A), Placing reflex test, the *ky/ky* mutant mouse fails to lift the head and the forelimbs to reach the edge of a table, whereas the control mouse can do so. (B), X-ray analysis of BDL and *ky/ky* mutant mice, arrow indicates the visible scoliosis in the *ky/ky* mutant mouse. images adapted from Blanco *et al.*<sup>1</sup>.

The *ky/ky* mutant mice exhibit a rare muscular dystrophy in postural, slow-twitching muscles including the soleus, psoas and erector spinae, which exhibits as diminished size of muscle fibres, internalized nuclei and an increase in the amount of connective tissue <sup>41</sup>. Electron microscopy analysis shows significant changes of the sarcomere banding dimensions and patterning in *ky/ky* soleus, including Z-line streaming and thickening of the Z-band <sup>42</sup>. In contrast the fast-contracting muscles are generally normal, such as the gastrocnemius and extensor digitorum longus (EDL) <sup>41</sup>. The slow-contracting muscles *from ky/ky* mice display a single postnatal phase of muscle fibre degeneration and regeneration between 3-5 weeks old. The regeneration completes at 47 days accompanied with severe muscle atrophy <sup>41</sup>. (figure 1.2C)

Normal soleus muscle contains 55 -60% of fibres expressing myosin heavy chain I (MHCI) and approximately 40% of fibres expressing MHCIIa, whereas in the adult *ky* mutant mice all muscle fibres express MHCI in the soleus muscle <sup>1,43</sup>. The body weight of *ky* mutant mice at all ages is 75% of that of the age matched controls. The muscle weight of soleus or EDL in *ky/ky* mice are up to 50% lighter than control mice, and therefore the ratio of body weight to muscle mass increases in *ky/ky* muscle <sup>43</sup>. Normal muscles in wild type (WT) animals undergo hypertrophic growth and adapt the expression of myosin heavy chain (HMC) and myosin light chain (MLC) isoforms in response to overload. However, the *ky/ky* EDL muscle, a muscle spared of visible myopathy, shows complete absence of hypertrophic response to compensatory overload. This indicates that *ky/ky* muscle has lost the ability to adapt its size in response to increased load and that the shifts in contractile isoforms to the slow type in *ky/ky* soleus muscle were possibly generated to increase their resistance to fatigue <sup>1</sup>.

### 1.3.2 The *ky* mutant human:

A pathology arising from homozygous, disruptive *ky* gene mutation was found in two Arab-Israeli brothers. The mutation causes a premature termination codon in exon 6 of the *ky* gene and possibly leads to nonsense mediated mRNA-decay<sup>3</sup>. Patients show congenital bilateral equinovarus foot deformity and suffered by progressive muscle weakness and atrophy of the lower limb since early infancy, which affects their walking ability - one brother can only walk short distance with crutches. The muscle weakness and atrophy also shows in the upper limbs of the younger brother (23 years old), which mainly affects the hand muscles, forearm and biceps and triceps muscles with preservation of the deltoid. The biopsy from quadriceps of this patient when he was 17 years old showed atrophic and necrotic fibres, variations of fibre size, centrally located nuclei, central mitochondrial depletion, unstructured core targetoid defects and streaming and thickening of the Z-disc<sup>3</sup>. The 34 year old patient showed less effect on his upper limbs, which maintain full muscle strength. However, he also suffers from elbow contractures, facial weakness, kyphosis with rigid spine and atrophic tongue, as does his younger brother<sup>3</sup>.

Another *ky* gene mutation causing a human neuromuscular disorder was found in a 7.5-year-old girl. The mutation is 1 base deletion leading to a frameshift and premature STOP codon, which is predicted to results in a truncated, non-functional protein. The girl shows generalized muscle weakness and contractures in her feet, hips and shoulders. She suffers with lordosis and progressive equinus contractures on her feet. Moreover, the muscle fibres showed size variations, internalized nuclei and Z-disc thickening in some fibres.<sup>2</sup>

The pathologies resulting from *ky* gene mutations share similar histological features between mice and humans, which exhibit as progressive muscular dystrophy, muscle weakness,

contractures, rigid spine/kyphosis or lordosis. Moreover, mutant muscle samples from humans and mice show atrophied and necrotic fibres, internalized nuclei and Z-disc streaming and thickening. All this evidence indicates that the KY protein is essential to maintain the normal function of skeletal muscle. However, a clear role for KY at the molecular level is still lacking. A previous study reviewed several KY interaction partners including titin (TTN), myosin binding protein C (MYBPC1), filamin C (FLNC) and immunoglobulin-like and fibronectin type 3 domain containing 1 (IGFN1) <sup>42</sup>. All known KY interaction partners are sarcomeric cytoskeletal muscle proteins, and all of them consist of repeats of immunoglobulin (Ig) and/or fibronectin-like (Fn3-like) domains. In striated muscle, FLNC acts as a flexible linker crosslinking actin at Z-disc. Mechanical tension-induced FLNC unfolding and conformational changes lead to degradation of FLNC via the Chaperone-Assisted Selective Autophagy (CASA) pathway. In this process, BAG3 facilitates the recruitment of chaperones (HSPA8 and HSPB8) to unfolded or damaged FLNC, then initiates FLNC ubiquitination and degradation through the autophagosome-lysosomal pathway <sup>44</sup>. In addition, under mechanical tension BAG3 also participates in FLNC transcription via release of the YAP/TAZ transcription factors from their inhibitors. The released transcription factors translocate to the nucleus and initiate FLNC transcription <sup>44</sup>. Thus, CASA is crucial for sensing mechanical stress and maintaining the balance of functional protein. Given FLNC is a client of CASA, which aggregates and distributes abnormally in slow ky/ky muscles <sup>42</sup>, it is possible that KY plays a role in the partially described CASA mechanism.

## 1.4 IGFN1:

### 1.4.1 Identification of the *Igfn1* locus:

A previous Y2H study using full length Ky protein as a bait identified a fragment of a novel protein, which mapped to the sequence ENSG00000163395 on human chromosome 1 (position 1q32.1). In mice, this fragment aligned to GENSCAN00000047301, which is a large predicted gene on mouse chromosome 1 (position qE4). This predicted gene was analysed by SMART (Simple Modular Architecture Research Tool) software, the results showed 11 globular domains and a large unstructured region located between the 3<sup>rd</sup> and 4<sup>th</sup> globular domains (figure 1.3). As these globular domains include immunoglobulin (Ig) and fibronectin type III (Fn3) domains, the assigned name of this predicted protein was Immunoglobulin-like and fibronectin type 3 domain containing 1 (IGFN1)<sup>42</sup>. The *Igfn1* locus shows strong evolutionary conservation between mice and humans<sup>4</sup>.



Figure 1.3: A diagram of the predicted domain composition of IGFN1. The oval shapes represent the globular domains. Figure adapted from Baker et al.<sup>4</sup>

### 1.4.2 Tissue distribution of *Igfn1* mRNA transcripts:

To reveal where transcription of *Igfn1* occurs in mice, a northern blot analysis was performed using probes from predicted *Igfn1* cDNA. The probes from 5'-end of *Igfn1* produced a single thick band in skeletal muscle. The 3'-end of *Igfn1* produced the same thick band in skeletal

muscle, as well as smears in heart, skeletal muscle and lung, which indicates that *Igfn1* may undergo a variety of splicing events, producing isoforms of several sizes (figure 1.4).<sup>4</sup>

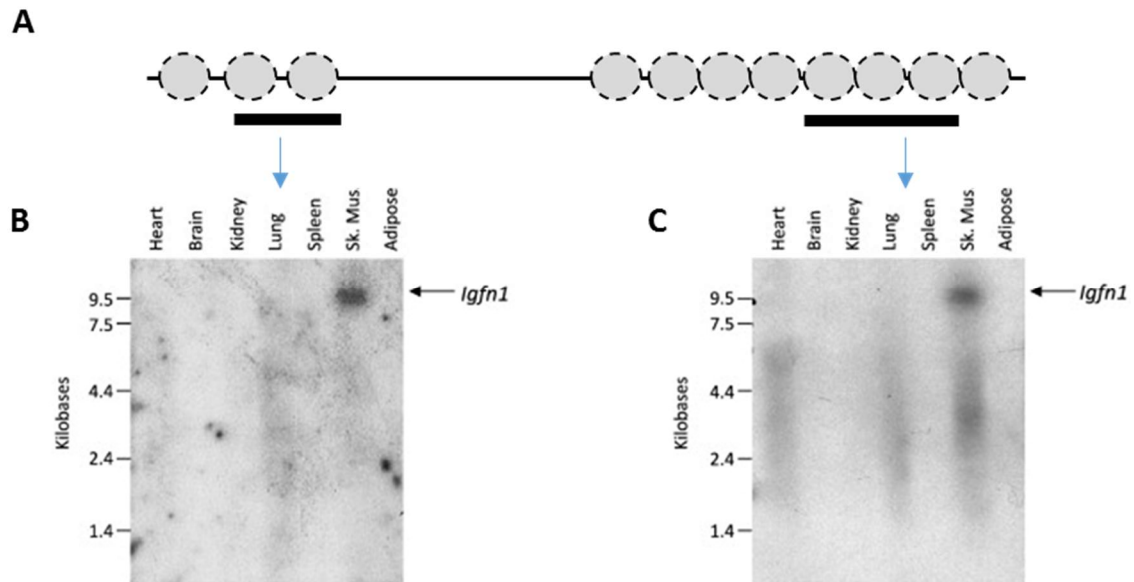


Figure 1.4: Northern blot analysis of *Igfn1* mRNA transcripts in mouse tissues. (A), a diagram of the *Igfn1* cDNA. black bar represents the *Igfn1* cDNA, the globular domains annotated with dashed circle shape, black bars represent the probes used in the northern blots. (B) and (C), northern blot analysis mRNA transcripts using radioactively labelled anti-sense probes. Short arrows labelled a large transcript detected in skeletal muscle by probes against both 3'- and 5' end of *Igfn1*. Part of figure (B and C) adapted from Baker et al.<sup>4</sup>

### 1.4.3 Identification of *Igfn1* cDNAs in skeletal muscle:

To isolate the full length *Igfn1* cDNA from mouse, several primers from 3'- and 5'-end of predicted sequence of *Igfn1* were used. At least 4 full length *Igfn1* cDNAs were identified, termed as *Igfn1*, *Igfn1\_v1*, *Igfn1\_v2* and *Igfn1\_v3*, which indicates that at least 4 isoforms of IGFN1 proteins originate from this locus. Both IGFN1 and IGFN1\_V1 contain all 11 globular domains, but only IGFN1 has the unstructured region located between the 3<sup>rd</sup> and 4<sup>th</sup> globular

domains. IGFN1\_V2 contains part of the unstructured region and all 8 globular domains at the C'-terminus. IGFN1\_V3 only contains 4 globular domains at the C'-terminus (figure 1.5).<sup>4</sup>

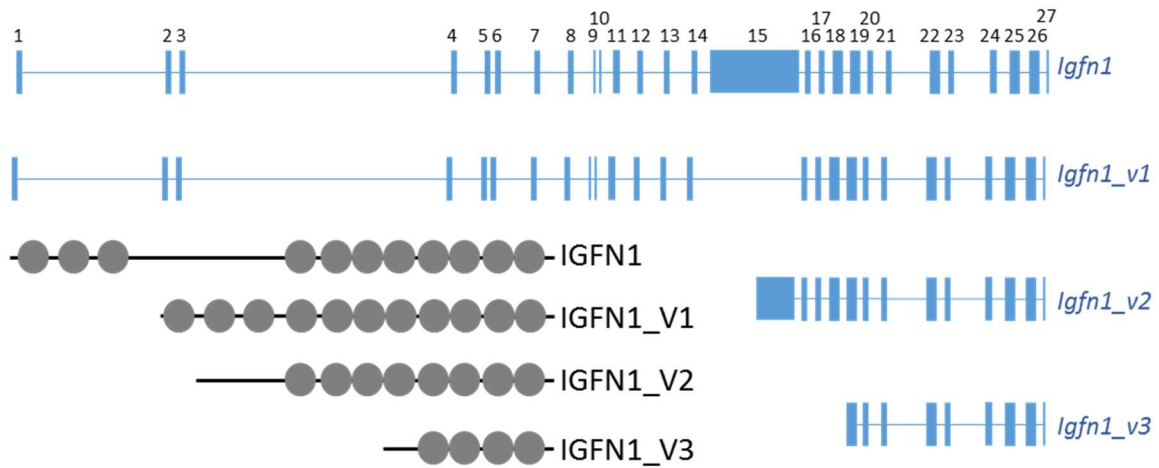


Figure 1.5: A diagram of the genomic structure of IGFN1 and domain composition of IGFN1. The blue bars represent exons in different *lgfn1* isoforms. The lower left hand side shows the protein domain composition of IGFN1, the grey circle shapes represent globular domains.

#### 1.4.4 Subcellular localization of IGFN1:

The subcellular localization of IGFN1 in adult mouse skeletal muscle was identified using immunohistochemistry and immunofluorescence with antibodies, Ab-US42 and Ab-Kip2b, against the N- and C-terminus of IGFN1 respectively. Both immunohistochemistry (figure 1.6A) and immunofluorescence (figure 1.6B and C) results showed a striated expression pattern and nuclear expression. The striated expression pattern was confirmed as Z-disc patterning by co-localization with the Z-band marker  $\alpha$ -actinin. Up to 40% of nuclei in the cross section of individual mid-hindlimb muscle show IGFN1 expression, whereas the number of nuclei from satellites cells only comprise <5% of total nuclei in mid-hind limb muscle. Therefore, nuclei

identified as expressing IGFN1 are likely to be the myonuclei rather than the nuclei from satellite cells. The z-disc and nuclear localizations of IGFN1 were also found in primary mouse neonatal cardiomyocytes by transduction of these cells with V5-tagged IGFN1<sub>(d1-d3)</sub>.<sup>4</sup>

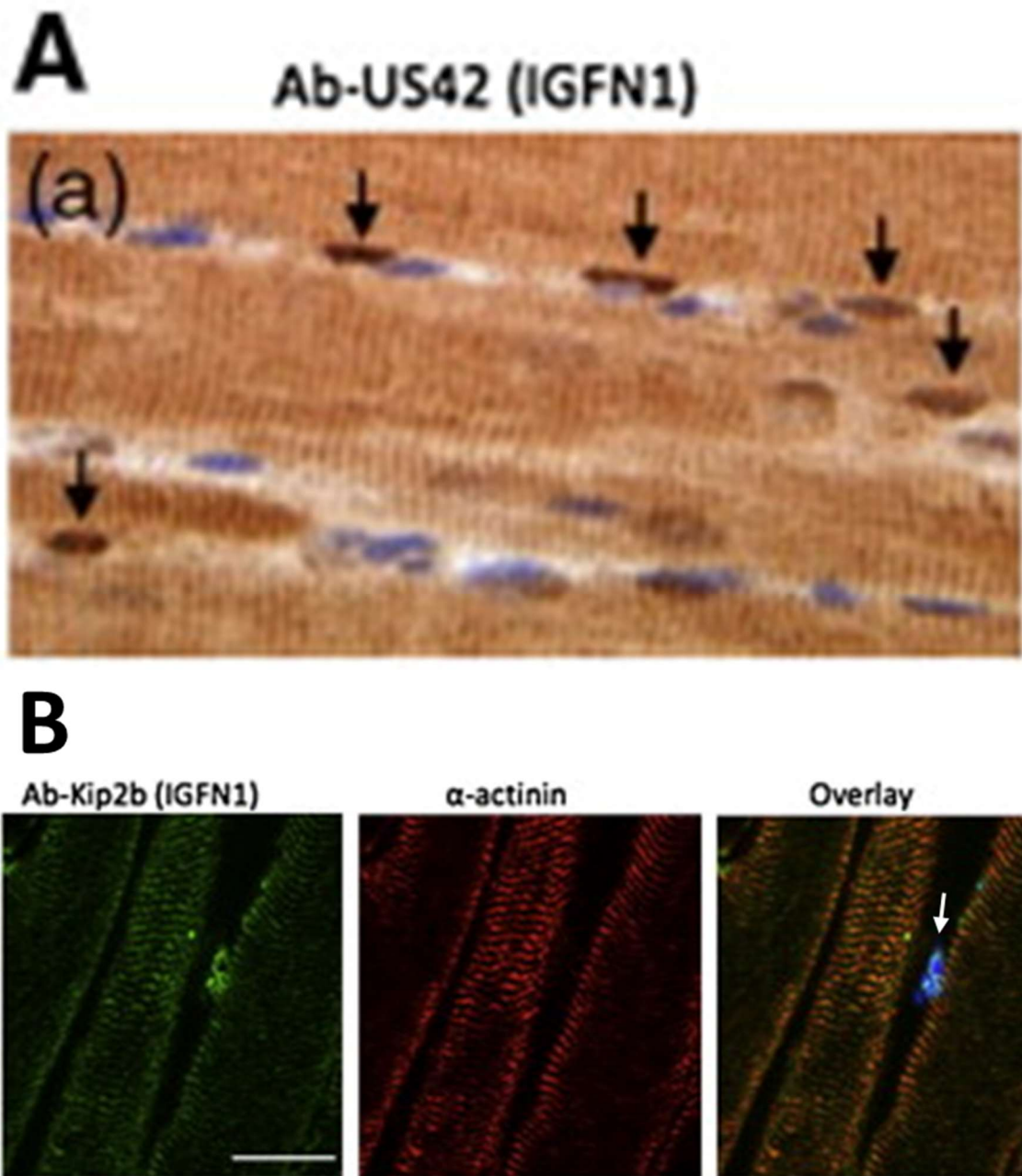


Figure 1.6: Subcellular localization of IGFN1 in adult mouse skeletal muscle and primary mouse neonatal cardiomyocytes.

(A), Immunohistochemistry of adult mouse skeletal muscle. (a), longitudinal sections of adult mouse skeletal muscle were analysed using immunohistochemistry with antibody Ab-US42 against the N-terminus of IGFN1. Arrows in (a) label the nuclear localization of IGFN1. (B), Immunofluorescence of adult mouse skeletal muscle with Ab-Kip2b antibody against the C-terminus of IGFN1. Z-disc localization confirmed by co-localizing the striated expression pattern with Z-disc marker  $\alpha$ -actinin. White arrow in B labels the nuclear localization of IGFN1. All the scale bars = 25  $\mu$ m. Figures adapted from Baker et al.<sup>4</sup>

#### 1.4.5 IGFN1 interaction partners:

A previous study identified several interaction partners of IGFN1 using two Y2H experiments. The first Y2H, using the bait against the sequence including all 8 globular domains (IGFN1<sub>(d4-d11)</sub>) at the C-terminal of IGFN1, identified 50 clones. Many IGFN1 interaction partners identified by IGFN1<sub>(d4-d11)</sub> are the same sarcomeric cytoskeletal proteins identified in a previous Y2H experiment using KY as a bait, including are FLNC, MYBPC1 and TTN, and other in-frame partners myomesin (MYOM2), actin (ACTA1), an uncharacterized transmembrane protein (TMCO7) and a Na<sup>+</sup>/K<sup>+</sup> ATPase beta chain protein (ATP1B1). The interactions between IGFN1<sub>(d4-d11)</sub> and the following interaction partners, MYOM2, BPC1, FLNC, TTN and ACTA1, were confirmed by in vitro pull-down assays. <sup>4</sup>

The second Y2H screen, using the bait against the sequence containing the first three globular domains at the N-terminus of IGFN1 IGFN1<sub>(d1-d3)</sub>, identified only 15 clones. The in-frame partners are a MLK-like mitogen-activated protein triple kinase (MLTK), four and a half LIM domains 2 (FHL2), PDZ and LIM domain 3 (PDLIM3), and a protein with unknown function (FAM96B). Interactions with IGFN1<sub>(d1-d3)</sub> were also confirmed by in vitro pull-down assays. <sup>4</sup>

The interactions between IGFN1 and FLNC or KY were confirmed by another independent method, immunoprecipitation. All these results suggested that IGFN1 proteins interaction with a variety of proteins, possibly forming biologically relevant protein complexes with FLNC and KY through Ig and Fn domains, since the Ig and Fn domains has shown to involved in protein interactions in many other scaromeric proteins <sup>4</sup>.

#### 1.4.6 Igfn1 transcription levels in hypertrophic or atrophic muscle:

Previous studies found that Igfn1 is upregulated in atrophic muscle caused by short term denervation<sup>45</sup> or activin A treatment<sup>46,47</sup>. Western blot using an antibody against IGFN1 in the *ky/ky* mouse showed that IGFN1 expression level was increased, while immunocytochemistry with IGFN1 antibodies showed that nuclear expression of IGFN1 in the *ky/ky* mouse decreased comparing to the control mouse (unpublished data from Jane Baker). The significance of IGFN1 changes in *ky/ky* mice has not been explored further. Igfn1 is downregulated in hypertrophic muscle treated with ActRIIB-Fc, whereas the transcription level of Igfn1 does not change in muscle hypertrophy resulting from myostatin deficiency<sup>48</sup>. In this context, ActRIIB-Fc is an inhibitor which can block both myostatin and activin to induce muscle growth<sup>49</sup>. Together this indicates that the function of IGFN1 in relation to muscle hypertrophy and atrophy possibly acts via KY or activin regulated signalling pathways.

In summary, the *Igfn1* locus is complex and contains at least 4 different cDNA splicing variants. It is highly conserved in all mammalian genomes examined. IGFN1 protein contains a series of globular domains which likely mediate the interactions between IGFN1 and other proteins. The interaction partners of IGFN1 have been identified by two Y2H screens and some of these interaction partners are the same as those identified in a Y2H screen examining KY interactions. Given that the *ky* gene mutation causes progressive muscular dystrophy in both human and mouse, and that KY interacts with IGFN1 and shares many interaction partners with IGFN1, it is suggested that KY and IGFN1 might operate in a common pathway to regulate muscle hypertrophic responses. The subcellular localization analysis of IGFN1 in adult mouse skeletal muscle and primary mouse neonatal cardiomyocytes found that IGFN1 localizes to the

Z-disc and nuclei. This may suggest that IGFN1 may play a role by transferring signals between nuclei and the Z-disc in a hypothetical IGFN1-KY pathway.

## 1.5 MLTK:

### 1.5.1 The genomic and proteomic features of MLTK:

A previous Y2H using IGFN1<sub>(d1-d3)</sub> as the bait identified several interaction partners<sup>4</sup>, including MLTK which attracts our attention due to its role in hypertrophic responses in cardiac muscle<sup>5</sup>. Moreover, MLTK was also found to be upregulated in EDL muscle of *ky/ky* mouse<sup>50</sup>, indicating that MLTK may also relate functionally with the IGFN1-KY pathway.

MLTK belongs to the mixed lineage kinase family, including MLK1, MLK2, MLK3, MLK4, leucine zipper kinase (LZK), dual leucine zipper kinase (DLK) and MLTKs<sup>51</sup>. All these MLK proteins contains two distinct structures, a kinase catalytic domain and a leucine zipper domain. The kinase domain contains features from both tyrosine kinase and serine/threonine kinases, which functionally activate the specific mitogen activated protein kinases (MAPKs) by phosphorylation<sup>52</sup>.

MLTK has two isoforms, MLTK $\alpha$  and MLTK $\beta$ , spliced from same gene on mouse chromosome 2C3 (human, chromosome 2q31.1). MLTK $\alpha$  is translated from 20 exons and composed of 803 residues, whereas MLTK $\beta$  is translated from 12 exons containing only 454 residues<sup>53</sup>. Both isoforms share the kinase domain (residues 16-227) and a leucine zipper (residues 287-322) at the N-terminus until residue 331. A previous study confirmed that the leucine zipper is responsible for MLTK $\alpha$  oligomerization<sup>54</sup>. The isoforms differ at their C-terminal: a sterile  $\alpha$ -motif (SAM) only exists in MLTK $\alpha$  (residues 337-408, see Figure 1.7), whereas MLTK $\beta$  only has a shorter C-terminus encoded by only one exon, which is not common to MLTK $\alpha$ . SAM

domains were found to be involved with protein interactions, polymeric formation and binding to RNA <sup>55</sup>. A study showed that the SAM domain is not essential for MLTK $\alpha$  oligomerization <sup>54</sup>.

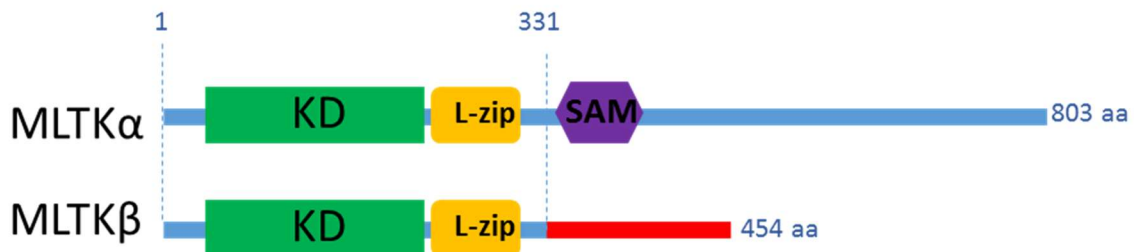


Figure 1.7: A diagram of the domain composition of MLTK $\alpha$  and MLTK $\beta$ . Both isoforms have identical sequence from residue 1 to 331. KD represents serine/threonine kinase domain. L-zip represents leucine zipper motif. SAM represents sterile  $\alpha$ -motif.

### 1.5.2 Tissue distribution of *mltk* mRNA transcripts:

A previous northern blot using probes against the unique C-terminus sequence of MLTK $\alpha$  or MLTK $\beta$  respectively identified *mltk* mRNA transcript levels in multiple human tissues. The analysis showed that MLTK $\alpha$  is encoded by a 3.5kb transcript with higher expression in the liver, no expression detected in the brain and leukocytes and intermediate expressions in the other examined tissues including heart, skeletal muscle, colon, thymus, spleen, kidney, small intestine, placenta and lung. In contrast, MLTK $\beta$ , encoded by a 7.5kb transcript, showed higher expression levels in skeletal muscle and heart, intermediate expressions in lung, placenta and small intestine and lesser expression in other tested tissues. <sup>51</sup>

Another northern blot used a probe (1022 bps) from mouse MLTK cDNA to analyse the *mltk* mRNA transcripts level in multiple human tissues. The blot showed that *Mltk $\beta$*  transcript is highly expressed in skeletal muscle and heart tissues, which is consistent with Bloem's results.

This probe detects another two bands, ~3.3kb and ~1.6kb, with lower expression levels only in skeletal muscle and heart tissues. The ~3.3kb band matches the molecular weight of *Mltka* transcript. However, the results are not fully compatible with Bloem's result which identified high expression levels in the liver<sup>53</sup>.

### 1.5.3 MLTK induces hypertrophic responses *in vitro* and *in vivo*:

Cardiac restricted overexpression of MLTK $\beta$  caused a hypertrophic response, impaired systolic function and diastolic function in the transgenic (Tg) heart. The hypertrophy phenotypes included an increase in the ratio of heart weight to body weight, myocardial fibrosis and disorganized myofibrils in MLTK $\beta$ -overexpressing Tg mice<sup>5</sup>. The MLTK-overexpressing Tg mice showed significant mortality under cardiac stress using chronic isoproterenol infusion, which is a well-known model of induced cardiac hypertrophy<sup>5</sup>.

MLTK functions as a mitogen activated protein kinase kinase kinase (MAPKKK) which can activate one or more MAPKK/MAPK cascades including the c-Jun N-terminal kinase (JNK)/stress-activated protein kinase (SAPK) pathway, p38 pathway, extracellular signal regulated kinase (ERK) pathway and the REK5/Big MAPK1 (BMK1) pathway<sup>53,56</sup>. In MLTK $\beta$ -overexpressing Tg mice, activation of the p38 pathway was significantly elevated compared with controls<sup>5</sup>. This suggests that MLTK $\beta$ -induced cardiac hypertrophy possibly operates through the p38 pathway.

Additionally, overexpression of MLTK $\beta$  in both cardiac myocytes and mouse heart altered fetal gene expression, which was found to be associated with cardiac hypertrophy<sup>5,57</sup>. The

alteration in fetal gene expression has also been observed in MLTK $\beta$ -overexpressing cardiac myocytes, in which protein synthesis was also significantly increased <sup>51</sup>.

Overexpression of MLTK $\alpha$  in H9c2 cardiomyoblast cells induced hypertrophic responses by increasing the organization of the actin fibres and the size of the cells. The kinase domain negative mutant failed to generate any of these changes. The fetal gene expression changes was also found in MLTK $\alpha$ -overexpressing cardiomyoblast cells <sup>54</sup>.

All this evidence suggests that MLTK is functionally related to cardiac muscle hypertrophic responses. Since both cardiac muscle and striated muscle contain similar sarcomeric structures, MLTK could possibly play a similar role to regulate hypertrophic growth in skeletal muscle.

#### 1.5.4 MLTK mutation:

A previous study found an autosomal recessive disorder caused by MLTK $\alpha$  mutation. The patients suffered by split-foot phenotype and nail anomalies. The mutations affected the SAM domain by missense alteration leading to domain dysfunction or intragenic deletion of exon 12 to 16 resulting in deletion of the SAM domain <sup>58</sup>.

CRISPR/Cas9 was used to generate an MLTK mutation in mouse exon 2, which completely knocks out both isoforms of MLTK. This lead to fully penetrant lethality caused by severe cardiac edema and growth retardation. In addition, CRISPR/Cas9 was used to generate another MLTK mutation by deleting the SAM domain. This caused hindlimb duplication phenotypes in 4 mice (four out of sixty-four mice). The mutations caused down regulation of

the *Trp63* gene, which is a split-hand/split-foot malformation disease gene. These results indicate that the function of MLTK $\alpha$  may be involved in limb development.<sup>58</sup>

In addition, MLTK mutations were found in six patients coming from three different families. Reverse transcription polymerase chain reaction and transcriptome analyses showed that the expression levels of MLTK were decreased. Patients suffer from muscle weakness, reduced ambulant ability, scoliosis and decreased ventilatory capacity. The muscle fibres show variable fibre size, predominance of type I fibres and central nuclei<sup>6</sup>. Intriguingly, there was no abnormal limb development shown in the human patients, which suggests that the SAM domain mutation causing the induction of split-hand/split-foot malformation disease<sup>58</sup> may be a gain of function effect. Predominance of type I and muscle weakness are features described in homozygous *ky* mice<sup>1</sup> and additionally both MLTK and KY interact with IGFN1. These results indicate that MLTK, IGFN1 and KY may be involved in the same pathway to regulate muscle hypertrophic responses or fibre type regulation.

### 1.5.5 More functions of MLTK:

MLTK can be activated by a variety of stressors including osmotic stress<sup>53,59,60</sup>, ionizing radiation<sup>61,62</sup>, ultraviolet radiation<sup>63</sup> and ribotoxic stress<sup>63,64</sup>. In cells, osmotic stress could activate the p38 MAPK pathway by activation of MLTK $\alpha$  and MLTK $\beta$  through autophosphorylation<sup>53,59,60</sup>. MLTK $\alpha$  was also found to respond to ionizing radiation-induced DNA damage checkpoints through two independent pathways: the p38 $\gamma$  pathway and the Chk2-Cdc25A pathway<sup>62</sup>.

MLTK proteins have been extensively studied in various kinds of cancers. MLTK $\alpha$  was found to be responsible for the induction of neoplastic cell transformation and tumorigenesis<sup>65</sup>. It plays as an effector of RhoC, controlling LPA-stimulated tumor cell invasion by regulation of myosin dynamics<sup>66</sup>. In addition, both MLTK $\alpha$  and MLTK $\beta$  play as key factors in cancer cell migration<sup>67</sup>. Additionally, MLTK is upregulated in some cancers, such as gastric tumours<sup>68</sup>, and downregulated in other cancers, such as hepatocellular carcinoma<sup>69</sup> and lung cancer<sup>70</sup>, which indicated MLTK may play different role in various cancers, possibly depending on tissue-specific interaction partners.

## 1.6 Aim of this thesis:

A previous study of IGFN1 illustrated that IGFN1 is an interaction partner of KY. The *ky* gene mutation leads to a dystrophic phenotype in mice and homozygous mutant mice fail to undergo hypertrophic responses to overloading. Moreover, the expression of IGFN1 closely relates to muscle hypertrophy and atrophy. In addition, IGFN1 contains the similar domain composition to other sarcomeric proteins and it located at nuclei and z-disc of skeletal muscle. Given that the z-disc experiences contractile forces directly, proteins at the z-disc are ideally placed to sense and respond to mechanical forces. All this evidence suggested that IGFN1 may play an important role in the regulation of hypertrophy/atrophy in skeletal muscle.

The Y2H of IGFN1 identified another interaction partner, MLTK. MLTK was found to be responsible for the induction of a hypertrophic response in cardiac muscle or cardiomyoblasts; MLTK is also upregulated in the *ky/ky* mouse. In addition, *Mltk* mutations cause phenotypes of myopathy showing some overlap with the *ky/ky* mouse, which indicated that MLTK is also

an important protein for regulation of skeletal muscle hypertrophy/atrophy. Taken together, the evidence indicates that MLTK, IGFN1 and KY may be involved in the same pathway to regulate muscle hypertrophic responses.

The aim of this thesis is to study the function of IGFN1 and MLTK in skeletal muscle. The main objectives of this study were to: -

- examine the subcellular localization of IGFN1 and MLTK by ectopic expression of fluorescence-labelled specific isoforms.
- identify the primary MLTK isoform in skeletal muscle by RT-PCR and western blot.
- identify the specific interactions between the two isoforms of IGFN1 and MLTK proteins.
- explore the function of IGFN1 and MLTK by *in vivo* overexpression and *in vitro* and *in vivo* knocking out IGFN1.

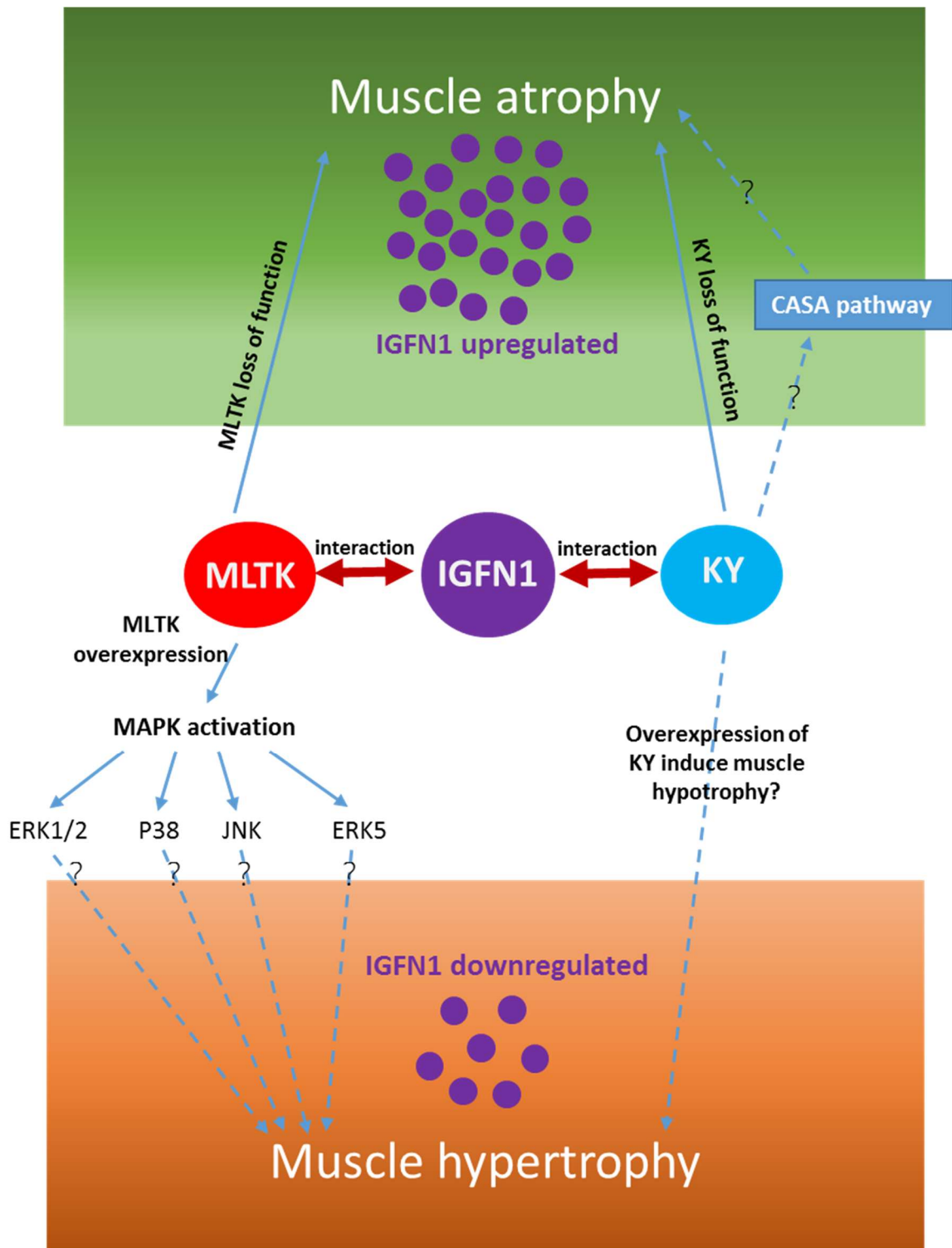


Figure 1.8: Signalling pathways possibly relate to MLTK, IGFN1 or KY.

# Chapter 2

## 2. Materials and methods

## 2.1 MATERIALS

### 2.1.1 General buffers

#### **TAE Buffer:**

- 1X Tris-acetate buffer (TAE) was prepared using 40 mM Tris (pH 7.6), 20 mM acetic acid and 1 mM EDTA.

#### **TE buffer:**

- 1X Tris-EDTA buffer (TE) was prepared using 10 mM Tris (pH 8 adjusted with HCl) and 1 mM EDTA

#### **9% formic acid:**

- 9% formic acid was prepared using 90 ml of formic acid and 910 ml ddH<sub>2</sub>O (double distilled water)

#### **PBS:**

- 1X phosphate buffered saline was prepared using 8 g NaCl, 0.2 g KCl, 1.44 g Na<sub>2</sub>HPO<sub>4</sub>, 0.24 g KH<sub>2</sub>PO<sub>4</sub>, adjusted the pH to 7.4 and topped up to 1 L with ddH<sub>2</sub>O.

#### **Mowiol medium:**

- 2.4 g of Mowiol 4-88, 6 g glycerol and 6 ml ddH<sub>2</sub>O were mixed for several hours at room temperature, before adding 12 ml of 0.2 M Tris-Cl (pH 8.5) and heating to 50 °C with occasional mixing until the Mowiol was fully dissolved. This was followed with

centrifugation at 5000 g for 15 minutes. 0.63g DABCO was added to reduce fluorescence fading. Aliquoted samples were stored at -20 °C.

#### **4% Paraformaldehyde (PFA):**

- To make 1 Litre of 4% PFA, 800 ml of PBS was added to a glass beaker and heated to ~60 °C with stirring in a ventilated hood. 40 g of PFA powder was added to the beaker. 1N NaOH was added dropwise until the solution cleared. The dissolved Paraformaldehyde was cooled, filtered, and topped up to 1 Litre with PBS. The final pH was adjusted with HCl. Aliquots of the solution were frozen for long term storage.

## **2.2 CELL STRAINS AND CULTURE**

### **2.2.1 Bacterial strains:**

For the expression of recombinant DNA plasmids, Subcloning Efficiency™ DH5α™ Competent Cells (Thermo Fisher) were used.

Genotype:

- F- Φ80lacZΔM15 Δ(lacZYA-argF) U169 recA1 endA1 hsdR17(rk-, mk+) phoA supE44 thi-1 gyrA96 relA1 λ-

For expression of Gateway recombinant DNA plasmid (Invitrogen), One Shot® Stbl3™ Chemically Competent *E. coli* (Thermo Fisher) were used.

Genotype:

- F-mcrB mrrhsdS20(rB-, mB-) recA13 supE44 ara-14 galK2 lacY1 proA2 rpsL20(StrR) xyl-5  $\lambda$ -leumtl-1

For propagating and maintaining Gateway® pcDNA™-DEST47 vectors, One Shot® ccdB Survival™ 2 T1R Chemically Competent Cells (Thermo Fisher) were used.

Genotype:

- F-mcrA  $\Delta$ (mrr-hsdRMS-mcrBC)  $\Phi$ 80lacZ $\Delta$ M15  $\Delta$ lacX74 recA1 ara $\Delta$ 139  $\Delta$ (ara-leu)7697 galU galK rpsL (StrR) endA1 nupG fhuA::IS2

### 2.2.2 Bacterial culture:

Lysogeny broth (LB) was used as media for bacterial growth (10 g NaCl, 10 g Tryptone, 5g yeast extract mixed in 1 litre ddH<sub>2</sub>O and then autoclaved), in which the appropriate antibiotic was added if required. Growth was performed in an incubator with shaking (200 rpm) at 37 °C for 16-20 hours.

1.5% (w/v) of agar was added to LB to generate solid LB agar plates for bacterial growth. LB plates were enriched with the appropriate antibiotic for selection of bacterial colonies expressing the target plasmid. The standard growth condition was 37 °C for 16-20 hours.

The antibiotics stocks were dissolved in autoclaved ddH<sub>2</sub>O, sterilized by passing through a 0.22 µm syringe filter (CORNING), aliquoted, and stored at -20 °C using the following stock concentrations:

- Ampicillin 100 mg/ml (1:1000 dilution for final concentration);
- Kanamycin 50 mg/ml (1:1000 dilution for final concentration).

Bacterial strains were preserved in sterilized 50% glycerol at -20 °C for frequent use and at -80 °C for long-term storage.

### 2.2.3 Mammalian cell lines:

The following cell lines were used in this work. All of them are adherent cell lines.

- COS7 is a kidney cell line from the African green monkey <sup>71</sup>.
- C2C12 is a mouse myoblast cell line from the thigh muscle of a C3H mouse strain <sup>72</sup>.
- 3T3 is a fibroblast cell line originally from Swiss albino mouse embryo tissue <sup>73</sup>.

### 2.2.4 Mammalian cell culture:

Mammalian cells were cultured in Dulbecco's Modified Eagle Medium (DMEM) (Life Technologies) supplemented with 10% Fetal Bovine Serum (FBS) (Life Technologies) and Penicillin-Streptomycin antibiotic solution (Life Technologies, final concentration is 100 units/mL of penicillin and 100 µg/mL of streptomycin) – this formulation is referred to as

growth medium in this thesis. Cells were normally seeded on T75, T25 or cell culture plates. Incubation was at 37 °C with 5% CO<sub>2</sub> until 80-90% confluent.

To subculture an adherent cell line, cells were rinsed with PBS, incubated with 0.25% trypsin-EDTA (Life Technologies) at 37 °C until cells detached from the growth surface, then re-plated at 5% confluence with growth medium.

For long term storage, trypsinized cells were centrifuged at 100 x g for 5-6 minutes to form a soft pellet, re-suspended in 10% DMSO/FBS (v/v) solutions and stored at -80 °C.

#### 2.2.5 C2C12 myotube differentiation:

To induce C2C12 myoblast fusion and myotube formation, C2C12 myoblasts were treated with differentiation medium (DMEM supplemented with 2% FBS and 1% Penicillin-Streptomycin antibiotic solution) when the cells confluence was higher than 90%. Subsequently, the differentiation medium was changed daily until the target time point.

#### 2.2.6 Cell transfection:

GenJet In Vitro DNA Transfection Reagent for C2C12 Cells (SignaGen Laboratories) was used to perform DNA transfection into C2C12 myoblasts. C2C12 cells were seeded in a flask or a cell culture dish depending on the purposes of the experiment (the cell culturing method is shown in section 2.2.4). When the cell density reached 80% confluence, cells were treated with 0.25% trypsin-EDTA to detach cells from the flask/culture dish (method is same as in

section 2.2.4), then detached cells were transfected by following the instructions provided with the reagent.

To perform DNA transfection into COS7 and 3T3 cells, the following reagents have been used and have shown good transfection efficiency:

- TurboFect™ Transfection Reagent (Thermo Scientific)
- Lipofectamine® LTX Reagent with PLUS™ Reagent (Invitrogen)
- PolyJet™ In Vitro DNA Transfection Reagent (SigmaGen Laboratories)

The transfections were undertaken following the manufacturer's instructions. The next day after transfection, the medium containing transfection reagent was changed to fresh pre-warmed growth medium. The following day the cells were washed twice with pre-warmed PBS and were then ready for immunofluorescence, protein extraction or other analyses.

### 2.2.7 Cell fixation:

Cells were washed with pre-warmed PBS, fixed with 4% PFA for 1 minute and washed with PBS and ddH<sub>2</sub>O respectively, then the cells are ready for antibody incubation steps. Some antibodies do not functionally interact with target proteins after 4% PFA fixation. In this case, the alternative method is to fix cells in ice-cold 100% methanol for 10 minutes at -20 °C, then replace methanol with ice-cold acetone for another 1 minute incubation at -20 °C. Compared to PFA fixation, methanol-acetone fixation can cause loss of integrity of intracellular structures in cells <sup>74</sup>, so the most commonly used method in this work is 4% PFA fixation.

### 2.2.8 Immunofluorescence on cells:

For immunofluorescence analysis on C2C12 myoblasts or myotubes, cells were grown or differentiated to the required time points and then fixed with 4% PFA as described in sections 2.2.4, 2.2.5 and section 2.2.7.

To label actin in C2C12 cells, fixed cells were incubated with Alexa Fluor 488<sup>®</sup> phalloidin (Life Technologies, 1:100 dilution) or Phalloidin-TRITC (P1951, Sigma, 1:100 dilution) for 30 minutes then washed twice with PBS.

To label  $\alpha$ -actin in the cells (antibody information on section 2.8.6), fixed cells were treated with 0.5% Triton X-100 in PBS for 1 minute to permeabilize the cells, then blocked in 4% bovine serum albumin (BSA,w/v)/PBS for 30 minutes, then incubated with Anti-Sarcomeric Alpha Actinin antibody [EA-53] (abcam, 1:150 dilution in 4% BSA/PBS) overnight at 4 °C. The next day, cells were washed three times with PBS (5-10 minutes per wash), then incubated with FITC conjugated secondary antibody (secondary information in section 2.8.7) in 4% BSA for 1 hour in darkness, afterwards, the cells were washed three times in PBS (5-10 minutes per wash).

For imaging, cells were mounted with either Vectormount (Vectorshield, containing DAPI) or Mowiol medium containing DAPI (for long-term storage). The images were captured using either a confocal microscope (Zeiss LSM 880 with Airyscan on an Axio Observer), or a fluorescence microscope (Microphot-FX Research Microscope).

## 2.2.9 Establishment of stable cell lines constitutively producing IGFN1-tdTomato or IGFN1\_V1-tdTomato

To generate a cell line stably expressing IGFN1 -tdTomato or IGFN1\_V1-tdTomato, C2C12 cells were seeded in 60 mm diameter cell culture dishes (Thermo Fisher Scientific) until 80% confluent. Both IGFN1-tdTomato- and IGFN1\_V1-tdTomato-containing plasmids were singly digested by PvuI restriction endonuclease (NEB), then transfected into C2C12 cells using GenJet In Vitro DNA Transfection Reagent for C2C12 Cells (SignaGen Laboratories) following the manufacturer's instructions. 24 hours after transfection, antibiotic G418 (Geneticin, Thermo Fisher Scientific, final concentration is 400 µg/ml) was added into the growth medium to select cells where the transposon containing the neomycin resistance gene was stably integrated into the genome. After 7 days under antibiotic selection, individual colonies were isolated, allowed to proliferate and examined under a fluorescence microscope to select colonies expressing tdTomato recombinant proteins.

## 2.3 Establishment of IGFN1 knockout cell lines

### 2.3.1 Mismatch cleavage assay

The targeting efficiency of the IGFN1 CRISPR/Cas vector (GeneCopoeia Inc ) was tested using a mismatch cleavage assay. 3T3 cells were grown in a T25 flask to ~90% confluency before transfection. 12 µg of IGFN1 CRISPR/Cas plasmid was transfected into 3T3 cells using GenJet in vitro DNA transfection reagent. Cells were harvested after 48 hours post- transfection. Genomic DNA was extracted from transfected 3T3 cells using GenElute™ Mammalian

Genomic DNA Miniprep Kit (Sigma, details in section 2.6.6). The IGFN1 CRISPR/Cas targeted region was amplified by PCR using the following primers (PCR method shown in section 2.6.1):

forward primer      CGGGCAGCTGATAAGTGTTA  
reverse primer      TGTGGGCAGAGGCATGTCATA

The PCR products were subjected to DNA re-hybridization followed by T7 endonuclease I (NEB) digestion. The results were checked on a 2% (w/vol) agarose gel (DNA gel electrophoresis methods show in section 2.6.3).

### 2.3.2 Establishment of IGFN1 knockout C2C12 cell lines

C2C12 cells were grown in 60 mm diameter cell culture dishes (Thermo Fisher Scientific) to 80-90% confluence. The cells were subsequently co-transfected with IGFN1 CRISPR/Cas and homologous recombination donor plasmids (GeneCopoeia Inc) using GenJet In Vitro DNA Transfection Reagent for C2C12 Cells (SignaGen Laboratories, transfection methods show in section 2.2.6) 48 hours after transfection, puromycin was added into the growth medium to select for colonies expressing the homologous recombination cassette for 7 days. Clonal selection by dilution was undertaken to generate colonies from single cells. To test whether the homologous recombination template was inserted into the right place, forward primers were placed on the *igfn1* genomic sequence before the homologous recombination arm1 (or after arm2) and the reverse primers were placed within the homologous recombination cassette (figure 7.2A; primers named as *igfn1* KO primer pair 1 and *igfn1* KO primer pair 2, the sequences are shown in section 2.6.1). To test whether the non-homologous end joining pathway generated random insertions or deletion around the CRISPR/Cas targeted sequence, a PCR forward primer was designed on homologous arm1 and reverse primer was selected on homologous arm2 (figure 7.2B; primers named as *igfn1* KO sequencing primer forward 3

and igfn1 KO sequencing primer reverse 3, the sequences were showed in section 2.6.1). All the PCR products were sent out for sequencing by LIGHTRUN™ Sequencing Service (GATC Biotech).

## 2.4 RT-PCR

### 2.4.1 RT–PCR testing MLTK $\alpha$ and MLTK $\beta$ endogenous expression levels in skeletal muscle

To detect the expression of endogenous MLTK $\alpha$  and MLTK $\beta$  transcripts in mouse skeletal muscle, total RNA was extracted from mouse hind limb muscle using TRIzol (Life Technologies), and cDNA was converted from mRNA using reverse transcriptase (QIAGEN). The cDNA concentration of each sample was measured, diluted to the same concentration and mixed with primers and SYBR Green Master Mix (Applied Biosystems) to form RT-PCR reactions on an optical 96 well plate. The primers for MLTK $\alpha$ , MLTK $\beta$  and housekeeping gene hypoxanthine-guanine phosphoribosyl transferase (HPRT) were as follows:

name of Primer	sequence
RT-PCR MLTK $\alpha$ -Forward	CATCGTCTCCAAGGGACACA
RT-PCR MLTK $\alpha$ -Reverse	GGTCCCCTCCTGAATCCTTA
RT-PCR MLTK $\beta$ -Forward	ACGTCTCAAGATGTGGGAGC
RT-PCR MLTK $\beta$ -Reverse	TGCACTGTTTGACTCCTCTGT
RT-PCR HPRT-Forward	GTTGGATACAGGCCAGACTTTGTTG
RT-PCR HPRT-Reverse	GATTCAACTTGCGCTCATCTTAGGC

Each reaction was performed in triplicate and plates were run and analysed on the StepOnePlus machines (Applied Biosciences) using a Fast PCR protocol.

## 2.4.2 RT-PCR confirm *Igfn1* gene knocking out in C2C12 cells

To detect the expression of endogenous *Igfn1* in C2C12 and *Igfn1* KO cell lines, mRNA was extracted from C2C12 myoblasts using GenElute DIRECT mRNA MINIPREP KIT (SIGMA), and the cDNA was converted from mRNA by Reverse transcriptase (QIAGEN) as in the previous section 2.4.1. The method and reagents used to perform RT-PCR are same as previous section 2.4.1. The reactions for *Igfn1* were carried out using the following primer sets:

name of Primer	Sequence
RT-PCR IGFN1-Forward	GGTATCGTCGACTTCCGGG
RT-PCR IGFN1-Reverse	GTCAAACGTAGCGACCCCT
RT-PCR HPRT-Forward	GTTGGATACAGGCCAGACTTTGTTG
RT-PCR HPRT-Reverse	GATTCAACTTGCGCTCATCTTAGGC

## 2.5 ELECTROPORATION AND MUSCLE SAMPLE PREPARATION

### 2.5.1 Transfection into skeletal muscle using *in vivo* electroporation

One hour before the electroporation procedure, mice were injected with 10  $\mu$ l of 0.4 U/ $\mu$ l hyaluronidase (in 0.9% saline). DNA was diluted to 800-1000 ng/ $\mu$ l in ddH<sub>2</sub>O, then 10  $\mu$ l of DNA samples were loaded into a sterile syringe. Mice were placed in an anesthetizing box with 4% isoflurane in O<sub>2</sub> supplied by an approved gas anaesthetic machine until deeply anaesthetised. Mice were then removed to a heating pad (37 °C) and continually anesthetized with a rodent face mask. Toe pinch reflex was used to test the anaesthetic depth. To reduce

the damage to the mouse, the DNA injections were performed through the skin, without exposing the muscle by anterior incision. Because extensor digitorum longus/ tibialis anterior (EDL/TA) muscle are physically confined within the hind limb and easy to access, all the injections were performed in these two muscle. Then electrodes were placed into to the same region as the injection site. The electrodes delivered 20 pulses, 20 ms in duration/each, at 1 Hz. The electroporated mice were returned to their cages and observed for recovery before being sent back to the animal room.

Note: All animal procedures strictly followed the Animals (Scientific Procedures) Act 1986 Amendment Regulations 2012. Procedures were performed by a competent person holding the appropriate personal and project licences for these protocols. (Project licence: 70/7855)

### 2.5.2 Skeletal muscle sample preparation and fixation

Mice were sacrificed at 7 days or longer after the electroporation by following the methods permitted by the Home Office (The Humane Killing of Animals under Schedule 1 to the Animals). The EDL/TA muscles were dissected out from the mouse, briefly fixed in PFA and snap frozen in liquid nitrogen-cooled isopentane prior to cryostat sectioning. For DNA or protein extraction, the dissected muscles were snap frozen in liquid nitrogen. The muscle samples were stored at -80 °C.

### 2.5.3 Embedding tissues into Wax

The muscle samples shipped from Tufts University School of Medicine were preserved in 10% formaline. Once the samples were received, 10% formaline was replaced with 70% ethanol and the samples were stored at 4 °C. To perform whole hind limb cross sections, muscle samples were decalcified in 9% formic acid to soften the bones overnight. The following morning decalcification was checked by bending the bones; if the bones can be bent, the decalcification is completed. Then muscle samples were washed in water twice for 10 minutes each to remove residual acid, which may contaminate the processing reagents. For muscle sample dehydration, samples were cross cut into pieces, which can fit into the embedding cassette and submerged in fresh 90% ethanol in a glass beaker for 2 hours with shaking, then the 90% ethanol was replaced with fresh absolute ethanol and samples were incubated for a further 2 hour with shaking. To remove alcohol and any remaining water from the muscle samples, samples were incubated twice with fresh xylene for 2 hours each in a safety cabinet with shaking. As much of the excess xylene as possible was removed from the samples by placing the cassettes on absorbent paper (without allowing the muscle samples to dry out) and quickly transferring the cassettes into a pot of molten wax (pre-warmed at 65 °C to melt the wax, any higher than 65 °C could possibly damage the wax) followed by incubation at 60 °C overnight. The next morning, cassettes were transferred twice into a new wax pot for 30mins incubation at 65 °C. To embed the samples in the wax, a hot plate and cool plate were prepared 1 hour before this process. The metal cassettes were placed on the cool plate and then samples were transferred from the plastic cassettes to the metal cassettes in the desired orientation. The metal cassette was then filled with melted wax and left to set on the cold

plate at -12 °C. Once the wax blocks were set, they were removed from the metal cassettes and ready for sectioning.

#### 2.5.4 Hematoxylin and eosin stain (H & E)

To perform H&E staining in fresh frozen muscle tissue, muscles were first sectioned by cryostat machine and the slides were kept at room temperature until dry. After that, samples were incubated in acetone for 5 seconds followed by air drying for 5 seconds. Sections were then incubated in Gill's Hematoxylin for 1 minute and subsequently washed gently on the back of the slides with running water until the water ran clear. The back of the slides were dried with tissue to remove the excess water. Afterwards, sections were incubated in eosin for 10 seconds then washed 6 times in 100% ethanol (20 seconds each with gentle shaking). Afterwards, slides were washed in Histo-Clear (National Diagnostics), mounted with DPX mounting medium (Fisher Scientific) and a cover-slip. Slides were kept under a heavy weight for 10 minutes to prevent the formation of air bubbles.

To perform H&E staining in wax-embedded muscle tissue, muscles were sectioned using a microtome. The sections were de-waxed in xylene twice for 10 minutes, rehydrated in 100% ethanol twice for 10 minutes, 90% ethanol for 5 minutes, 70% ethanol for 5 minutes and final wash with ddH<sub>2</sub>O for 2 minutes. After that, the slides were incubated in Gill's Hematoxylin for 1 minute. The remainder of the protocol is the same as the previous H&E staining methods for fresh frozen muscle tissue.

## 2.6 MOLECULAR TECHNIQUES

### 2.6.1 Polymerase chain reaction (PCR)

The GoTaq® Green Master Mix (Promega) was used to amplify PCR products less than 1000 bp long throughout the course of this project. The primers were designed using the primer-blast programme (<http://www.ncbi.nlm.nih.gov/tools/primer-blast/>) and the sequences are listed below:

name of Primer	Sequence
<i>igfn1</i> KO sequencing primer forward 1	TGCTCATGTGCCTAGCATGT
<i>igfn1</i> KO sequencing primer reverse 1	CAGATCGTACCAAGGGCGAA
<i>igfn1</i> KO sequencing primer forward 2	AGGAACGAAGTCCCTAAAGAAACA
<i>igfn1</i> KO sequencing primer reverse 2	CTAAGAGGTGTTCCACTCCCAA
<i>igfn1</i> KO sequencing primer forward 3	CGGGCAGCTGATAAGTGTTA
<i>igfn1</i> KO sequencing primer reverse 3	TGTGGGCAGAGGCATGTCATA
tdTomato-forward	ATCTAGAATGGCTAGCGTGAGCAAGGGCGAGGAG
tdTomato-reverse	CGTTGGGATCTTTCGAATTACTTGTACAGCTCGTCCATGC

PCR was performed using the following standard method and programme (MJ Research PTC-200 Thermal Cycler):

Componet	50 µL rxn	Final conc
GoTaq® Green Master Mix, 2X	25 µL	1x
Forward primer (10 µM)	X µL	0.1–1.0 µM
Reverse primer (10 µM)	X µL	0.1–1.0 µM
Template DNA	1 µL	<250ng
H <sub>2</sub> O	add to 50 µL	

Cycle step	Temp.	time	Cycles
Initial Denaturation	94-95 °C	2 mins	1

Denaturation	94-95 °C	10 s	
Annealing	60-67 °C	15 s	30-35
Extension	72 °C	1 min per kb	
Final extension	72 °C	1 min	1

The Phusion High-Fidelity DNA Polymerase (Thermo Fisher Scientific) was used for PCR amplification MLTK $\alpha$  and MLTK $\beta$  from mouse cDNA library following manufacturer's instructions. The PCR primers were designed by the primer-blast programme (<http://www.ncbi.nlm.nih.gov/tools/primer-blast/>) based on the published sequence from Ensembl databases (<http://www.ensembl.org>). To ligate PCR products into pENTR/TEV/D-TOPO vector, CACC sequence were added on the 5' end of the forward primers. the primer sequences are listed below:

name of Primer	Sequence
MLTK $\alpha$ forward primer	CACCGCCAGATTTTGTGGACGTTT
MLTK $\alpha$ reverse primer	GGCCGAAAGTTGCCTGTGTGTC
MLTK $\beta$ forward primer	CACCGCCAGATTTTGTGGACGTTT
MLTK $\beta$ reverse primer	ATCCACATCATTCTCAGCATCG

The PCR using the following standard method and programme (MJ Research PTC-200 Thermal Cycler):

Componet	50 $\mu$ L rxn	Final conc
	add to 50	
H <sub>2</sub> O	$\mu$ L	
5x Phusion GC buffer	10 $\mu$ L	1X
2 mM dNTPs	5 $\mu$ L	200 $\mu$ M each
Forward primer (2 $\mu$ M)	12.5 $\mu$ L	0.5 $\mu$ M
Reverse primer (2 $\mu$ M)	12.5 $\mu$ L	0.5 $\mu$ M
Template DNA	1 $\mu$ L	
DMSO	1.5 $\mu$ L	3%
Phusion DNA Polymerase	0.5 $\mu$ L	0.02 U/ $\mu$ L

Cycle step	Temp.	time	Cycles
Initial Denaturation	98 °C	2 mins	1
Denaturation	98 °C	10 s	
Annealing	55 °C	20 s	30
Extension	72 °C	30-40 s per kb	
Final extension	72 °C	10 mins	1

### 2.6.2 Purification of PCR products

To perform downstream analysis, such as sequencing, ligation, restriction enzyme digestion and so on, PCR products were purified using a PCR Purification Kit (Qiagen) to remove unwanted enzymes, primers, nucleotides and salts following the manufacturer's instructions. The purified samples were eluted in 30µl ddH<sub>2</sub>O.

### 2.6.3 Agarose gel electrophoresis

All PCR results were first analysed by agarose gel electrophoresis. For detection of PCR products larger than 1000 bp, the agarose percentage (W/V) of the gel was 1%. 2% gels were used to resolve DNA products less than 1000 bp. Gels were supplemented with ethidium bromide dye (1:10000 dilution) to allow DNA visualisation. Reactions performed using GoTaq® Green Master Mix already contained loading dye and could therefore be loaded directly onto the gel. Other DNA samples were mixed with DNA Orange G before loading onto the gel. 1 kb or 100 bp DNA ladders (NEB) were used as DNA size markers. Gels were run in

1xTAE buffer at 80v until the dye front was approximately 70% of the way down the gel and analysed using a Gel Doc 2000 UV transilluminator system (Bio-Rad).

#### 2.6.4 Gel extraction of DNA

To extract DNA from resolved bands on an agarose gel, gels were placed on a UV transilluminator box after gel electrophoresis. The target bands were excised and transferred into a 2ml eppendorf. DNA was extracted from the gel using a QIAquick Gel Extraction Kit (QIAGEN) following the manufacturer's instructions.

#### 2.6.5 Sequencing of DNA

All the sequencing work during this project was performed using LIGHTRUN™ sequencing service (GATC Biotech). The samples were diluted and mixed with sequencing primer following the service provider's instructions.

#### 2.6.6 Preparation of DNA from mammalian cells

Cells were grown in a T25 flask until approximately 80-90% confluence, harvested by trypsinization and centrifuged at 100 x g for 5-6 minutes to form a soft pellet (cell culture protocols are shown in section 2.2.4). The DNA from the pellet was extracted using a GenElute™ Mammalian Genomic DNA Miniprep Kit (Sigma) following the manufacturer's instructions.

### 2.6.7 Preparation of DNA from muscle

To isolate genomic DNA from mouse skeletal muscle, flash frozen muscle was ground in liquid nitrogen and re-suspended in Digestion Solution from GeneJET Genomic DNA Purification Kit (Thermo scientific). The extraction process followed the instructions provided by manufacturer.

## 2.7 CLONING

### 2.7.1 Ligations into pENTR/D-TOPO Entry Gateway vector (Invitrogen)

PCR amplicons from *mtk $\alpha$*  and *mtk $\beta$*  were cloned into the pENTR/D-TOPO vector following manufacturer's instructions (pENTR™ /D-TOPO® Cloning Kits, Life Technologies).

### 2.7.2 TdTomato replacement of cycle 3 GFP in pcDNA™-DEST47 Vector

TdTomato DNA sequence was amplified from pRSET-B tdTomato plasmid, the NheI and BstBI restriction enzyme digestion sequences were added at 5' and 3' end of tdTomato sequence by PCR (the primer sequence and PCR information are shown in section 2.6.1). Both tdTomato and pcDNA™-DEST47 Vector (Life Technologies) were digested by NheI and BstBI restriction enzymes and ligated together to form a new vector, termed as pcDNA-DEST-tdTomato, by T4 DNA Ligase (NEB) at 16 °C overnight. After that, the ligation products were transformed into competent cells (details in section 2.2.1 and 2.7.4), then plated on LB agar with appropriate

antibiotic and incubated at 37 °C overnight. The following morning, bacterial clones were picked randomly and screened by PCR amplification (details in section 2.6.1) and restriction enzyme digestion to identify correct ligations (details in 2.7.7).

### 2.7.3 Gateway cloning

To convert DNA from pENTR/D-TOPO vector (entry vector) to Gateway destination vectors, 300ng of entry clone was mixed with 150 ng destination vector, 4µl of 5X LR Clonase Reaction Buffer (Gateway® LR Clonase® Enzyme Mix, Life Technologies), and made up to 16 µl with TE buffer, then 4µl of LR Clonase enzyme mix (Gateway® LR Clonase® Enzyme Mix, Life Technologies) was added into the reaction and incubated at room temperature for 60 minutes. To stop the reaction, 2µl of Proteinase K solution was added to the reaction and incubated at 37 °C for 10 minutes. After this, the reaction was ready for transformation into chemically competent cells (The details of competent cells are listed in section 2.2.1 and 2.7.4) before being plated on LB agar with appropriate antibiotic and incubated at 37 °C overnight. The following morning, the clones were picked randomly and checked by PCR amplification (details in section 2.6.1) and restriction enzyme digestion (details in 2.7.7).

### 2.7.4 Transformation of chemically competent cells

Plasmid DNA was mixed with competent cells on ice for 30 minutes, then cells were heat-shocked at 42 °C for exactly 30 seconds, followed by 2 minutes incubation on ice. To allow

cells to recover and begin expression of the relevant selective marker, 450 µl of S.O.C. (Super Optimal Broth) medium was added into the cells followed by incubation at 37 °C for 1 hour with shaking. Cells were pelleted by centrifugation at 5000 x g for 1 minute, re-suspended in ~100 µl of S.O.C. medium, plated onto selective plates and incubated at 37 °C overnight. The following day, single colonies on the selective plates were selected and grown in 5ml LB medium for further analysis.

### 2.7.5 Plasmid preparation from bacterial cultures

For mini-preparations, 5ml bacterial cultures grown overnight at 37 °C with shaking were pelleted at 13000 x g for 5 minutes. The plasmid extraction was performed using Wizard® Plus SV Minipreps DNA Purification System (Promega) or QIAprep Spin Miniprep Kit (Qiagen) following the manufacturer's instructions.

A PowerPrep HP Plasmid Maxiprep Kit (Origene) was used to produce higher yields of plasmids (more than 200µg per purification). 200-300ml bacterial cultures were pelleted at 13000 x g for 5 minute after overnight incubation at 37 °C with shaking. Plasmid extractions were performed following the manufacturer's instructions.

### 2.7.6 DNA quantification

DNA concentration and quality were tested using a NanoDrop 1000 Spectrophotometer (Thermo Fisher Scientific)

### 2.7.7 Restriction digests

All the restriction enzymes used in this projects were provided by New England Biolabs (NEB). The reactions were set up following the instructions provided on the NEB website. The digestion products were analysed by agarose gel electrophoresis (details of agarose gel electrophoresis are found in section 2.6.3).

## 2.8 PROTEIN ANALYSIS:

### 2.8.1 Protein sample preparation from cells:

To prepare protein lysate from C2C12 or COS7 cells, cells in a T75 flask at 80% confluence were washed twice with PBS and then lysed with 500  $\mu$ l of RIPA buffer (Sigma, contains 10 mM Tris-Cl (pH 8.0), 1 mM EDTA, 0.5 mM EGTA, 1% Triton X-100, 0.1% sodium deoxycholate, 0.1% SDS, 140 mM NaCl and 1 mM PMSF) enriched with protease inhibitor (PI, Roche). Lysates were treated with three cycles of freeze/thaw and centrifuged at 13,000 g for 15 minutes at 4 °C. The protein concentration was determined by the Bradford assay (section 2.8.3).

### 2.8.2 Protein sample preparation from muscle

To prepare protein lysate from muscle tissue, mice were sacrificed and the skeletal muscle from the hind limbs were dissected. The muscle was ground in liquid nitrogen and re-suspended in RIPA buffer/PI followed by three cycles of freeze/thaw. The muscle lysates were

centrifuged at 13,000 g for 15 minutes at 4 °C, the supernatants were collected and the total protein concentration was measured by the Bradford assay (section 2.8.3).

### 2.8.3 Bradford assay

To produce a protein standard curve, bovine serum albumin (BSA) was diluted in a 20% RIPA/PI solution (v/v in H<sub>2</sub>O) to following concentrations: 0 mg/ml, 0.2 mg/ml, 0.4 mg/ml, 0.6 mg/ml, 0.8 mg/ml and 1 mg/ml. 1 µl of protein samples were diluted in 4 µl of H<sub>2</sub>O, and then mix with 45 µl of 20% of RIPA/PI to achieve 50x dilution of protein samples. The dilution of the RIPA buffer solution was necessary to bring the detergent levels within the tolerable range for the Bradford reagent. 10 µl of diluted protein samples or protein standards were mixed with 200 µl of Bradford reagent (Sigma); loaded into 96-well Plate (Fisher Scientific) and measured with MRX Microplate Reader (DYNEX). All the samples were measured in triplicate; the results were calculated from the average of the measurements.

### 2.8.4 SDS-PAGE

To perform sodium dodecyl sulfate polyacrylamide gel electrophoresis (SDS-PAGE), protein samples were pre-mixed with NuPAGE 4x LDS sample buffer and 10x sample reducing agent (Invitrogen) and other reagents following the manufacturer's instructions. Samples were denatured at 70 °C for 10 minutes before loading onto either NuPAGE® Novex® 3–8% Tris-Acetate Gel (Invitrogen, to separate large molecular weight proteins) or NuPAGE® Novex® 4–12% Bis-Tris Gel (Life Technologies) based on the molecular weight of the target protein. The gels were run using either 1x NuPAGE® Tris-Acetate SDS Running Buffer (Invitrogen, for Tris-Acetate gels) or 1x NuPAGE® MOPS SDS Running Buffer (Invitrogen, for Bis-Tris gels) in an

XCell SureLock™ Mini-Cell Electrophoresis System (Invitrogen) at 100 v for approximately 1 hour.

### 2.8.5 Western blotting

Protein transfer from the resolved gel to a nitrocellulose membrane was performed using iBlot® Gel Transfer Device (Invitrogen) with iBlot® Transfer Stacks (Invitrogen, nitrocellulose membrane). To test the transfer efficiency, 2ml Ponceau S solution (Sigma) was added on membrane and incubated for 5 minutes, then washed with running water to visualize protein bands. The membrane was blocked in 5% milk/PBST solution (5g of Marvel Dried Skimmed Milk Powder in 100 ml PBS, 0.1% Tween20 (Fisher Biotech) in PBS) for 1 hour with shaking at room temperature. Primary antibodies were diluted in 5% milk/PBS solution and incubated on the membrane overnight at 4 °C on an orbital shaker. On the following day, Membranes were washed three times with 0.2% Tween20/PBS solution for 10 minutes each, incubated with HRP conjugated species specific secondary antibodies (diluted in 5% milk/PBS solution) for 1 hour at room temperature on an orbital shaker, and then washed with 0.2% Tween20/PBS solution. ECL Western Blotting Detection Reagent (GE Healthcare) was added to the membrane and Hyperfilm ECL (GE Healthcare) was used to visualize the peroxidase activity. Film was processed and fixed using an Xograph.

## 2.8.6 Primary antibodies

The following primary antibodies were used in this work:

Primary antibodies	WB dilution	IF dilution	Company	Host Species/Clonality/Isotype
Anti-Sarcomeric $\alpha$ -actinin antibody [EA-53] (ab9465)	-	1:150	Abcam	mouse monoclonal IgG ( IgG1)
mouse monoclonal anti-V5 antibody (R960-25)	1:5000	-	Invitrogen	mouse monoclonal IgG ( IgG2a)
Anti-GFP (11814460001)	1:1000	-	Roche	mouse monoclonal IgG ( IgG1 $\kappa$ )
Anti-His Antibody (27-4710-01)	1:3000	-	GE Healthcare	mouse monoclonal IgG ( IgG2)
Anti-desmin (D76)		2-5 $\mu$ g/ml	DSHB	mouse monoclonal IgG ( IgG1)
Anti-Myosin Heavy Chain Type IIB (BF-F3)	-	2-5 $\mu$ g/ml	DSHB	mouse monoclonal IgM
Anti-Myosin Heavy Chain Type IIA (SC-71)		2-5 $\mu$ g/ml	DSHB	mouse monoclonal IgG ( IgG1)
Anti-Myosin heavy chain (A4.840 slow fibers)		2-5 $\mu$ g/ml	DSHB	mouse monoclonal IgM
Anti-MLTK Rabbit polyclonal antibody (14945-1-ap)	1:5000	1:100	PROTEINTECH EUROPE	rabbit polyclonal IgG
Anti-RFP ( 600-401-379)	1:5000	-	Rockland	rabbit polyclonal IgG

## 2.8.7 Secondary antibodies

The following secondary antibodies were used in this work:

Secondary antibodies	WB dilution	IF dilution	Company
goat anti-mouse IgG (whole molecule)-FITC conjugate (F9006)	-	1:150	SIGMA-ALDRICH
goat anti-rabbit IgG (whole molecule)-FITC conjugate (F6005)	-	1:150	SIGMA-ALDRICH
goat anti-rabbit IgG (whole molecule)-HRP (A8275)	1:10 000	-	SIGMA-ALDRICH
goat anti-mouse IgG (whole molecule)-HRP (A4416)	1:10 000		SIGMA-ALDRICH
Phalloidin-TRITC (P1951)	-	50 ug/ml final concentration	SIGMA-ALDRICH
Alexa Fluor 488® phalloidin	-	1:100	Life technologies
anti-mouse IgM-FITC (F9259)		1:150	SIGMA-ALDRICH

## 2.8.8 Stripping of western blot membrane using restore plus reagent

To remove antibodies from the membrane, a sufficient volume of Restore Western Blot Stripping Buffer (Thermo Scientific) was added to cover the membrane followed by incubation for 5 to 15 minutes at 37 °C. The membrane was washed in PBS, re-blocked in 5% milk/PBS solution and re-used for further analysis.

## 2.9 Identification of interactions between IGFN1 and MLTK

### 2.9.1 Immunoprecipitation

IGFN1-v5 or IGFN1\_V1-v5 was co-expressed with either MLTK $\alpha$ -GFP or MLTK $\beta$ -tdTomato in COS7 cells (the details of transfection protocols are in section 2.2.6). The co-transfected cells were incubated in RIPA buffer (Sigma) to lyse the cells and prepare protein lysate (details shown in section 2.8.1).

The concentration of total protein in the lysate was measured with Bradford assay (section 2.8.3). To confirm expression of target protein, cell lysates were tested by WB using antibodies against v5 and GFP (WB methods as section 2.8.5). Samples were precleared in 20 $\mu$ l of the mouse IgG Agarose (Sigma) with 1 hour rotating incubation at 4 °C, and centrifuged at 2000g for 3 minutes then split into two aliquots. one aliquot was incubated with 40 $\mu$ l Anti-V5 Agarose Affinity Gel (antibody produced in mouse, Sigma), and the second aliquot was incubated with mouse IgG Agarose (Sigma, containing the same amount of agarose beads as Anti-V5 Agarose Affinity Gel) as negative control. Both aliquots were incubated overnight with rotation at 4 °C. the following morning, samples were centrifuged at 2000g for 3 minutes. supernatants were removed and saved for further analysis. The agarose beads were washed 4 times with 1 ml PBS and centrifuged to remove the PBS. After the final wash, agarose beads were incubated with 40 $\mu$ l of SDS running buffer at 75 °C for 10 minutes, then the supernatants were loaded into NuPAGE<sup>®</sup> Novex 3-8% Tris-Acetate, 1.0 mm, 10 well gels (Invitrogen) and analysed by WB (details of SDS-PAGE shown in section 2.8.4, and the details of WB shown in section 2.8.5). Anti-GFP primary antibody (Roche, details in section 2.8.6) was applied to detect the presence of MLTK $\alpha$ -GFP or MLTK $\beta$ -GFP. The anti-V5 primary antibody (Invitrogen,

details in section 2.8.6) was applied to confirmed V5-tagged protein binding to the Anti-V5 Agarose Affinity Gel.

### 2.9.2 Pull down of COS7-produced MLTK-GFP by *E.coli*-produced IGFN1-His (from Matthew Winder, placement student)

His-tagged IGFN1\_V1, IGFN1<sub>(d1-d3)</sub>, IGFN1<sub>(d8-d11)</sub> and LacZ were produced by expression of pET161-DESTIgf1\_v1, pET161-DESTIgf1(d1-d3), pET161-DESTIgf1(d8-d11) plasmids in *E.coli* and affinity purified by Ni-NTA agarose beads (Life Technologies). MLTK $\alpha$ -GFP and MLTK $\beta$ -GFP were produced from COS7 cells by transfection the cells with pcDNA-DEST47-MLTK $\alpha$  or pcDNA-DEST47-MLTK $\beta$ , then transfected cells were incubated in RIPA buffer to prepare protein lysate (details shown in section 2.8.1). For the pull-down assay, the his-tagged IGFN1\_V1, IGFN1<sub>(d1-d3)</sub>, IGFN1<sub>(d8-d11)</sub> and LacZ bounded Ni-NTA agarose beads were blocked in 500ul of blocking buffer ( 20 mM HEPES, pH7.4; 300 mM NaCl, 0.05% NP-40, 10% glycerol and 3% BSA) with rotating overnight at 4 °C. Cell lysates containing MLTK $\alpha$ -GFP or MLTK $\beta$ -GFP were pre-cleared with 1  $\mu$ g of LacZ bound Ni-NTA agarose beads in the presence of 500 $\mu$ l binding buffer (20 mM HEPES, pH7.4; 300 mM NaCl; 0.05% NP-40; 10% glycerol and 1% BSA). Then the precleared samples were split into aliquots, incubated with either immobilised his-IGFN1\_v1, his-IGFN1(d1-d3), his-IGFN1(d8-d11) or his- LacZ for 1 hour at 4 °C with rotating. The beads were subsequently washed three times with Native Wash Buffer (20 mM imidazole; pH 8.0). 5 $\mu$ l of beads were used for SDS-PAGE analysis and stained with Coomassie Brilliant Blue to test the His-tagged protein binding efficiency to the Ni-NTA agarose beads. WB was used to analyse the pull-down assay. Anti-GFP antibody (Roche, details in section 2.8.6.) was

used to detect the presence of MLTK $\alpha$ -GFP or MLTK $\beta$ -GFP. The successful pull-down experiments showed the GFP conjugated MLTK $\alpha$  or MLTK $\beta$  on the blot.

## 2.10 Statistics

All the t-tests were performed after normality tests using D' Agostino's test. Data which did not pass the normality test was log-transformed then re-tested for normality. Normally distributed data was analysed using either paired or un-paired t-tests. Two types of unpaired t-test were used in this thesis - one was used to test for significant differences between two samples assuming equal variance, another one used to test for significant differences between two samples assuming unequal variance. The equal variance test was performed by F-test. Non-normally distributed data were analysed using either Wilcoxon signed-rank tests (paired data) or Mann-Whitney tests (unpaired data). To analyse the difference among three or more samples, single factor ANOVA was used in normally distributed data, and Kruskal-Wallis H testing was used in non-normally distributed data. Single factor ANOVA tests were followed by post hoc tests to analyse the differences between samples, in which Tukey's honestly significant difference (HSD) post hoc test was used to analyse data containing homogeneity of variances, whereas the Games Howell post hoc test was used to analyse data not containing homogeneity of variances.

## 2.11 Co-localization analysis

To prepare whole-mount immunostaining, muscle samples were dissected into small pieces along the muscle fibres and fixed with 4% PFA for 30 mins, followed with permeabilisation

with 0.5% Triton X-100 for 10 minutes. To stain the Z-disc, muscle samples were blocked in 4% bovine serum albumin (BSA, w/v)/PBS for at least 30 minutes, then incubated with Anti-Sarcomeric Alpha Actinin antibody [EA-53] (abcam, 1:150 dilutions in 4% BSA/PBS) overnight at 4 °C. The next day, muscles were washed three times with PBS (10 mins per wash), then incubated with FITC conjugated secondary antibody (see section 2.8.7) in 4% BSA for 3 hours in darkness. Afterwards, muscles were washed three times in PBS (10 mins per wash). The immunostained muscles were placed on a glass slide and mounted with Mowiol medium (section 2.1.1 General buffers), then covered with a coverslip, gently pressing the coverslip to flatten the muscle samples. All the images used for co-localization analysis were captured objectively using a confocal microscope with either a 60X or 40X oil immersion objective lens. The co-localization analysis was performed by imageJ software (Fiji version), the mean value of Mander's Colocalization coefficients were calculated from at least 2 images (the number of images used in each experiment is indicated in the results).

# Chapter 3

## RESULTS

3. Ectopic expression of IGFN1 and MLTK isoforms *in vitro* and *in vivo*: subcellular localizations

### 3.1 INTRODUCTION

The protein KY is essential to maintain postural muscles and underlies a unique type of muscular dystrophy. Mutations in the *ky* gene lead to muscular dystrophy and prominent spinal deformity in mice and humans<sup>1-3</sup>. In the mouse model, the homozygous mutant (*ky/ky*) muscles are much weaker, smaller and slower-contracting than muscles from control mice<sup>43</sup>. However, the typical features of muscular dystrophy only appear in slow-contracting skeletal muscle<sup>41</sup>. Moreover, the expected hypertrophy of normal muscles in response to the application of increased mechanical loading does not occur in *ky/ky* mice<sup>1</sup>.

A yeast two-hybrid screen (Y2H) identified IGFN1 (immunoglobulin-like and fibronectin type 3 domain containing 1) as interacting partner with the KY protein<sup>42</sup>. *Igfn1* mRNA transcripts are present in skeletal muscle, heart and lung<sup>4</sup>. The *Igfn1* gene is located on mouse chromosome 1, and encodes at least four isoforms: IGFN1, IGFN1\_V1, IGFN1-V2 and IGFN1-V3. Both IGFN1 and IGFN1\_V1 contain 11 globular domains, but only IGFN1 has an unstructured region between the 3<sup>rd</sup> and 4<sup>th</sup> globular domains<sup>4</sup> (Figure 1.5).

In mouse skeletal muscle, IGFN1 was detected in both the nucleus and the Z-disc by two different antibodies, Ab-US42 (against the N-terminus of IGFN1) and Ab-Kip2b (against the C-terminus of IGFN1)<sup>4</sup>. A V5-tagged construct coding for the first 3 globular domains of IGFN1 (IGFN1(d1-d3)) transduced into primary cardiomyocytes also showed Z-disc and nuclear localization for the resulting recombinant protein<sup>4</sup>. Ab-US42 and Ab-Kip2b antibodies cannot distinguish between specific IGFN1 isoforms. To distinguish potential differences in subcellular localization between IGFN1 and IGFN1\_V1, constructs encoding the recombinant

proteins IGFN1-tdTomato and IGFN1\_V1-tdTomato were generated. These were then expressed in a non-muscle cell line (COS7), a muscle cell line (C2C12) and mouse skeletal muscle.

A Y2H screen performed previously using IGFN1 as bait identified MLTK as an interaction partner. This interaction attracted attention because transcriptomics had previously shown that MLTK is substantially up-regulated in *ky/ky* mouse *Extensor digitorum longus* (EDL) muscle<sup>50</sup>. The *Mltk* gene codes for two isoforms, MLTK $\alpha$  (also known as ZAK) and MLTK $\beta$  (also known as MLK7)<sup>53</sup>. Residues 1-331 of MLTK $\alpha$  are identical to those of MLTK $\beta$ , and they include a serine/threonine kinase domain (residues 16-227) and a leucine zipper motif (residues 287-322). The isoforms differ at their C-terminal: a sterile  $\alpha$ -motif (SAM) only exists in MLTK $\alpha$  (residues 337-408, see Figure 1.7). SAM domains are involved in protein-protein interactions and oligomerization<sup>55</sup>, a previous study showed that the SAM domain in MLTK $\alpha$  is not necessary for MLTK $\alpha$  oligomerization<sup>54</sup>. It is possibly related with limb development, with a SAM domain mutation in MLTK $\alpha$  leading to split-foot phenotype and nail anomalies in humans<sup>58</sup>. MLTK $\alpha$  is composed of 803 residues, whereas MLTK $\beta$  only has 454 residues<sup>53</sup>. Northern blots have previously shown that MLTK $\beta$  is highly expressed in heart and skeletal muscle<sup>51</sup>. In cardiomyoblasts, MLTK $\alpha$  increases the organization of actin fibres and the size of the cells, which indicates MLTK $\alpha$  could induce the hypertrophy of the cardiomyoblasts<sup>54</sup>. A transgenic mouse with tissue-specific overexpression of MLTK $\beta$  in the heart showed myocardial fibrosis and hypertrophy<sup>5</sup>. As a first step towards the functional characterization of MLTK in muscle, here we have looked at the subcellular localization of MLTKs in COS7 cells, C2C12 myoblast cells and adult skeletal muscle.

## 3.2 RESULTS

### 3.2.1 IGFN1-tdTomato and IGFN1\_V1-tdTomato subcellular localization in COS7

In order to study the function of IGFN1 and IGFN1\_V1 in skeletal muscle, two tdTomato expression constructs containing IGFN1 or IGFN1\_V1 were built. Tdtomato fluorescent protein was designed to tag onto IGFN1 or IGFN1\_V1 protein at their C-terminal. IGFN1-tdTomato and IGFN1\_V1-tdTomato constructs were tested in a non-muscle cell line (COS7 - a cell line derived from monkey kidney tissue) due to this cell line being easy to transfect. Both constructs could express IGFN1-tdTomato or IGFN1\_V1-tdTomato, showing strong red fluorescence. In COS7 cells, IGFN1-tdtomato mainly localised to the cytoplasm, with only a few cells having nuclear expression patterns (Figure 3.1A). IGFN1\_V1-tdTomato is also localised to the cytoplasm and the nucleus, although the nuclear expression pattern appears much brighter (Figure 3.1B).

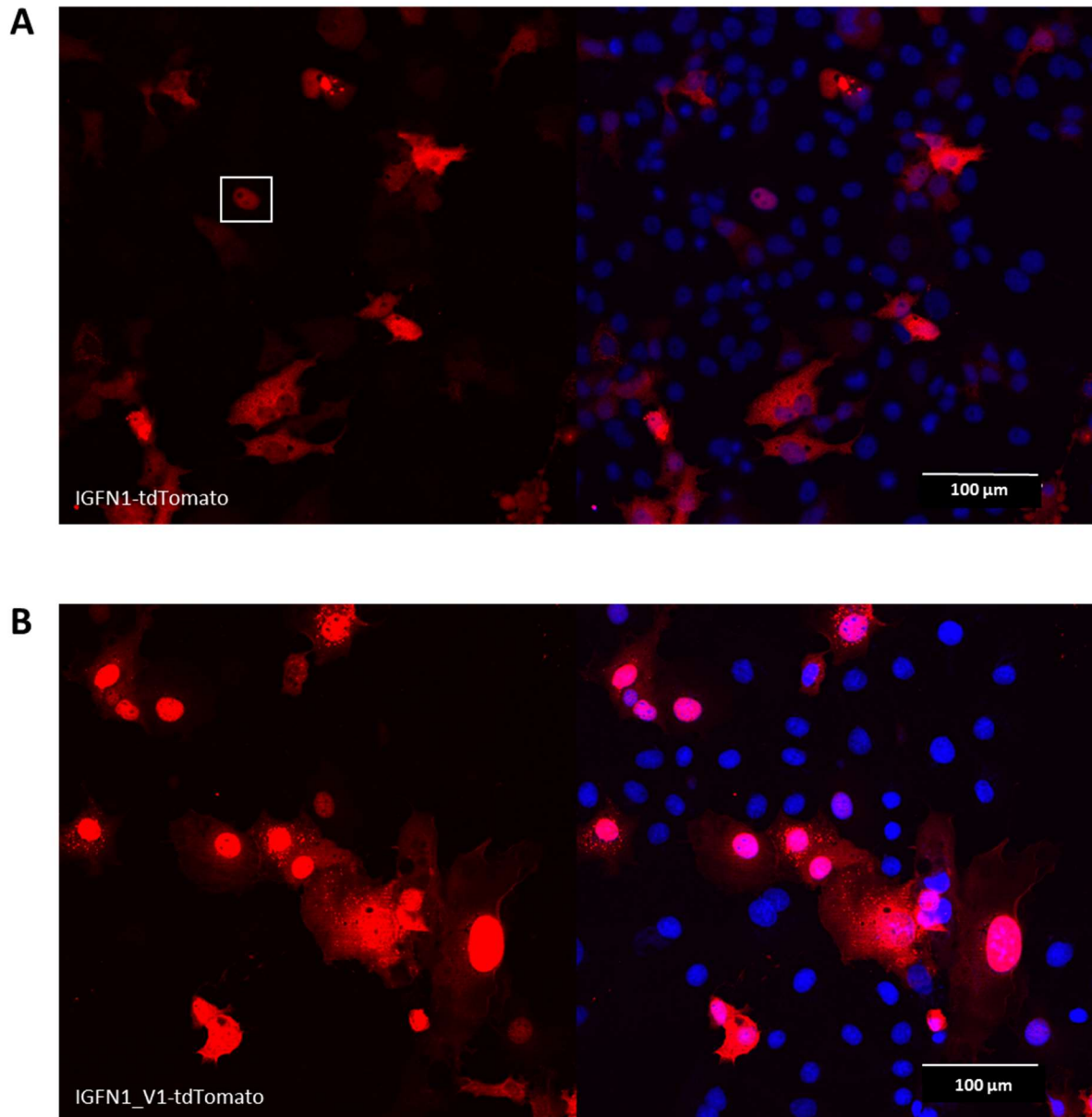


Figure 3.1: IGFN1-tdTomato and IGFN1\_V1-tdTomato subcellular localization in COS7 cells. IGFN1-tdTomato (A) and IGFN1\_V1-tdTomato (B) subcellular localization in COS7 cells. The red colour comes from fluorescent protein tag tdTomato, the blue colour comes from DAPI stained nuclei. The square in (A) highlights a cell showing nuclear expression of the recombinant protein. Both experiments were repeated more than three times, the images shown above are representative images.

### 3.2.2 IGFN1-tdTomato and IGFN1\_V1-tdTomato subcellular localization in C2C12

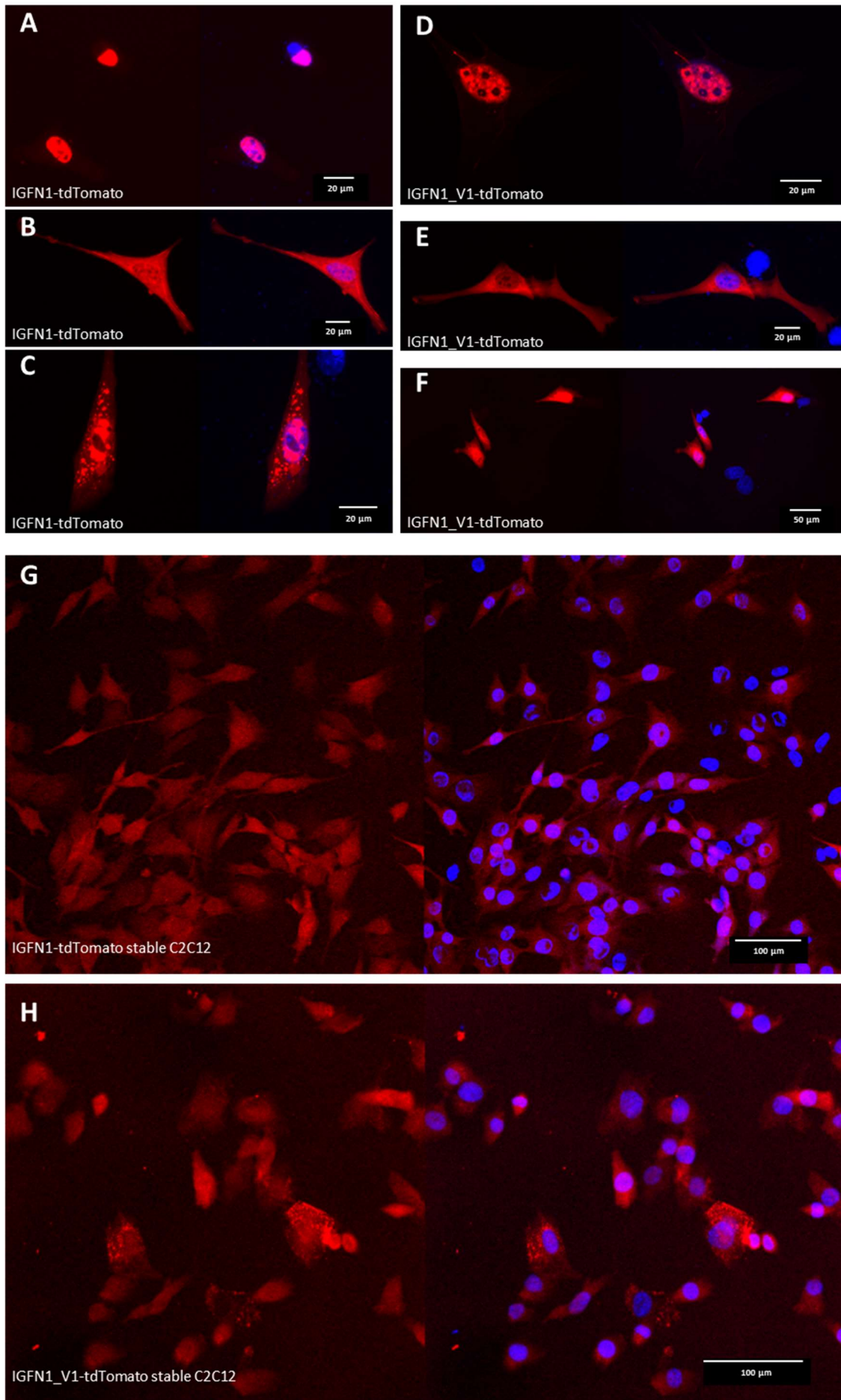
To reveal the subcellular localization of IGFN1 and IGFN1\_V1 in mouse myoblasts, a type of cell able to fuse together to form muscle fibres during muscle myogenesis, IGFN1-tdTomato and IGFN1\_V1-tdTomato were transiently transfected into C2C12 cells (a mouse myoblast cell line). Cells show three distinctive expression patterns for IGFN1-tdtomato and IGFN1\_V1-tdTomato: nuclear expression only (figure 3.2A and D), cytoplasmic expression only (figure 3.2B and E) or nuclear and cytoplasmic expression (figure 3.2C and F). This suggests that in myoblasts IGFN1 and IGFN1\_V1 shuttle between the nucleus and the cytoplasm in response to environmental cues.

Skeletal muscle cells are long tubes, muscle fibres or myofibres, which contain multiple nuclei. Muscle fibres result from the fusion of many myoblasts during muscle differentiation or myogenesis. Since C2C12 myoblasts are difficult to transiently transfect with good efficiency, and given that transiently transfected genes usually only express for a short time before reducing in intensity after cell divisions or other affections, C2C12 cell lines stably expressing IGFN1-tdTomato and IGFN1\_V1-tdTomato were generated for stable expression of these IGFN1 proteins during cell differentiation. To select stable cell lines, constructs encoding recombinant IGFN1-tdTomato or IGFN1\_V1-tdTomato were linearized and transfected into C2C12 cells. 48 hours after transfection, due to the constructs containing a *neo* gene selection marker, geneticin (G418) was used to select resistant cell colonies expressing *neo* for 7 days. These colonies were expanded and stored for future usage. In this experiment, only one clone was selected for stable expression of each IGFN1-tdTomato and IGFN1\_V1-tdTomato.

These stable cell lines were used to study the localisation patterns of IGFN1 and IGFN1\_V1 during differentiation *in vitro*. Both IGFN1-tdTomato and IGFN1\_V1-tdTomato mainly localise

to the cytoplasm of the stable cell lines during the proliferative stage (myoblasts), only few examples of nuclear localisation have been observed in IGFN1-tdTomato expressing cells (figure 3.2G and H). After seven days in differentiation medium, IGFN1-tdTomato expressing cells were not able to form myotubes (figure 3.2I). Using  $\alpha$ -actinin as differentiation marker, due to the expression level of  $\alpha$ -actinin increasing during cell differentiation<sup>75</sup>, showed little expression of  $\alpha$ -actinin in this cell line (figure 3.2I), indicating that the IGFN1-tdTomato derived cell line could potentially begin to differentiate, but the process was not able to complete. IGFN1\_V1-tdTomato expressing cells differentiate into myotubes after seven days in differentiation medium. In this case, the recombinant protein was present in the cytoplasm only (figure 3.2J). The  $\alpha$ -actinin-FITC staining results showed strong green fluorescence in these myotubes, indicating that IGFN1\_V1-tdTomato expressing cells can differentiate further than IGFN1-tdTomato expressing cells (figure 3.2J).

The fluorescence levels from both stable cell lines are not as strong as those in transiently transfected cells (The fluorescence intensity seen in figure 3.2G, H, I and J were increased through longer exposure times). Once the foreign gene integrates into genome, it may fall into a region where expression depends on a weaker promoter, resulting in lower levels of expression. It is also possible that constantly overexpressing high levels of IGFN1 or IGFN1\_V1 is toxic and thereby selected against.



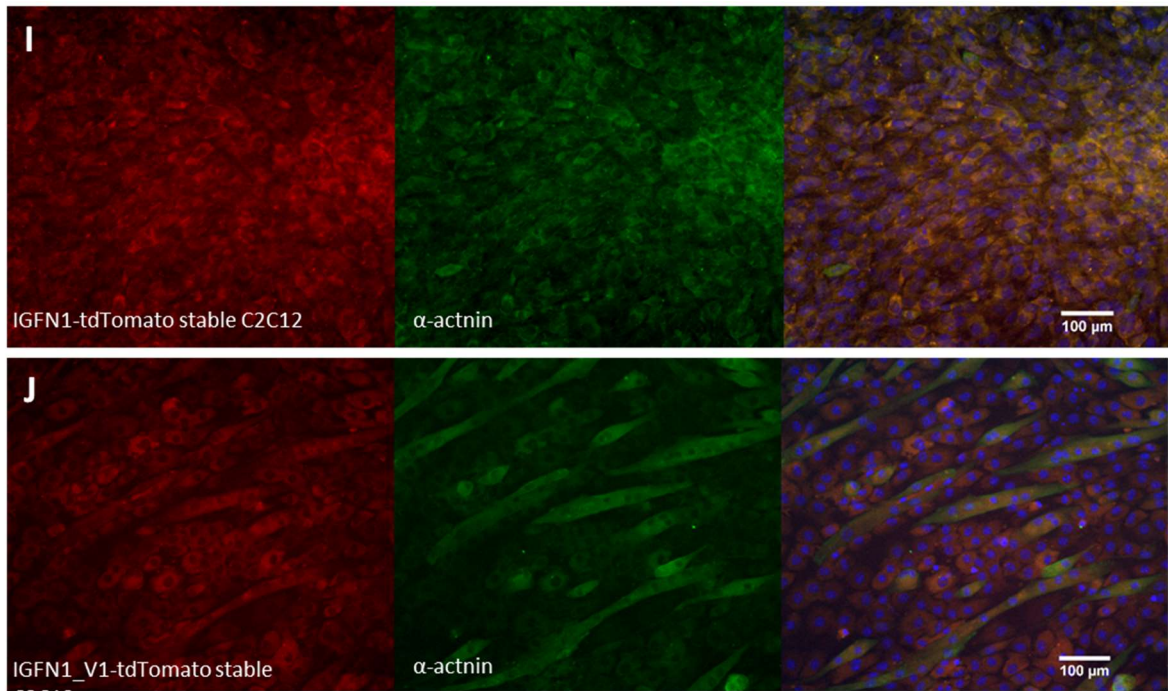


Figure 3.2: IGFN1-tdTomato and IGFN1\_V1-tdTomato subcellular localization in C2C12. (A),(B),(C), represent IGFN1-tdTomato subcellular localization with transiently transfected construct expression of IGFN1-tdTomato in C2C12 cells. (D),(E),(F), represent IGFN1\_V1-tdTomato subcellular localization when IGFN1\_V1-tdTomato was transiently transfected into C2C12 cells. (G), image shows IGFN1-tdTomato stably expressed in C2C12 myoblasts. (H), image shows IGFN1\_V1-tdTomato stably expressed in C2C12 myoblasts. (I), Differentiated IGFN1-tdTomato stably expressing C2C12 myoblasts. (J), Differentiated IGFN1\_V1 stably expressed in C2C12 myoblasts. The cells, used in I and J, were grown in the differentiation medium for 7 days. Red colour comes from fluorescent protein tag, tdTomato. Green fluorescence in I and J comes from α-actinin-FITC. Blue colour comes from DAPI stained nuclei. All the experiments described above were repeated more than three times, the images shown above are representative images.

### 3.2.3 IGFN1 and IGFN1\_V1 subcellular localization in skeletal muscle

Previous work in our group using antibodies Ab-US42 (against the N-terminus of IGFN1) and Ab-Kip2b (against the C-terminus of IGFN1) indicated that one or more IGFN1 isoforms are present at the Z-disc and the nucleus<sup>4</sup>. According to the position of the epitopes used to raise Ab-US42 and Ab-Kip2b antibodies, these antibodies can potentially detect both IGFN1 and IGFN1\_V1 isoforms. Therefore, the previous immunofluorescence results from adult skeletal muscle with these antibodies is not evidence of specific localization for either of these isoforms. To address isoform specific localization, tdTomato tagged versions of IGFN1 and IGFN1\_V1 were electroporated into mouse Extensor digitorum longus/ Tibialis Anterior (EDL/TA) muscle. After seven days of expression, mice were sacrificed and electroporated muscles were dissected, then muscle were prepared as whole mount samples for confocal imaging. The results showed that both IGFN1-tdTomato and IGFN1\_V1-tdTomato are expressed in the nucleus as well as in the cytoplasm with a striated expression pattern (figure 3.3). To prove that these striations were Z-discs, an antibody against  $\alpha$ -actinin and a FITC-conjugated secondary antibody were used to label the Z-disc with green fluorescence in IGFN1\_V1-tdTomato expressing muscle fibres.  $\alpha$ -actinin protein is one of the major components of the Z-disc. Co-localization analysis was performed using ImageJ software to illustrate the co-localization between IGFN1\_V1-tdTomato and  $\alpha$ -actinin (figure 3.3D). The mean value of Mander's Colocalization coefficients were calculated for each image used for co-localization analysis (in here called  $M_{\text{IGFN1\_V1-tdTomato}}$  and  $M_{\alpha\text{-actinin}}$ , the results were calculated from 4 individual experiments). A coefficient of 1 represents the perfect co-localization and one of 0 represents no co-localization. In this experiment,  $M_{\text{IGFN1\_V1-tdTomato}} = 0.9998$  and  $M_{\alpha\text{-actinin}} = 0.9993$  indicating that almost all of the green signal overlap with the red.

The white pixels in figure 3.3D represent the overlapped pixels. The results confirmed the striated expression pattern from IGFN1\_V1-tdTomato is located at the Z-disc.

The large molecular size of IGFN1-tdTomato [ $\sim 189\text{kDa}$ ] probably explains the poorer electroporation efficiency observed with this construct in several attempts. This precluded the same localization analysis from being undertaken since the number of IGFN1-tdTomato expressing fibres were not enough for characterisation. However, consistent with previous results, we can conclude that IGFN1\_V1-tdTomato locates to the Z-disc and the nucleus.

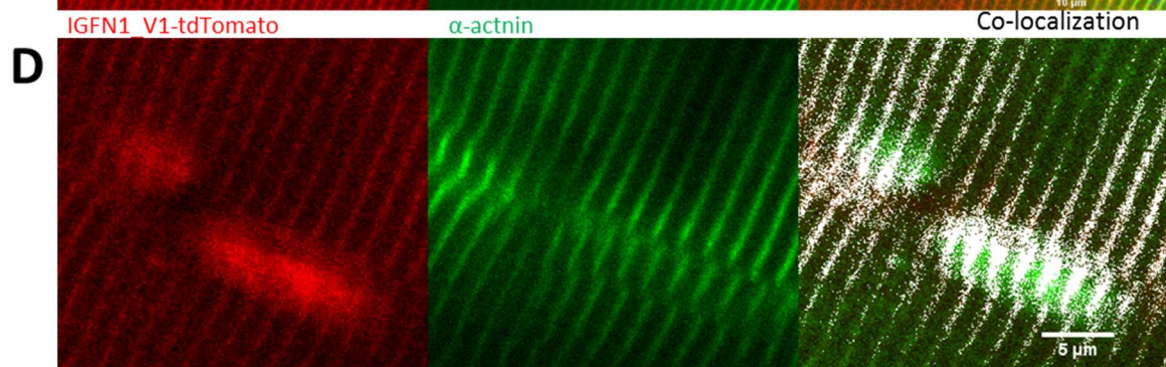
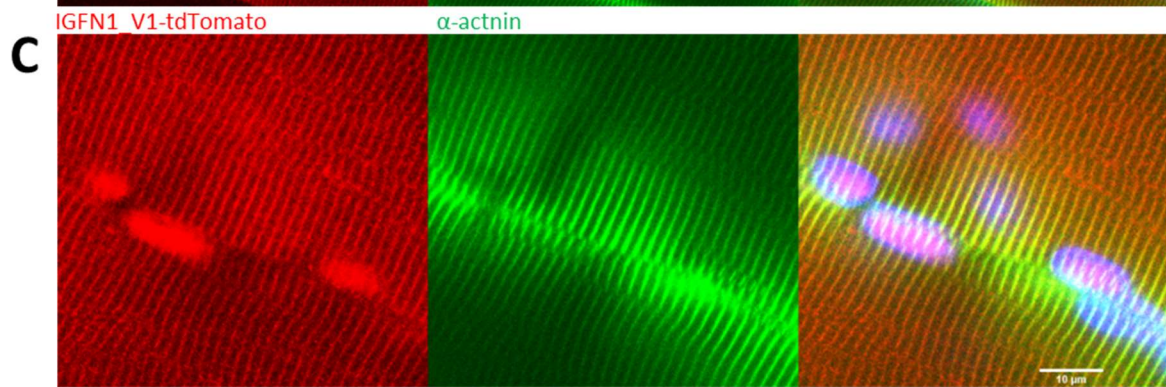
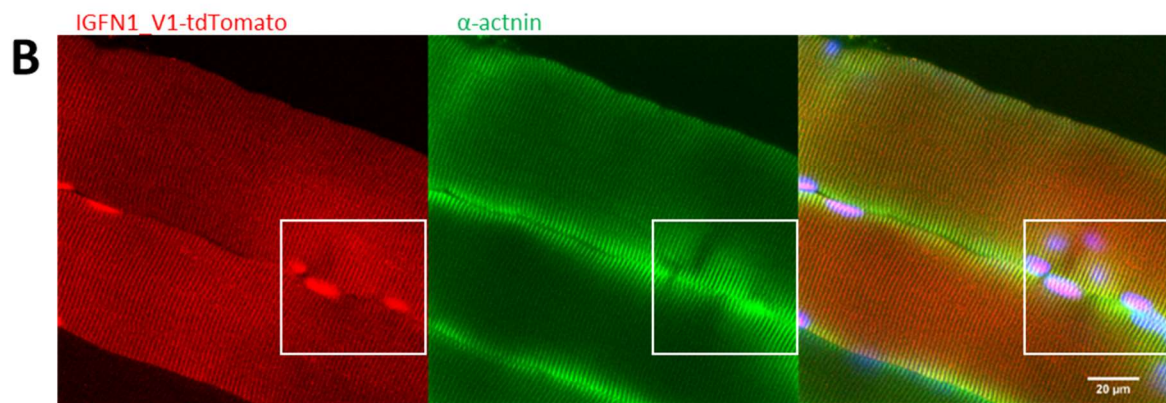
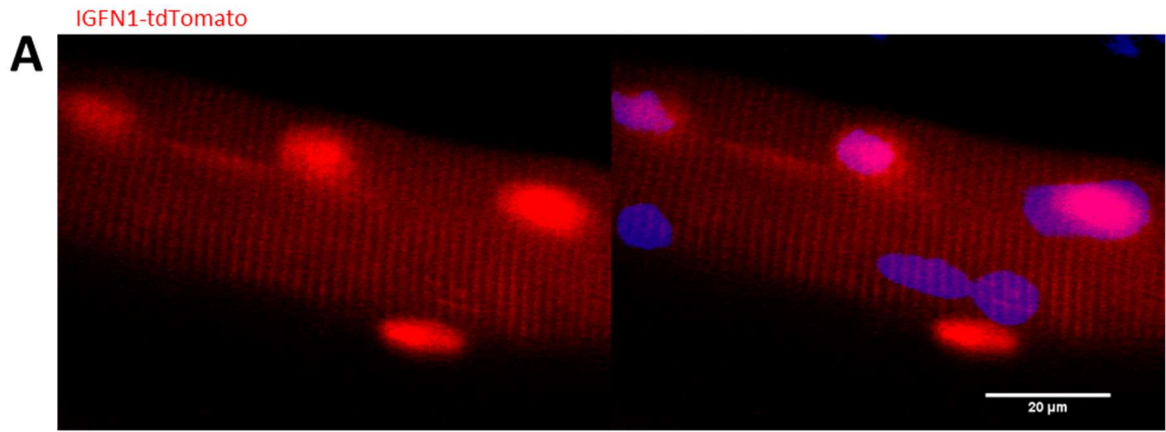


Figure 3.3: IGFN1-tdTomato and IGFN1\_V1-tdTomato subcellular localization in mouse skeletal muscle.

(A), ectopic expression IGFN1-tdTomato in mouse EDL/TA muscle by electroporation. (B), ectopic expression IGFN1\_V1-tdTomato in mouse EDL/TA muscle by electroporation.  $\alpha$ -actinin antibody (EA-53) and FITC secondary antibody were used to stain Z-disc in a whole mount muscle fibres. (C), expanded images from the corresponding white squares shown in B. (D), co-localization analysis showing Z-disc localization by imageJ, white pixels represent overlapped pixels in both red and green channels. The red fluorescence comes from tdTomato labelled proteins, the blue fluorescence is DAPI stained nuclei and the green fluorescence comes from  $\alpha$ -actinin (using a FITC conjugated secondary antibody). All the figures were captured using a confocal microscope to examine whole mount muscle fibres. The mice were injected at the ages of 5-8 weeks. To reduce the damage to the mouse, the DNA injections were performed through the skin, without exposing the muscle by anterior incision. Because EDL/TA muscle are physically confined within the hind limb and easy to access, all the injections were performed in these two muscle. All the experiments described above were repeated more than three times, the images shown above are representative images.

### 3.2.4 Subcellular localization of MLTK $\alpha$ and MLTK $\beta$ in COS7

In order to study the function of MLTKs, constructs encoding recombinant MLTK $\alpha$ -GFP and MLTK $\beta$ -GFP were built and tested by transient transfection of these constructs into COS7 cells. MLTK $\alpha$ -GFP and MLTK $\beta$ -GFP localized to the cytoplasm and in the nucleus. MLTK $\beta$ -GFP shows more nuclear expression than MLTK $\alpha$ -GFP (figure 3.4). The subcellular localization results for MLTK $\alpha$ -GFP and MLTK $\beta$ -GFP were similar to Gotoh's study which used HA-tagged MLTK $\alpha$  and MLTK $\beta$ <sup>53</sup>. This proved that labelling MLTK proteins at the C-terminus with GFP does not affect MLTKs protein subcellular localization.

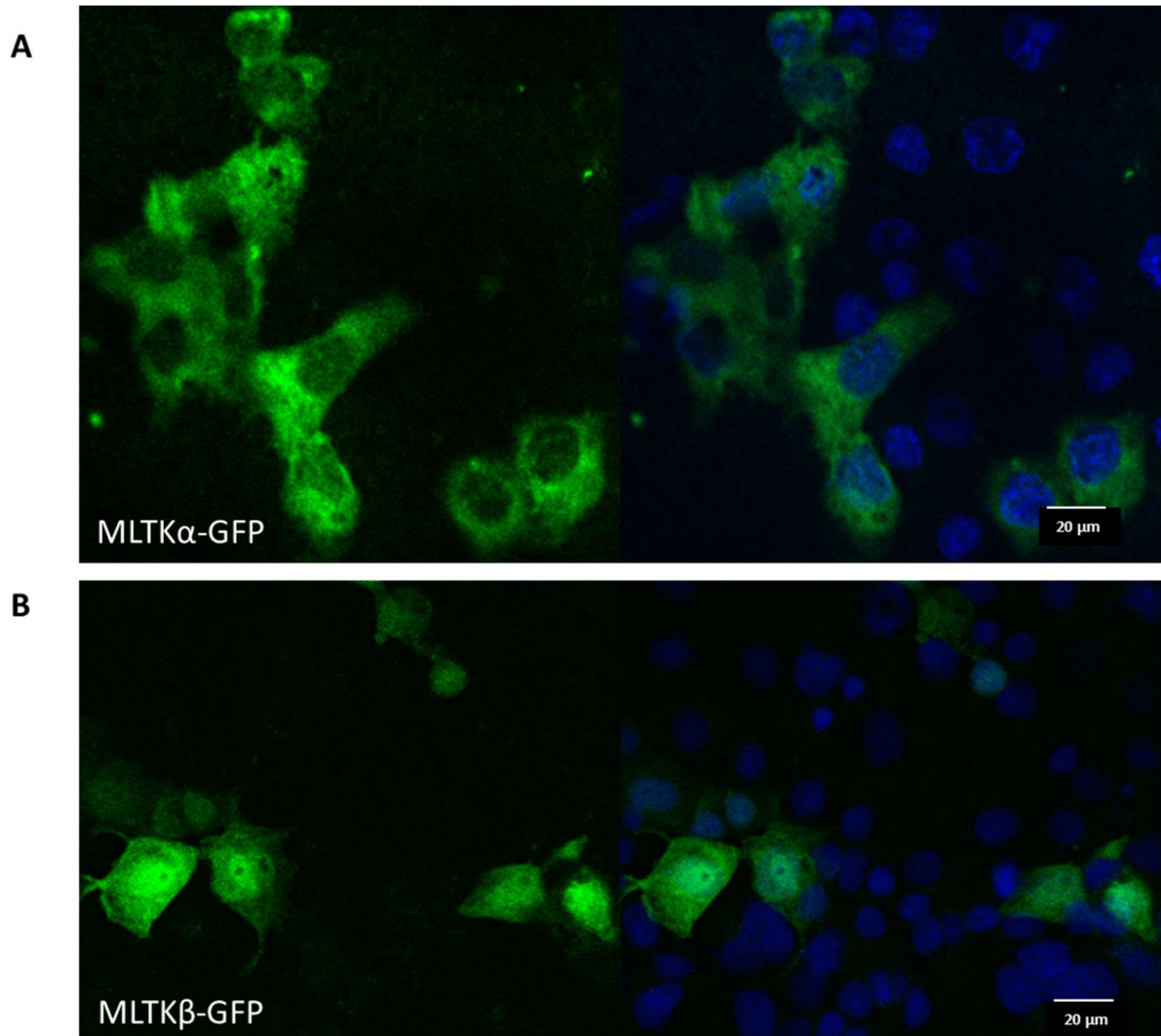


Figure 3.4: MLTK $\alpha$ -GFP and MLTK $\beta$ -GFP subcellular localization in COS7 cells. MLTK $\alpha$ -GFP (A) and MLTK $\beta$ -GFP (B) subcellular localization in COS7 cells. Green fluorescence comes from GFP labelled recombinant proteins, blue fluorescence represents DAPI stained nuclei. All the experiments described above were repeated more than three times, the images shown above are representative images.

### 3.2.5 MLTK $\alpha$ and MLTK $\beta$ subcellular localization in skeletal muscle

To study MLTK subcellular localization in skeletal muscle, MLTK $\alpha$ -tdTomato and MLTK $\beta$ -tdTomato were electroporated into mouse TA/EDL muscles from the hind limb. After seven days of expression, electroporated muscles were dissected and processed for confocal microscopy as before. Both MLTK $\alpha$ -tdTomato and MLTK $\beta$ -tdTomato showed a striated expression pattern but no nuclear expression (figure 3.5A and B; white arrows in figure 3.5A and B point at examples of nuclei showing DAPI signal but no red fluorescence). Colocalization analyses were performed as before (in section 3.2.3: IGFN1 and IGFN1\_V1 subcellular localization in skeletal muscle) and showed that MLTK $\beta$ -tdTomato localizes at the Z-disc (the mean values of Mander's Colocalization coefficients:  $M_{\text{MLTK}\beta\text{-tdTomato}}=0.9310$ ,  $M_{\alpha\text{-actinin}}=0.9970$ , datas were calculated from 3 images; Figure 3.5C - white pixels represent overlapped pixels). In addition, the striated expression pattern contained wide and narrow stripes in both MLTK $\alpha$ -tdTomato and MLTK $\beta$ -tdTomato expressing fibres, the narrow stripes were not easy to visualize below 40x magnification. Based on the localization of the narrow stripes it appears likely that these are at the M-line, though further analysis is needed to confirm this. In figure 3.5D and E, the narrow stripes (yellow arrows) alternate with the wide stripes (white arrows). Moreover, MLTK $\alpha$ -tdTomato and MLTK $\beta$ -tdTomato showed expression as parallel lines running along the length of the muscle fibres, (blue arrows in figure 3.5D and F). Taken together, these results demonstrated that in skeletal muscle MLTKs accumulate at the Z-disc and additional subcellular localizations but not in the nucleus.

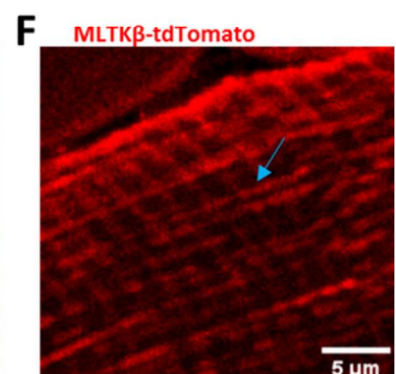
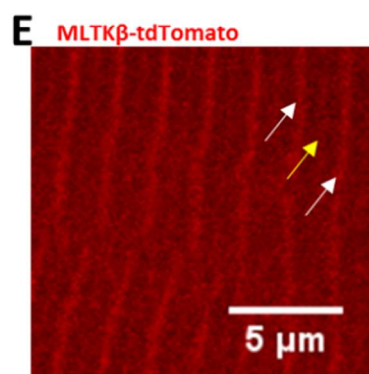
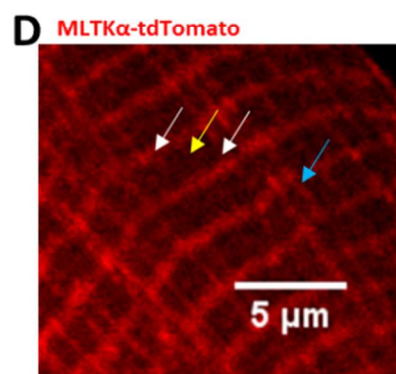
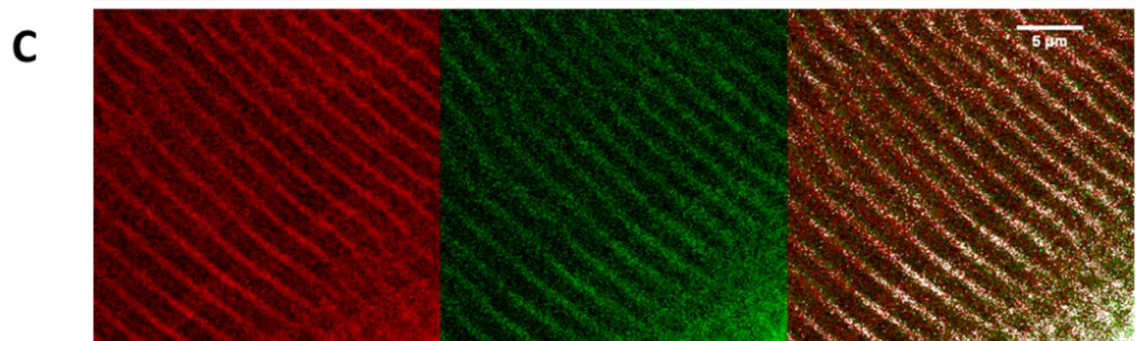
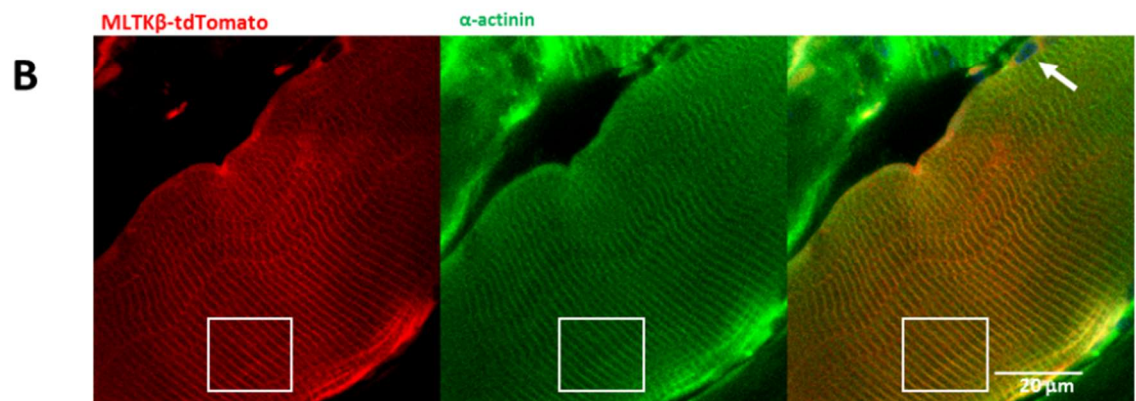
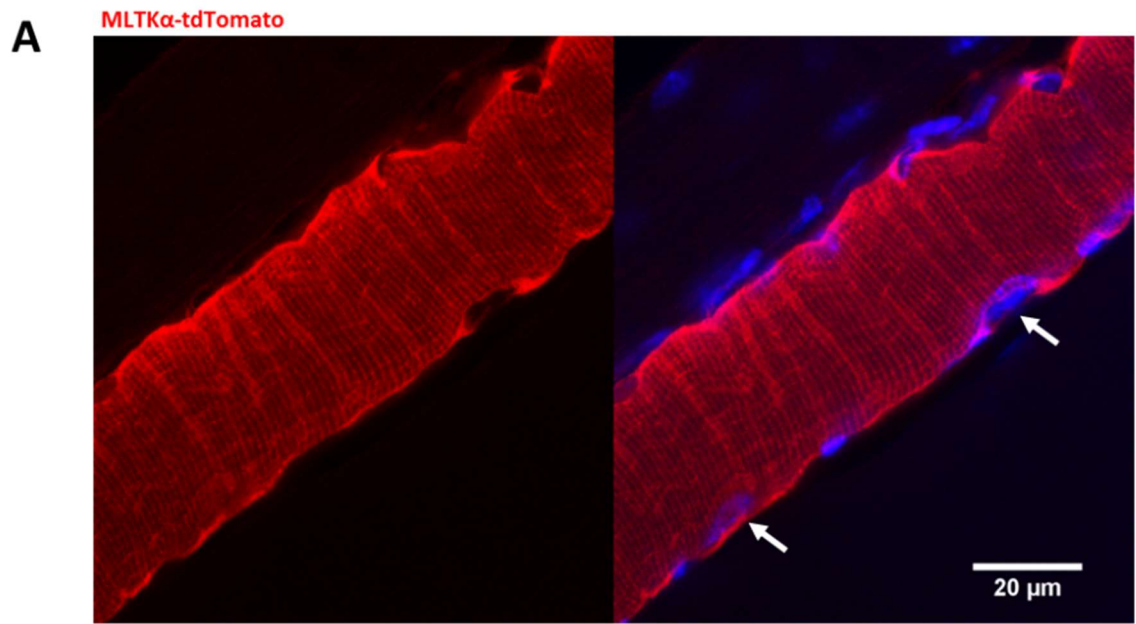


Figure 3.5: MLTK $\alpha$ -tdTomato and MLTK $\beta$ -tdTomato subcellular localization in skeletal muscle. (A), MLTK $\alpha$ -tdTomato expression in an electroporated muscle fibre. (B). MLTK $\beta$ -tdTomato expression in an electroporated muscle fibre, the fibres were stained with EA-53 against  $\alpha$ -actinin with a FITC-conjugated secondary antibody. (C), Co-localization analysis. White pixels are the co-localized pixels for MLTK $\beta$ -tdTomato and  $\alpha$ -actinin (FITC signal). D,E,F higher magnification images showing MLTK $\alpha$  or MLTK $\beta$  is not only expressed at the Z-disc. White arrows point at the Z-disc. Yellow arrows point at another band, based on the localization it can only be the M-line. Blue arrows point at fluorescent lines running parallel to the long axis of the fibres. All the images in this figure were prepared from TA/EDL muscle electroporated with constructs encoding either MLTK $\alpha$ -tdTomato or MLTK $\beta$ -tdTomato. Red fluorescence represents tdTomato labelled MLTK $\alpha$  or MLTK $\beta$ . Green fluorescence represents  $\alpha$ -actinin and FITC conjugated secondary antibodies staining at the Z-disc. Blue is DAPI stained nuclei. The mice were injected at the ages of 5-8 weeks. All the experiments described above were repeated more than three times, the images shown above are representative images.

### 3.3 CONCLUSION:

In this chapter the subcellular localizations of IGFN1, IGFN1\_V1, MLTK $\alpha$  and MLTK $\beta$  were investigated in COS7 cells, C2C12 myoblasts and mouse skeletal muscle. In the non-muscle cell line COS7, recombinant IGFN1 and IGFN1\_V1 expressed in the cytoplasm and the nucleus. IGFN1\_V1-tdTomato showed more nuclear expression than IGFN1-tdTomato. In the C2C12 muscle myoblast cell line, IGFN1-tdTomato and IGFN1\_V1-tdTomato showed no significant localization differences, both of them expressed either only in the nucleus or in cytoplasm or in both localizations. This indicated that IGFN1-tdTomato and IGFN1\_V1-tdTomato may shuttle between the nucleus and the cytoplasm. In mouse skeletal muscle, IGFN1\_V1 was confirmed expressed in the nucleus and the Z-disc. IGFN1-tdTomato also showed nuclear expression as well as a striated expression pattern.

In this chapter, Cycle3-GFP were used to tag MLTK $\alpha$  and MLTK $\beta$  at 3' terminal. The results of transfection showed that both MLTK $\alpha$  and MLTK $\beta$  located in cytoplasm, MLTK $\beta$  was found to also localise to the nucleus. Because the green fluorescence from cycle3-GFP was not strong as tdTomato, tdTomato-tagged MLTK $\alpha$  and MLTK $\beta$  were used to study their localizations in skeletal muscle. In skeletal muscle, MLTK $\beta$  was confirmed to be located at the Z-disc. In both MLTK $\alpha$  and MLTK $\beta$  expressing fibres, narrow stripes alternated with the wide stripes expression patterns as seen in higher magnification images. This indicated that Z-disc was not the only subcellular location to which the MLTK proteins located. The results also showed a linear localisation pattern running parallel alongside the fibres for both MLTK isoforms. The results demonstrated that MLTK $\alpha$  and MLTK $\beta$  may be associated with a wider variety of cytoskeletal structures than IGFN1.

Because IGFN1s and MLTKs are known interaction partners and both of them were found localised to the Z-disc of skeletal muscle cells, the results suggest that the Z-disc may be the place where IGFN1 interacts with MLTK.

Given the fact that most of the fibres in TA/EDL muscles are fast fibres, whether the subcellular localization of IGFN1s and MLTKs in slow fibres are same as in fast fibres was not known. In the mouse hind limb, soleus muscle is the only muscle containing a high proportion of slow fibres. The soleus is located in the centre of the mouse hind limb. Due to the position of soleus muscle and the relatively small size of this muscle compared to TA/EDL muscle, it is hard to generate expression of IGFN1s-tdTomato or MLTKs-tdTomato in this muscle by using our current electroporation methods. To explore the localization of IGFN1s and MLTKs in slow fibres, soleus muscle electroporation will be performed in the future, using anterior incision to expose the muscle for precise positioning of DNA injections and electroporation needles.

# Chapter 4

## RESULTS

### 4. Interaction between IGFN1\_V1 and MLTLKs

## 4.1 INTRODUCTION

Previous yeast two hybrid (Y2H) screening identified that IGFN1 interacts with MLTK<sup>4</sup>. The bait sequence of the Y2H contained the 1<sup>st</sup> to 3<sup>rd</sup> globular domain of IGFN1, which exist in both IGFN1 and IGFN1\_V1. The identified prey sequence, a 200 amino acid fragment of MLTK spanning the beginning of the N-terminus, is common to both MLTK $\alpha$  and MLTK $\beta$ . Therefore, the Y2H screen did not identify specific interactions between individual IGFN1 and MLTK isoforms. Here, immunoprecipitation (IP) assays using full length isoforms were performed in order to validate the Y2H interactions.

## 4.2 RESULTS

### 4.2.1 Pull down using recombinant IGFN1\_V1-v5 and MLTK $\alpha$ -GFP or MLTK $\beta$ -GFP from transfected COS7 cells

To test interactions between specific isoforms of IGFN1 and MLTK, immunoprecipitation experiments were performed using IGFN1-v5 or IGFN1\_V1-v5 and MLTK $\alpha$ -GFP or MLTK $\beta$ -GFP recombinant proteins in co-transfected COS7 cells. This experiment was performed using v5 antibody conjugated agarose beads to immunoprecipitate the v5-tagged IGFN1 isoform. If the interaction exists between the specific isoforms of IGFN1 and MLTK, GFP-tagged MLTK $\alpha$  or MLTK $\beta$  will be co-precipitated with v5-tagged IGFN1 isoforms and v5 antibody conjugated agarose beads. The presence of recombinant MLTK $\alpha$ -GFP or MLTK $\beta$ -GFP in the immunoprecipitate was then tested with antibodies against GFP.

Both MLTK $\alpha$ -GFP and MLTK $\beta$ -GFP were precipitated with either IGFN1-v5 or IGFN1\_V1-v5. For the first IP experiment, the negative control failed to present because of experimental error (Figure 4.1A). A second IP used IgG conjugated beads as a negative control to test that the interactions are specific and not the result of non-specific binding to the conjugated beads. The result shows that both MLTK $\alpha$ -GFP [ $\sim$  118 kDa] and MLTK $\beta$ -GFP [ $\sim$  78 kDa] are pulled down with IGFN1\_V1-v5 [ $\sim$  136kDa] but not with IgG conjugated agarose beads alone (figure 4.1B), indicating that both MLTK $\alpha$ -GFP and MLTK $\beta$ -GFP interact with IGFN1\_V1-v5 in this assay. In this experiment, a cross-reacting band appeared on the anti-GFP blot in close proximity to the MLTK $\beta$ -GFP band, possibly the heavy chain ( $\sim$  50kDa) of denatured or reduced primary antibody present in the immunoprecipitate. However, the two bands are distinct and the MLTK $\beta$ -GFP band was only identified in this lane. Due to the difficulty of expressing the large IGFN1-v5 [ $\sim$ 303kDa] in COS7 cells at sufficient levels, the second experiment was unable to test interactions between IGFN1-v5 and MLTK $\alpha$ -GFP or MLTK $\beta$ -GFP, therefore the following work focuses on IGFN1\_V1 alone to study the interactions between IGFN1s and MLTKs.

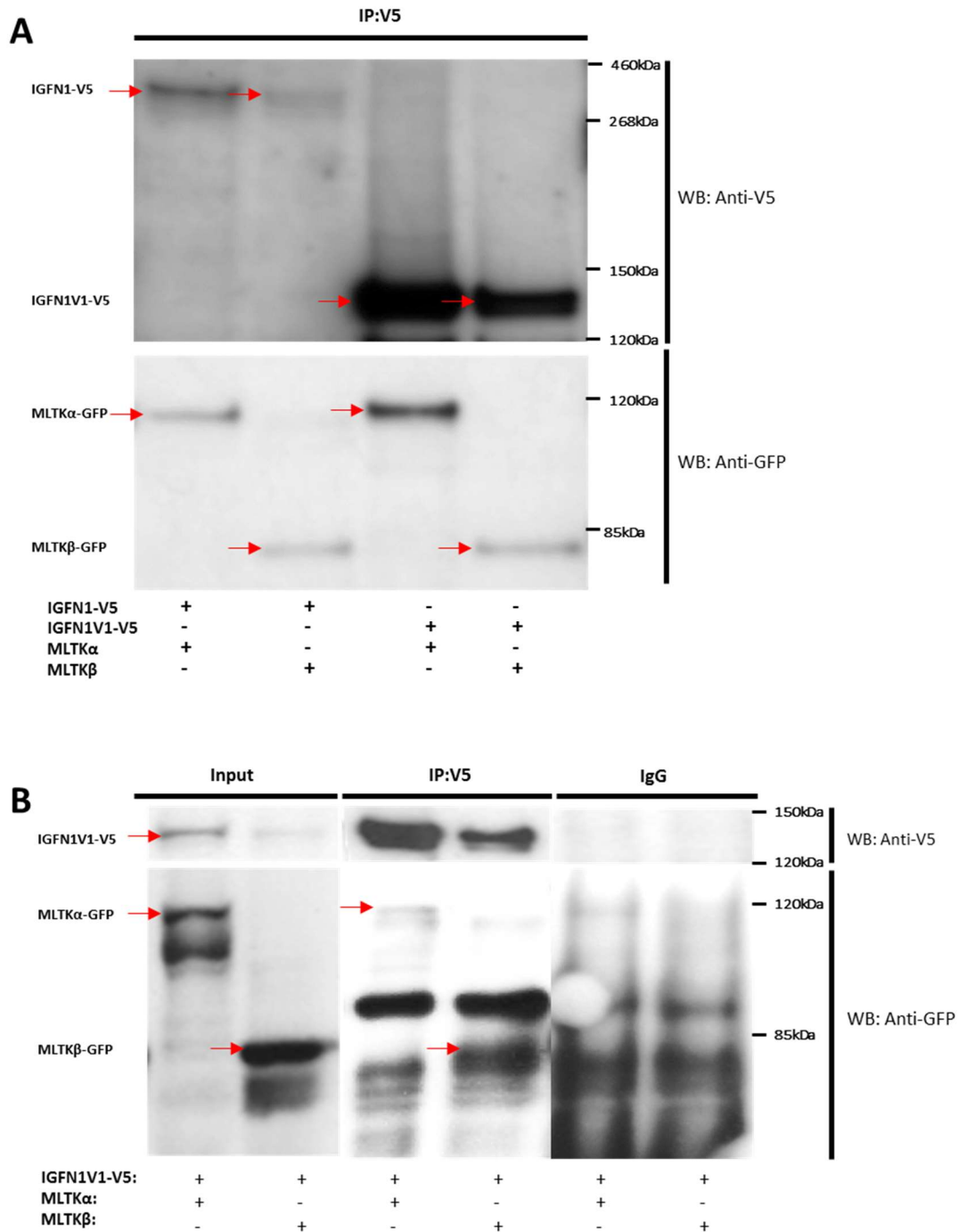


Figure 4.1: Pull down assays analysis the interactions between specific isoform of IGFN1 and MLTK.

Pull-down assays in co-transfected COS7 cells using recombinant IGFN1-v5 [ $\sim 303$ kDa] or IGFN1\_v1-v5 [ $\sim 136$ kDa] and MLTK  $\alpha$ -GFP [ $\sim 118$ kDa] or MLTK  $\beta$ -GFP [ $\sim 78$ kDa], as indicated. (A) and (B) are independent pull-down experiments. The red arrows identify the individual isoforms. The blue arrows indicate an unexpected band, likely arising from non-specific interactions. Experimental error caused negative control experiment fail for the first IP (A). The second IP (B) added the negative control to show that the signals from the IP results are specific. The IP experiments were repeated 3 times; all the results were similar; this figure represents the clearest result to present.

#### 4.2.2 Pull down using recombinant IGFN1\_V1-his from *E.coli* and MLTK $\alpha$ -GFP or MLTK $\beta$ -GFP from transfected COS7 (from Matthew Winder, placement student)

IP results showed that IGFN1\_V1-v5 interacts with both MLTK $\alpha$ -GFP and MLTK $\beta$ -GFP. To investigate where the interaction site(s) are in IGFN1\_V1, two constructs, a his-tagged IGFN1<sub>(d1-d3)</sub> containing the first three globular domains from the N-terminal and a his-tagged IGFN1<sub>(d8-d11)</sub> containing the 8<sup>th</sup> to 11<sup>th</sup> globular domains were expressed in *E.coli*. IGFN1\_V1-his, IGFN1<sub>(d1-d3)</sub>-his and IGFN1<sub>(d8-d11)</sub>-his were used as baits in a pull down assay to test interactions with MLTK $\alpha$ -GFP or MLTK $\beta$ -GFP produced from transfected COS7 cells.

The results show that IGFN1\_V1-his, IGFN1<sub>(d1-d3)</sub>-his and IGFN1<sub>(d8-d11)</sub>-his are able to pull down both MLTK $\alpha$ -GFP and MLTK $\beta$ -GFP. MLTK $\alpha$ -GFP was not pulled down with the negative control, LacZ-his. This proved that MLTK $\alpha$ -GFP specifically interacts with IGFN1\_V1-his, IGFN1<sub>(d1-d3)</sub>-his and IGFN1<sub>(d8-d11)</sub>-his. However, a faint band showed in the negative control of MLTK $\beta$ -GFP pull-down. If the MLTK $\beta$ -GFP band in the negative control is due to non-specific interactions with LacZ, given that the input levels of LacZ are similar to or greater than the input levels of IGFN1 isoforms (figure 4.2B), this would appear to represent a much weaker interaction than would account for the band intensity in the lanes from the IGFN1 isoforms (figure 4.2A). It therefore seems likely that the IGFN1-MLTK $\beta$  interactions are genuine. The band in the negative control might also be explained by the large amount of protein used, this would increase the levels of non-specific binding to the beads and the washing step may not have completely washed all the MLTK $\beta$ -GFP off. It may also be the result of a loading error. In summary, the results show that both IGFN1<sub>(d1-d3)</sub>-his and IGFN1<sub>(d8-d11)</sub>-his interact with

MLTK $\alpha$ -GFP and MLTK $\beta$ -GFP, which indicates that IGFN1\_V1 contains more than one binding site for MLTK $\alpha$ -GFP and MLTK $\beta$ -GFP.

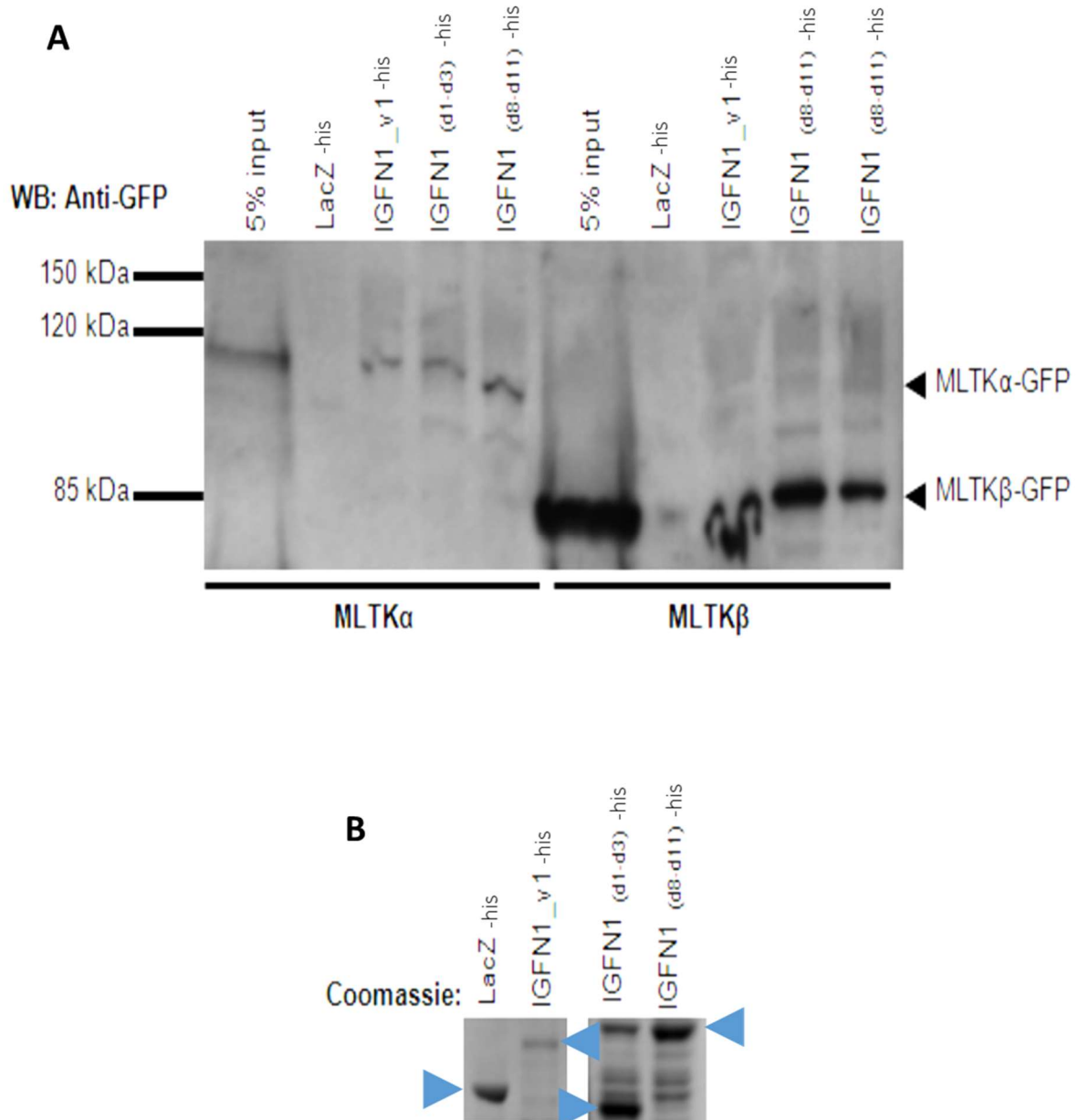


Figure 4.2: Pull-down assays analyze MLTK interaction sites on IGFN1\_V1.

(A), pull down assays show that *E.coli* produced recombinant proteins IGFN1\_V1-his [ $\sim$ 136kDa], IGFN1 (d1-d3)-his [ $\sim$ 38kDa] and IGFN1 (d8-d11)-his [ $\sim$ 72kDa] interact with MLTK $\alpha$ -GFP [ $\sim$  118kDa] and MLTK $\beta$ -GFP [ $\sim$ 78kDa], which were produced in COS7 cells. (B), comparative amounts of purified IGFN1\_V1-his, IGFN1(d1-d3)-his, IGFN1 (d8-d11)-his and LacZ-his proteins used in each pull down were displayed in coomassie stained gel. Blue arrows label the expected band.

### 4.2.3 IGFN1\_V1-tdTomato co-expression with MLTK $\alpha$ -GFP or MLTK $\beta$ -GFP in skeletal muscle

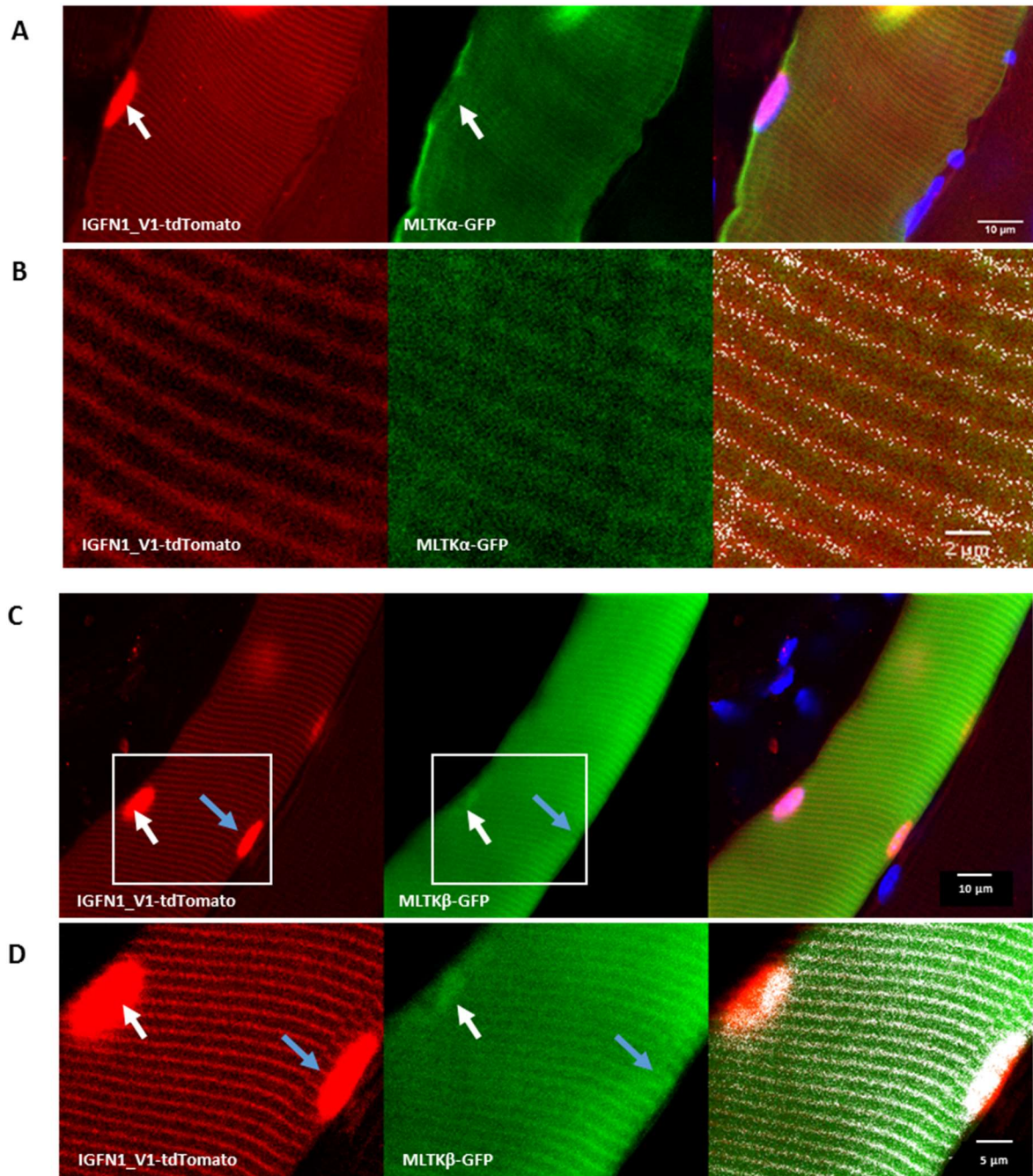
The previous pull down assay confirmed that IGFN1\_V1-v5 interacts with both MLTK $\alpha$ -GFP and MLTK $\beta$ -GFP. In chapter 3, MLTK $\alpha$ -tdTomato, MLTK $\beta$ -tdTomato and IGFN1\_V1-tdTomato were found to localize at the Z-disc. Therefore, the Z-disc is likely to be the place where interactions occur in skeletal muscle. To verify this hypothesis, IGFN1\_V1-tdTomato was co-expressed with MLTK $\alpha$ -GFP or MLTK $\beta$ -GFP by electroporating constructs expressing these proteins in the EDL/TA muscle of 5-8 week old mice. Following 7 days of expression, mice were sacrificed, and electroporated muscles were dissected, sectioned or prepared as whole mounts to obtain fluorescence images.

In co-transfected fibres, Z-disc co-localization was found in both IGFN1\_V1-tdTomato and MLTK $\alpha$ -GFP expressing fibres (figure 4.3A). ImageJ co-localization analysis was performed as in section 3.2.3, the mean values of Mander's Colocalization coefficients are  $M_{\text{IGFN1\_V1-tdTomato}} = 0.9949$  and  $M_{\text{MLTK}\alpha\text{-GFP}} = 0.9980$  (these data were calculated from 2 individual images). The co-localization analysis results indicated that IGFN1\_V1-tdTomato and MLTK $\alpha$ -GFP partially co-localized at the Z-disc (see distribution of white pixels in figure 4.3B). As in previous electroporations, IGFN1\_V1-tdTomato also shows localization to the nucleus, but MLTK $\alpha$ -GFP was not observed in the nucleus in any fibre showing co-expression of both recombinant proteins (figure 4.3A shows an illustrative example in which the arrow points at a nucleus positive for IGFN1\_V1-tdTomato and negative for MLTK $\alpha$ -GFP expression).

To analyse the co-localization between IGFN1\_V1-tdTomato and MLTK $\beta$ -GFP, the co-localization analysis was performed as before in section 3.2.3, the mean values of Mander's Colocalization coefficients are  $M_{IGFN1\_V1-tdTomato} = 0.9876$  and  $M_{MLTK\beta-GFP} = 0.9933$  (these data were calculated from 4 individual images). For both red and green channels, the Mander's Colocalization coefficients are close to 1, which indicates that most of the pixels in both channels overlap. The white pixels in figure 4.3D represent the overlapped pixels in both red and green channels. These results proved that IGFN1\_V1-tdTomato and MLTK $\beta$ -GFP co-localized at the Z-disc. Interestingly, nuclear localization of MLTK $\beta$ -GFP was also found in IGFN1\_V1-tdTomato and MLTK $\beta$ -GFP co-transfected fibres (Figure 4.3C shows an example of a nucleus expression both IGFN1\_V1-tdTomato and MLTK $\beta$ -GFP). Although the intensity of MLTK $\beta$ -GFP expression is not as strong as that of IGFN1\_V1-tdTomato, nuclear expression of MLTK $\beta$ -GFP could be clearly distinguished over background levels (see an example Figure 4.3D showing a confocal optical section at the level of two nuclei expressing IGFN1\_V1-tdTomato in the same fibre; only one of these nuclei shows clear MLTK $\beta$ -GFP expression). Since nuclear localization of MLTK $\beta$  was not observed in fibres transfected with only MLTK $\beta$ -tdTomato (figures in chapter 3 figure 3.6), it is plausible that IGFN1\_V1-tdTomato drives MLTK $\beta$ -GFP into the nucleus in co-transfected fibres.

To confirm this, IGFN1\_V1-tdTomato expressing muscles were dissected, fixed with 4% PFA, sectioned and immuno-stained with anti-MLTK antibody (Anti-MLTK Rabbit polyclonal antibody, PROTEINTECH EUROPE) and FITC conjugated secondary antibody. The IGFN1\_V1-tdTomato showed localization in both the Z-disc and the nucleus (Figures 4.3 E and F), the immunostaining results show strong green signal in nuclei, which are positive for IGFN1\_V1-tdTomato (arrows in figure 4.3E and F label MLTK expressing nuclei). This signal was not observed in non-transfected fibres or with secondary antibody only (figure 4.3G, yellow

arrows label a fibre without IGFN1-tdTomato expression and MLTK nucleus accumulation), supporting the notion that IGFN1\_V1-tdTomato also drives endogenous MLTK $\beta$ -GFP into the nucleus.



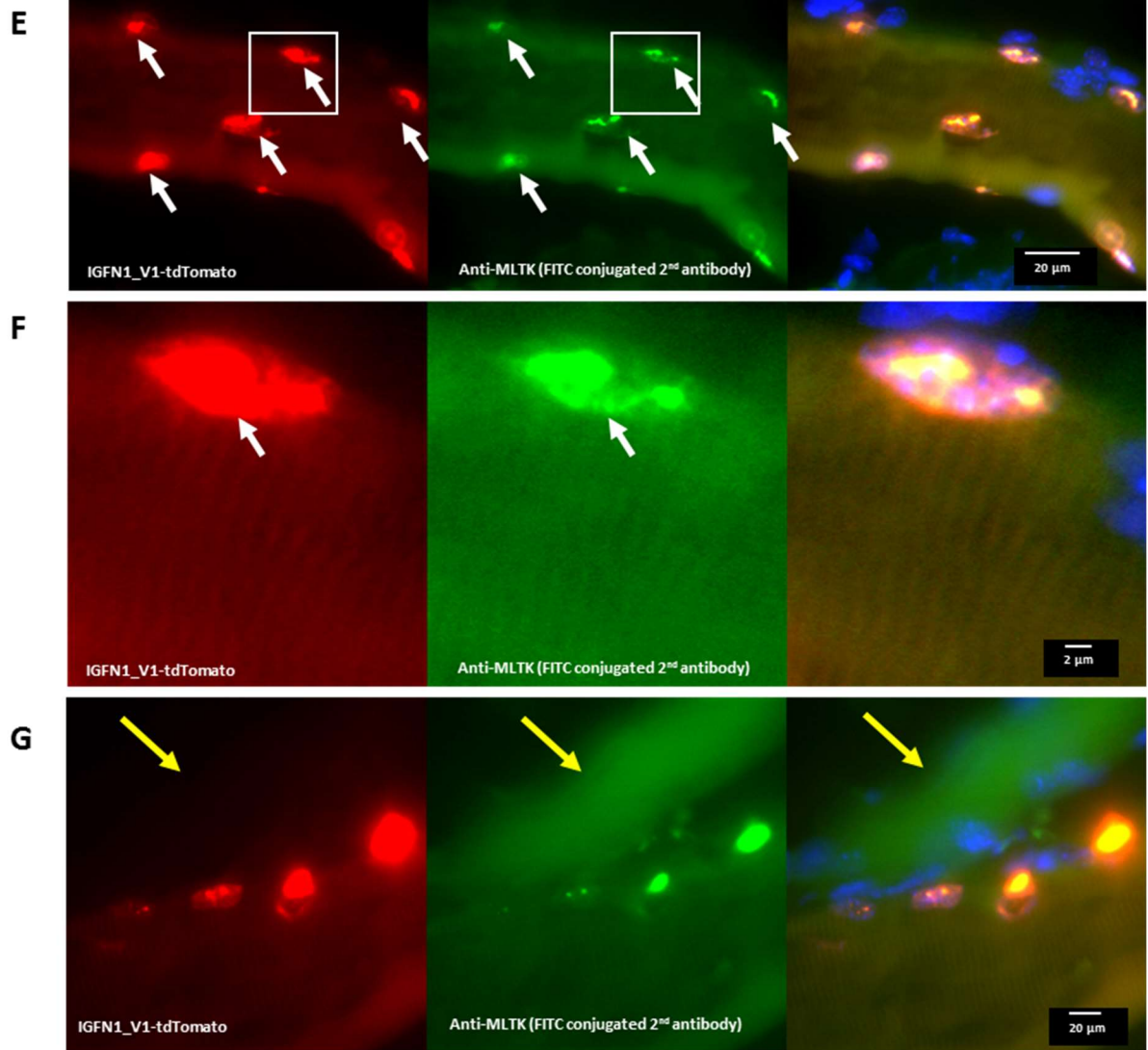


Figure 4.3: Electroporation of IGFN1\_V1-tdTomato and MLTK $\alpha$ -GFP or MLTK $\beta$ -GFP in EDL/TA muscle in vivo.

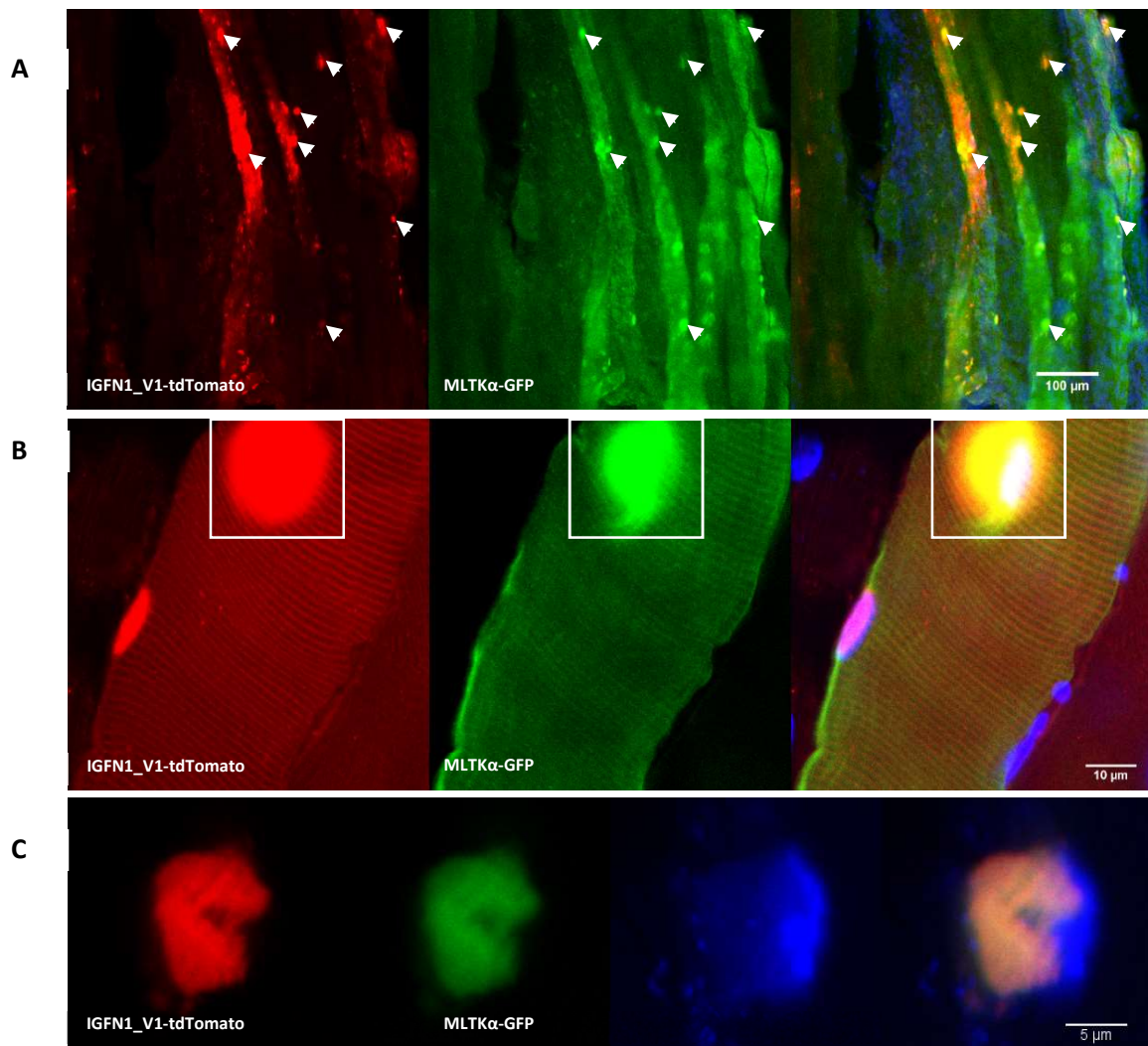
(A), Illustrative confocal microscope images from an EDL/TA muscle fibre showing expression of IGFN1\_V1-tdTomato and MLTK $\alpha$ -GFP. Arrow points at a nucleus expressing IGFN1\_V1-tdTomato. Note the absence of MLTK $\alpha$ -GFP expression in this nucleus. (B), Co-localization analysis of IGFN1\_V1-tdTomato and MLTK $\alpha$ -GFP from a co-transfected fibre done by ImageJ. White pixels indicate co-localization of red and green pixels. (C), Illustrative confocal microscope images from an EDL/TA muscle fibre showing expression of IGFN1\_V1-tdTomato and MLTK $\beta$ -GFP. Arrows label nuclei expressing both IGFN1\_V1-tdTomato and MLTK $\beta$ -GFP. (D), Co-localization analysis of IGFN1\_V1-tdTomato and MLTK $\beta$ -GFP from inset shown in C (white square) using ImageJ. Arrows label nuclei expressing both IGFN1\_V1-tdTomato and MLTK $\beta$ -GFP, and white pixels show co-localization of green and red pixels. In A, B, C and D, mice were sacrificed after 7 days of expression and the muscles were dissected and prepared as whole mounts. (E), immunostaining of IGFN1\_V1-tdTomato expressing fibre with MLTK antibody and FITC conjugated secondary antibody. (F), Detailed view from the white square in figure E. Arrows in E and F label nuclei that contains IGFN1\_V1-tdTomato and endogenous MLTK. (G), immunostaining of IGFN1\_V1-tdTomato expressing fibre with MLTK antibody and FITC conjugated secondary antibody. The fibre labelled with yellow arrow has not been transfected with IGFN1\_V1-tdTomato, and the endogenous MLTK did not accumulate in the nucleus of this fibre. In E, F and G, mice were sacrificed after 7 days of expression, IGFN1\_V1-tdTomato expressing muscles were dissected, fixed with 4% PFA, sectioned and immuno-stained with anti-MLTK antibody (Anti-MLTK Rabbit polyclonal antibody, PROTEINTECH EUROPE) and FITC conjugated secondary antibody. All the mice used in this figure were injected at age of 5-8 weeks. All the experiments described above were repeated more than three times, the images shown above are representative images.

#### 4.2.4 Co-expression of IGFN1\_V1-tdTomato with MLTK $\alpha$ -GFP or MLTK $\beta$ -GFP causes both proteins to become aggregated around nuclei in skeletal muscle

A phenotype was observed in previous sections, in which co-expression of IGFN1\_V1-tdTomato and MLTK $\alpha$ -GFP or MLTK $\beta$ -GFP showed colocalization in large patches in the fibres. Arrows in figure 4.4A and D label some of the apparent aggregations showing strong fluorescence in both red and green channels. This expression pattern was not observed in IGFN1\_V1-tdTomato, MLTK $\alpha$ -GFP or MLTK $\beta$ -GFP single transfections. Figure 4.4B and E show that the fluorescence intensity of aggregations is much stronger than fluorescence intensity in the Z-disc or in nucleus, indicating higher accumulation of these proteins in these putative aggregates than in the Z-disc or nucleus. These patches seem to be located in or around the nucleus (Figure 4.4C). Because the fluorescence intensity of these patches (figure 4.4B and E) is too high to define their morphology and exact distribution, figures 4.4C and F were captured under a reduced exposure time. This views showed that these patches are not within the nucleus but around it. The reason why these patches formed and locate around the nuclei is still unknown.

Usually, newly generated polypeptides need to fold into a distinct three-dimensional conformation and go through further modifications to form a functional protein <sup>76</sup>. If even a small mistake occurs during protein folding, it may result in misfolded proteins which are prone to form aggregates <sup>77</sup>. One estimate is that up to 30% of newly generated proteins are not folded properly <sup>78</sup>. Overexpression of a large amount of high molecular weight recombinant proteins in muscle cells possibly results in mass of misfolded proteins production. Because IGFN1\_V1 and MLTK proteins are interaction partners, the interactions may still exist between misfolded IGFN1\_V1 and MLTK recombinant proteins, and this may increase the

possibility of forming protein aggregations. This may explain that the aggregations are only observed in the co-expression fibres rather than in IGFN1\_V1-tdTomato, MLTK $\alpha$ -GFP or MLTK $\beta$ -GFP singly expressing fibres. Misfolded proteins are usually recognized by ubiquitin E3 ligases, which form polyubiquitinated protein and lead to proteasome-mediated protein degradation <sup>79</sup>. To test whether these aggregations are caused by protein misfolding, an antibody against ubiquitin can be used to immunostain ubiquitin in IGFN1\_V1-tdTomato and MLTK $\alpha$ -GFP or MLTK $\beta$ -GFP co-expression fibres in order to determine whether ubiquitin localizes at these patches.



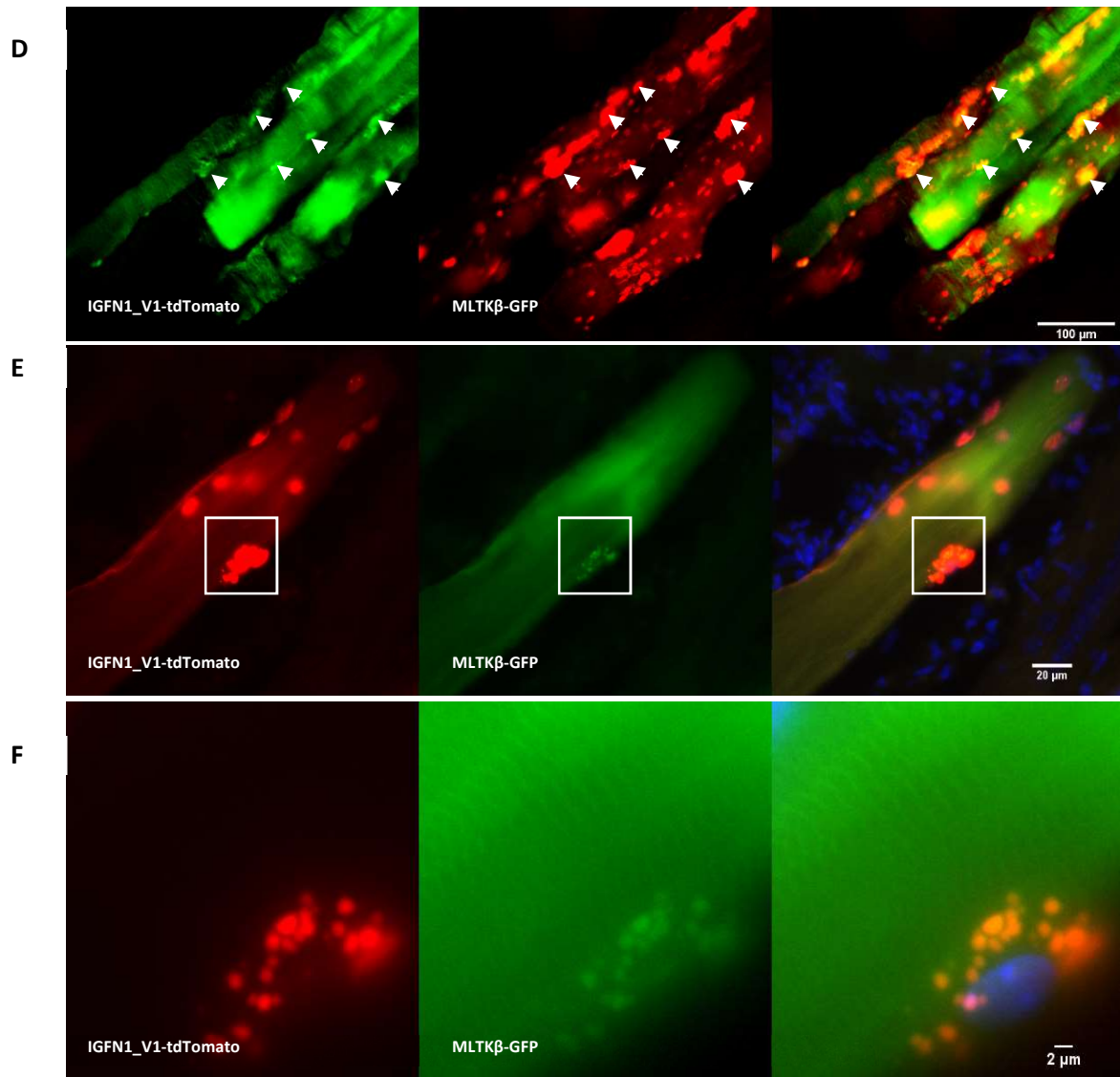


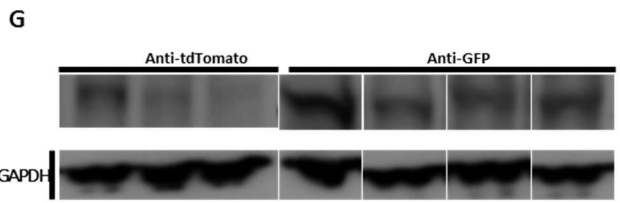
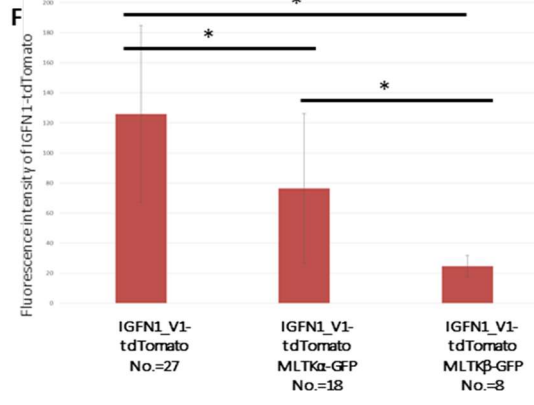
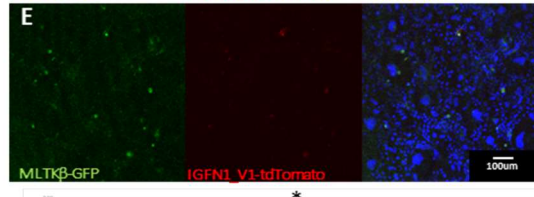
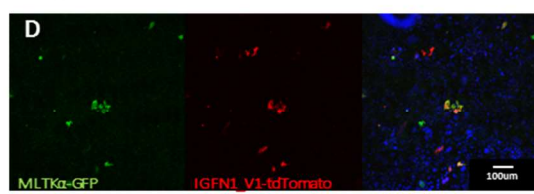
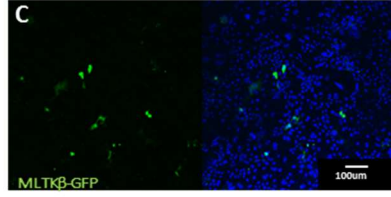
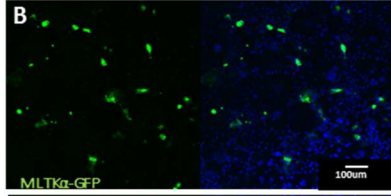
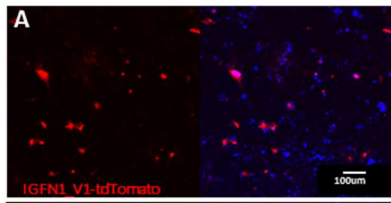
Figure 4.4: Co-expression in vivo of IGFN1\_V1-tdTomato with MLTK $\alpha$ -GFP or MLTK $\beta$ -GFP causes apparent aggregations of the recombinant proteins.

(A), Co-expression of IGFN1\_V1-tdTomato and MLTK $\alpha$ -GFP in skeletal muscle by electroporation. Image was captured under the 10x magnification. Arrows label putative aggregates. (B), Detail of a muscle fibre expressing both IGFN1\_V1-tdTomato and MLTK $\alpha$ -GFP taken at 60x magnification. White square labels a putative aggregate. (C), Detailed view of the square inset in image B, the exposure time of image C was reduced to visualize the morphology of aggregation. (D), Co-expression of IGFN1\_V1-tdTomato and MLTK $\beta$ -GFP in skeletal muscle by electroporation. Image was captured under the 10x magnification. Arrows label putative aggregations. (E), muscle fibre expressing both IGFN1\_V1-tdTomato and MLTK $\beta$ -GFP at 40x magnification. White square labels a cluster of putative aggregates. (F), magnified image from inset in E, the exposure time of image F was reduced to visualize the morphology of the patches. Electroporations in this figure use 5-8 weeks old mice sacrificed after 7 days of expression of recombinant proteins. The electroporated EDL/TA muscles were dissected, sectioned or prepared as whole mounts to obtain fluorescence images. Blue colour in this figure is DAPI stained nuclei. All the experiments described above were repeated more than three times, the images shown above are representative images.

#### 4.2.5 Co-expression of IGFN1\_V1-tdTomato with MLTK $\alpha$ -GFP or MLTK $\beta$ -GFP in COS7 leads to decreased IGFN1\_V1-tdTomato expression

A phenotype was observed in the pull down assays from COS7 cells in that IGFN1\_V1-tdTomato expression was highly reduced when co-expressed with MLTK $\alpha$ -GFP or MLTK $\beta$ -GFP. To confirm this observation, the same amount of IGFN1\_V1-tdTomato was singly-transfected or co-transfected with MLTK $\alpha$ -GFP or MLTK $\beta$ -GFP in COS7 cells. After 48 hours, transfected cells were fixed with 4% PFA and fluorescence images were obtained with the same exposure time and magnification. Figures 4.5A-E, show that both the fluorescence intensity and the number of IGFN1\_V1-tdTomato expressing cells are reduced in IGFN1\_V1-tdTomato and MLTK $\alpha$ -GFP co-transfected cells when compared to single transfections of IGFN1\_V1-TdTomato. The same was also true in IGFN1\_V1-tdTomato and MLTK $\beta$ -GFP co-transfected cells. Quantifications of fluorescence intensity of IGFN1\_V1-tdTomato in single transfection and co-transfected cells confirmed this previous observation (figure 4.5F). Western blotting (figure 4.5G) showed that reduction of IGFN1\_V1-tdTomato expression is most apparent when IGFN1\_V1-tdTomato is co-transfected with MLTK $\beta$ -GFP. Statistical analysis of this blot combined with another two blots (not shown), confirmed that IGFN1\_V1-tdtomato expression level significantly decreases when co-expressed with MLTK $\alpha$ -GFP or MLTK $\beta$ -GFP (figure 4.5H). Co-expression does not affect MLTK $\alpha$ -GFP or MLTK $\beta$ -GFP expression levels compared to MLTK $\alpha$ -GFP or MLTK $\beta$ -GFP single transfections (figure 4.5I and J). To prove that reduced IGFN1\_V1-tdTomato expression is not caused by MLTK $\alpha$ -GFP or MLTK $\beta$ -GFP expression increasing cell death, the cell death rate was calculated in cells transfected with IGFN1\_V1-tdTomato and co-transfections of IGFN1\_V1-tdTomato with MLTK $\alpha$ -GFP or MLTK $\beta$ -GFP. The results show that there was no significant cell death rate difference between

the transfection experiments (Figure 4.5K). The aim of this project is to study the function of IGFN1 and MLTK in skeletal muscle. Because the COS7 cells is not a muscle cell line, and the expression reduction of IGFN1\_V1-tdTomato has not been observed in IGFN1\_V1-tdTomato and MLTK $\alpha$ -GFP or MLTK $\beta$ -GFP co-expressed fibres, the cause of IGFN1\_V1-tdTomato expression reduction when co-transfected with either MLTK in the context of COS7 cells remains unclear and was not explored further.



IGFN1V1-tdTomato: + + + - + - +  
 MLTKα-GFP: - + - + - + -  
 MLTKβ-GFP: - - + - - + +

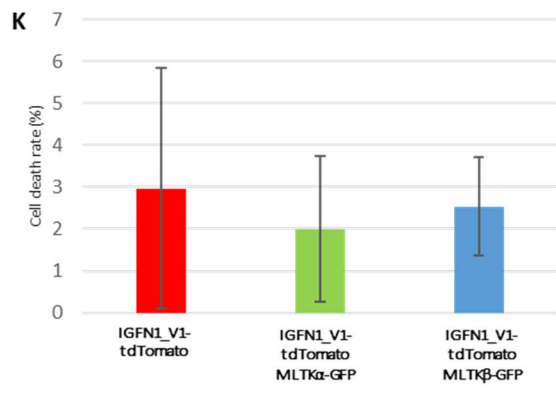
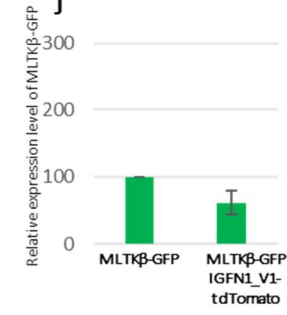
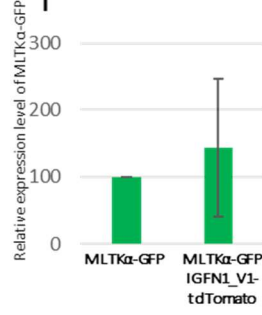
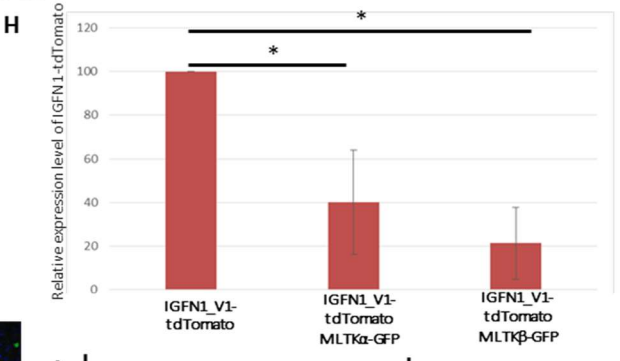


Figure:4.5 Co-expression of IGFN1\_V1-tdTomato with MLTK $\alpha$ -GFP or MLTK $\beta$ -GFP in COS7 cells. Fluorescence images A-C represent IGFN1\_V1-tdTomato (A), MLTK $\alpha$ -GFP (B) or MLTK $\beta$ -GFP (C) singly transfected COS7 cells. (D), fluorescence images of COS7 cells co-transfected with IGFN1\_V1-tdTomato and MLTK $\alpha$ -GFP. (E), fluorescence images of COS7 cells co-transfected with IGFN1\_V1-tdTomato and MLTK $\beta$ -GFP. All the fluorescence images (A-E) obtained with the same exposure time and magnification. (F), fluorescence intensity measurements of IGFN1\_V1-tdTomato expressing cells on the fluorescence images such as A, D and E. The results calculated from three independent experiments (N=3). Red numbers in this figure represent the number of IGFN1\_V1-tdTomato expressed cells in each measurement. (G), Western blots using anti-tdTomato and anti-GFP antibodies on COS7 extracts from IGFN1\_V1-tdTomato single transfection or co-transfection of IGFN1\_V1-tdTomato with MLTK $\alpha$ -GFP or MLTK $\beta$ -GFP. (H), a histogram showing the average expression level of IGFN1\_V1-tdTomato in transfected cells as indicated. (I and J), a histogram showing expression levels of MLTK $\alpha$ -GFP and MLTK $\beta$ -GFP in transfected cells as indicated. The results presented in figure H and I are calculated from three independent experiments (N=3). (K), cell death rate quantifications in transfected cells as indicated. Trypan Blue was used to stain the dead cells, and the cells were counted by using a haemocytometer. The results are calculated from three independent experiments (N=3). Error bars represents the standard deviation of the measurement. \*represents significant difference calculated by a T-test. (p $\leq$ 0.05)

### 4.3 CONCLUSION

The aim of this chapter was to explore *in vitro* interactions and co-localization of ectopically overexpressed IGFN1\_V1 and MLTK $\alpha$  or MLTK $\beta$ . A previous Y2H study found that fragments of IGFN1 interact with fragment of MLTK common to both isoforms <sup>4</sup>. These Y2H assays did not explore specific interactions between full IGFN1 and MLTK isoforms. To address whether full-length isoforms interact, an immunoprecipitation experiment was done using IGFN1-v5 or IGFN1\_V1-v5 and MLTK $\alpha$ -GFP or MLTK $\beta$ -GFP recombinant proteins co-transfected COS7 cells. The immunoprecipitation results confirmed that IGFN1\_V1-v5 interacts with both MLTK $\alpha$ -GFP and MLTK $\beta$ -GFP. Due to the difficulty of expressing the large IGFN1-v5 [ $\sim$ 303kDa] in COS7 cells at sufficient levels, the interactions between IGFN1-v5 and MLTK $\alpha$ -GFP or MLTK $\beta$ -GFP have not been fully examined. These limitations meant that subsequent work focused on interactions between IGFN1\_V1 and MLTK $\alpha$  or MLTK $\beta$ .

Since the interactions have been demonstrated between IGFN1\_V1-v5 and MLTK $\alpha$ -GFP or MLTK $\beta$ -GFP, the next experiment was to study where the interaction site(s) are in IGFN1\_V1. This was performed by a placement student, Matthew Winder. The results showed that all the *E.coli*-produced his-tagged IGFN1\_V1, IGFN1<sub>(d1-d3)</sub> and IGFN1<sub>(d8-d11)</sub> are able to interact with both MLTK $\alpha$ -GFP and MLTK $\beta$ -GFP produced from transfected COS7 cells. This indicated that more than one interaction sites exist, one in the 1<sup>st</sup> to 3<sup>rd</sup> globular domains and the other in the 8<sup>th</sup> to 11<sup>th</sup> globular domains of IGFN1\_V1.

To test whether IGFN1\_V1-tdTomato and MLTK $\alpha$ -GFP or MLTK $\beta$ -GFP interactions occur in skeletal muscle, IGFN1\_V1-tdTomato was co-expressed with MLTK $\alpha$ -GFP or MLTK $\beta$ -GFP by electroporating constructs expressing these proteins in mouse EDL/TA muscle. The results showed that IGFN1\_V1-tdTomato co-locates with MLTK $\alpha$ -GFP or MLTK $\beta$ -GFP in the Z-disc

(figure 4.3). Meanwhile, MLTK $\beta$ -GFP was found to be co-located with IGFN1\_V1-tdTomato in the nucleus, the nuclear localization was not observed in a fibres expressing MLTK $\beta$  recombinant protein alone. An anti-MLTK antibody on sections of IGFN1\_V1-tdTomato expressing fibres showed that endogenous MLTK accumulates in nucleus, suggesting that IGFN1\_V1-tdTomato drives MLTK $\beta$  into the nucleus.

A distinctive phenotype with co-transfection of TA/EDL muscle was that co-expression IGFN1\_V1-tdTomato with either MLTK $\alpha$ -GFP or MLTK $\beta$ -GFP caused both proteins to form patches or cluster of small apparent aggregates around the nucleus. These putative aggregates were not observed in IGFN1\_V1-tdTomato, MLTK $\alpha$ -GFP or MLTK $\beta$ -GFP single transfections. The cause of these aggregations remains unclear and was not explored further. However, since these have not been observed with other ectopically expressed proteins using the same vectors (e.g., GFPmax, tdTomato, KY-v5, etc.), it is likely that these aggregates reflect an increased tendency for interacting proteins to form insoluble aggregates when co-transfected. Given IGFN1 has multiple MLTK interaction domains, high levels of expression of both proteins may cause the formation of large protein complexes, which promote aggregate formation.

# Chapter 5

## RESULTS

### 5. Quantifications of MLTK isoforms in skeletal muscle

## 5.1 INTRODUCTION

Previous northern blot experiments identified that MLTK is highly expressed in heart and skeletal muscle in humans. The probe used in this experiment was a 1022 bp MLTK cDNA fragment amplified from mouse tissue using a cDNA Subtraction kit. This 1022 bp fragment was also used to clone mouse MLTK $\alpha$  and MLTK $\beta$  isoforms by 5' and 3' RACE (Rapid amplification of cDNA ends)<sup>53</sup>. Given that the 1022 bp fragment was amplified from a region common to both MLTK $\alpha$  and MLTK $\beta$ , using this fragment as a probe in northern blotting experiments is able to identify both MLTK $\alpha$  and MLTK $\beta$  isoforms. The northern blot revealed high expression of a ~7.5kb isoform in heart and skeletal muscle, corresponding to the known sequence length of MLTK $\beta$  indicating that MLTK $\beta$  is the primary isoform in these tissues in humans. Another northern blot using isoform specific probes identified that MLTK $\beta$  also highly expressed in skeletal muscle and heart. it also identified that MLTK $\beta$  intermediately expressed in lung, placenta and small intestine and lesser expressed in other tested tissues. Moreover, MLTK $\alpha$  was found that it highly expressed in liver, intermediately expressed in other tested tissues except the brain and leukocytes<sup>53</sup>. The second northern blot results is not fully compatible with the first one. To address this issue, this chapter identifies the expression levels of MLTK $\alpha$  and MLTK $\beta$  in mouse skeletal muscle by real time PCR (RT-PCR).

## 5.2 RESULTS

### 5.2.1 Real-time PCR primer selection

In order to study the expression levels of MLTK $\alpha$  and MLTK $\beta$  in mouse skeletal muscle by RT-PCR, primer pairs were designed to target isoform-specific regions of MLTK $\alpha$  and MLTK $\beta$ . Figure 5.1A shows that all 4 primers pairs were designed to span exon-exon junctions to avoid amplification from genomic sequence. The annealing temperatures of these primers are all between 58 °C and 60 °C. The sequences of these primers are shown in figure 5.1B. The primer sequences used for the housekeeping gene hypoxanthine-guanine phosphoribosyl transferase (HPRT) were selected from the literature and have been widely used in many publications, e.g.,<sup>80</sup>. To test whether these primers are able to specifically amplify only the target PCR products, polymerase chain reaction (PCR) was performed on mouse muscle cDNA. The results show that only one strong DNA band is produced for each primer pair, which is of the expected size (figure 5.1C). The negative control reaction, using water in place of DNA template, produced no product (figure 5.1D), indicating that the PCR products in figure 5.1C are not the result of non-specific amplifications, primer-dimers or contamination.

Differences in primer sequence and product size can result in large variations in amplification efficiency, which can confound the interpretation of RT-PCR results. To avoid this, primer efficiency tests were performed to select the primer pairs with similar amplification efficiency. In this test, cDNA templates were diluted several times to build standard curves and calculate primer efficiency. The dilutions were 10 ng/reaction, 7 ng/reaction, 4 ng/reaction and 1 ng/reaction. The results showed that the efficiency of MLTK $\alpha$  primer pair 1 is 118.763%,

MLTK $\alpha$  primer pair 2 is 105.099%, MLTK $\beta$  primer pair 1 is 104.224% and MLTK $\beta$  primer pair 2 is 98.557% (100% efficiency represents that the PCR product of interest is doubling with each cycle during the logarithmic phase.). Based on these results, MLTK $\alpha$  primer pair 2 and MLTK $\beta$  primer pair 1 were selected to perform RT-PCR test in skeletal muscle.

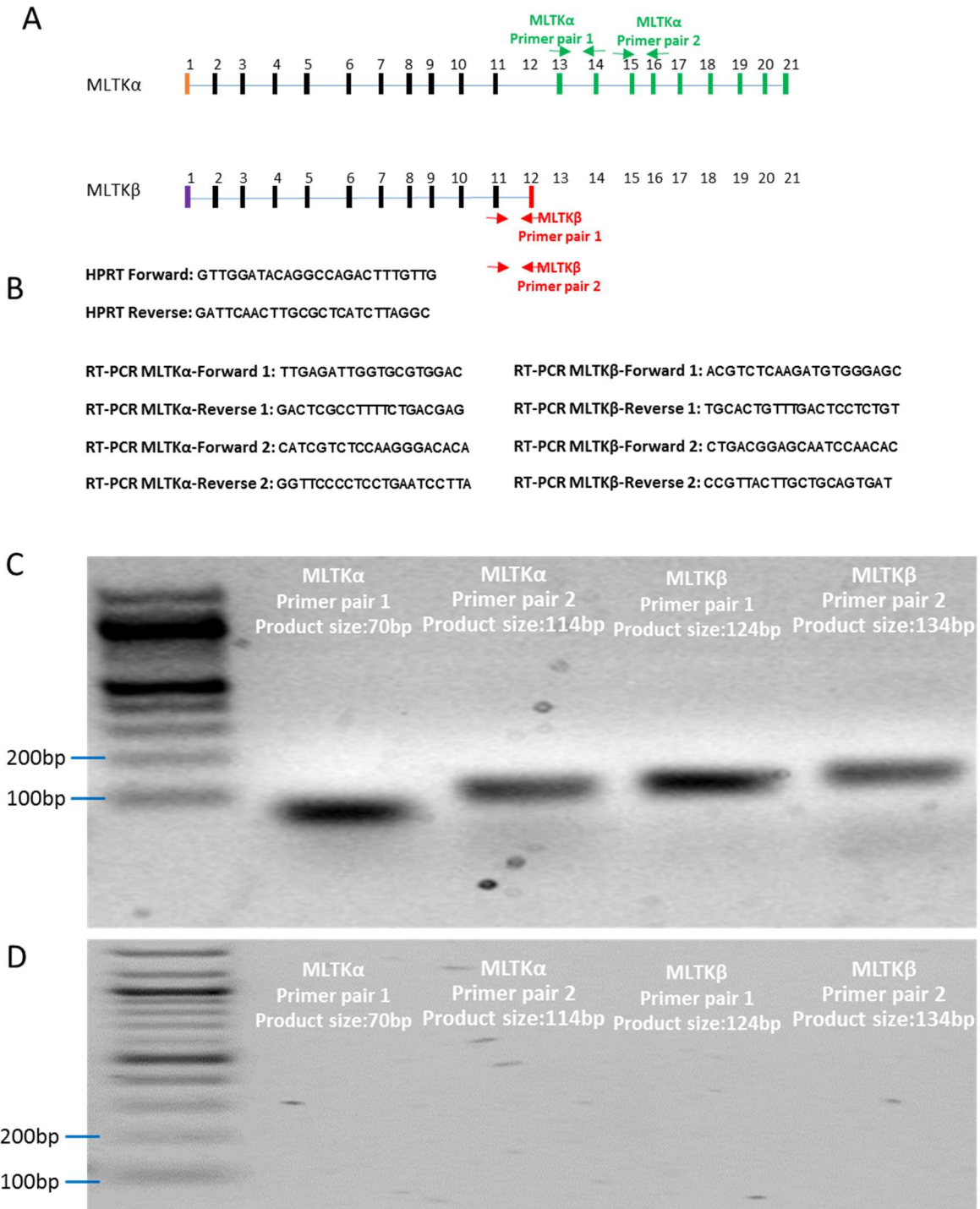


Figure 5.1: RT-PCR primer pair design and amplification test.

(A), Exon position schematics of MLTK $\alpha$  and MLTK $\beta$ , arrows represent RT-PCR primers. (B), RT-PCR primer sequences of HPRT (housekeeping gene), MLTK $\alpha$  and MLTK $\beta$ . (C), Standard PCR test of RT-PCR primers shows specific amplification of the target sequence from cDNA. (D), No template controls confirm that products from C do not result from contamination and non-specific amplifications. The gels used in C and D are 2% agarose gel. Electrophoresis runs at 80v for 30 mins.

## 5.2.2 MLTK $\beta$ is the primary isoform in mouse skeletal muscle

To perform real-time PCR (RT-PCR), three mice were sacrificed and the hindlimb skeletal muscles were dissected to provide tissue for mRNA extraction. cDNA was converted from mRNA, and the cDNA concentration of each sample was measured, diluted to the same concentration and mixed with primers and SYBR Green Master Mix to form RT-PCR reactions on an optical 96 well plate. Each reaction was performed in triplicate and plates were run and analysed on the StepOnePlus machines using a Fast PCR protocol. During the amplification, SYBR Green dye binds to the double stranded DNA and emits fluorescence light, which is detected by the plate reader. The fluorescence intensity increases with DNA amplifications, as this results in higher levels of double stranded DNA. The level of fluorescence will cross a threshold after a certain number of amplification cycles. This number of cycles is defined as the Ct value, which is used to calculate fold changes in target gene expression compared to the control. The equations show below were used for these calculations.

$$\text{Fold Change} = 2^{-\Delta(\Delta C_T)}$$

$$\Delta C_T = C_{T_{\text{target}}} - C_{T_{\text{HPRT}}}$$

$$\Delta(\Delta C_T) = \Delta C_{T_{\text{stimulated}}} - \Delta C_{T_{\text{control}}}$$

Here, target represents MLTK $\alpha$  or MLTK $\beta$ .  $\Delta C_{T_{\text{stimulated}}}$  is  $C_{T_{\text{MLTK}\alpha}} - C_{T_{\text{HPRT}}}$  or  $C_{T_{\text{MLTK}\beta}} - C_{T_{\text{HPRT}}}$ .

$\Delta C_{T_{\text{control}}}$  is  $C_{T_{\text{HPRT}}} - C_{T_{\text{HPRT}}} = 0$ . In this test, HPRT not only represents a housekeeping gene used to calculate the relative expression levels of the MLTK isoforms, it also represents an internal control as the fold change of HPRT between individual samples ought to be 1 (indicating no expression changes of the housekeeping gene between samples).

The RT-PCR results show that the expression level of MLTK $\alpha$  is 14.7 times lower than HPRT in skeletal muscle, but the expression level of MLTK $\beta$  is 4.38 times higher than HPRT (figure 5.2). The result also shows that the expression level of MLTK $\beta$  is 64.4 times ( $4.38/0.068=64.4$ ) higher than MLTK $\alpha$  expression in mouse skeletal muscle. The results therefore indicate that MLTK $\beta$  is the primary isoform in mouse skeletal muscle.

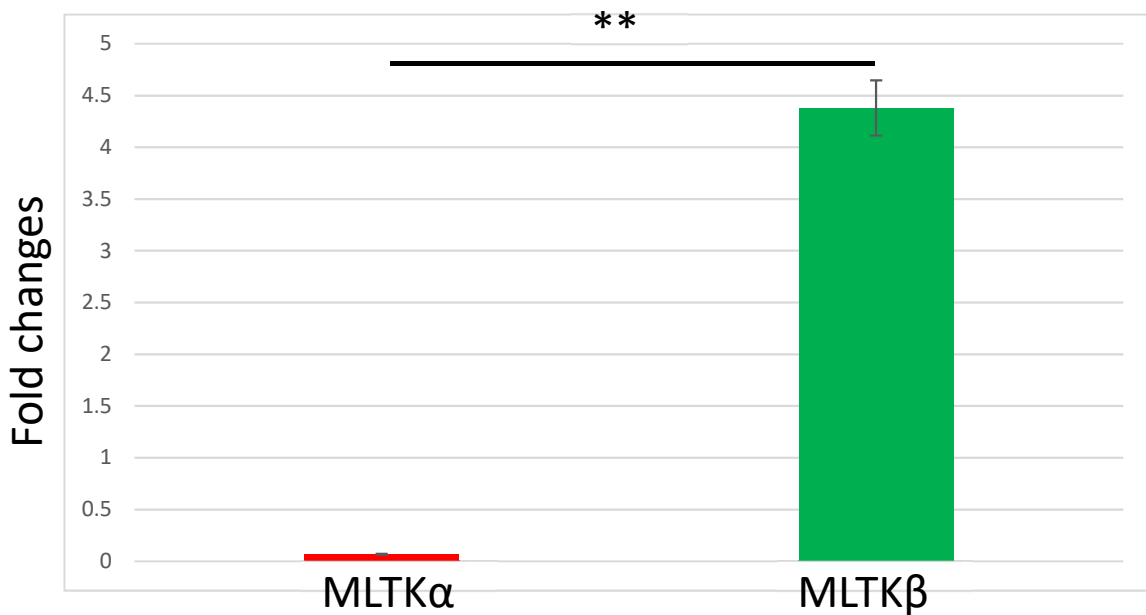


Figure 5.2: Real-time PCR quantification of MLTK $\alpha$  and MLTK $\beta$  relative expression levels in mouse skeletal muscle.

The primer sequences and efficiency tests are shown in 5.2.1. The relative expression level of MLTK $\alpha$  or MLTK $\beta$  were calculated by normalizing the data to HPRT expression (assuming that HPRT expression level is 1). Error bars represent the standard deviation of three independent cDNA templates. \*\* represents  $P \leq 0.001$ .

### 5.3 CONCLUSIONS

The aim of this chapter is to quantify the expression levels of MLTK $\alpha$  and MLTK $\beta$  in mouse skeletal muscle by RT-PCR and thereby determine the primary isoform. The primers used in this experiment were selected by PCR and primer efficiency tests from 4 primer pairs. The

results show that all these primer pairs are able to specifically amplify the target sequence. MLTK $\alpha$  primer pair 2 and MLTK $\beta$  primer pair 1 have highly similar efficiency and were therefore selected to test MLTK $\alpha$  and MLTK $\beta$  expression levels in mouse skeletal muscle. The RT-PCR result showed that the expression level of MLTK $\beta$  is 64.4 times higher than MLTK $\alpha$  in mouse skeletal muscle, indicating that MLTK $\beta$  is the primary isoform. This indicates that MLTK $\beta$  may be the more physiologically important isoform, and therefore experiments in this project have focused on the role of this isoform in skeletal muscle.

# Chapter 6

## RESULTS

### 6. Effects of MLTK $\beta$ and IGFN1\_V1 overexpression on muscle fibre size and morphology

## 6.1 INTRODUCTION

Previous MLTK studies found that transgenic overexpression of MLTK $\beta$  in mouse heart tissue results in cardiac hypertrophy<sup>5</sup>, and overexpression of MLTK $\alpha$  in H9c2 cardiomyoblast cells induces hypertrophic growth<sup>54</sup>. MLTK was also found to be upregulated in the *ky/ky* mutant mouse model of recessive, hereditary kyphoscoliosis which is unable to undergo compensatory hypertrophy<sup>50</sup>. These results indicate that MLTK proteins may be functionally related to hypertrophic growth in the heart.

Chapter 1 has shown that MLTK is located at the Z-disc in skeletal muscle. Given that skeletal muscle shares many structural and physiological properties with cardiac muscle, including sarcomeric structures such as the Z-disc, the role of MLTK might be conserved between these two tissues. Therefore, one aim of this chapter is to evaluate whether overexpression of MLTK protein is able to induce hypertrophic growth in skeletal muscle.

The expression level of IGFN1 is upregulated during muscle atrophy caused by short term denervation<sup>45</sup> or activin A treatment<sup>46</sup> and is downregulated in hypertrophic muscle resulting from ActRIIB-Fc treatment<sup>48</sup>. This shows that IGFN1 expression levels correlate inversely to skeletal muscle growth and thus indicates that IGFN1 may be involved in the regulation or mediation of hypertrophic/atrophic signalling pathways. To investigate more about the correlations between IGFN1 expression levels and changes in skeletal muscle mass, the second aim of this chapter is to test the effects of IGFN1 overexpression on fibre size in skeletal muscle.

## 6.2 RESULTS

### 6.2.1 *In vivo* overexpression of MLTK $\alpha$ -tdTomato or MLTK $\beta$ -tdTomato induces muscle fibre growth

To test whether overexpression of MLTK protein is able to induce hypertrophic growth in skeletal muscle, DNA constructs encoding MLTK $\alpha$ -tdTomato or MLTK $\beta$ -tdTomato were injected into mouse EDL/TA muscle and transfected via *in vivo* electroporation. After allowing the construct to express for seven or nineteen days (extended expression over nineteen days was used to examine whether long-term overexpression will cause different morphology changes), mice were sacrificed and the electroporated muscles were dissected. Tissue samples were briefly fixed in 4% PFA and snap frozen in liquid nitrogen-cooled isopentane prior to cryostat sectioning. Images were obtained from cross sections by confocal microscopy (figure 6.1A, B and C). The red fluorescent fibres in Figure 6.1 A, B and C indicate fibres expressing MLTK $\alpha$ -tdTomato, MLTK $\beta$ -tdTomato and tdTomato respectively. Transfected fibres are labelled with yellow circles, and untransfected fibres are labelled with blue circles. An increase in fibre cross-sectional area can be observed in fibres expressing MLTK $\alpha$ -tdTomato and MLTK $\beta$ -tdTomato but not in fibres expressing tdTomato.

Comparison of fibre cross-sectional area between different muscles and mice is difficult as the location of fibres within the muscle that have been efficiently transfected can vary due to placement of the electrodes and the site of DNA injection. As there is a high level of variation in cross-sectional area in different regions of a muscle, noise associated with comparing between mice may mask modest size differences between transfected and untransfected

fibres. Therefore, the fibre size changes caused by construct overexpression can be only accurately obtained between transfected and un-transfected fibres in same region of a single muscle.

MLTK $\alpha$ -tdTomato was overexpressed in two mice, MLTK $\beta$ -tdTomato was overexpressed in three mice, and another three mice were used to overexpress tdTomato as a control for any changes in fibre size associated with the transfection protocol. All the mice used in this experiment are male and between 5-8 weeks old. The results show that the cross-sectional area of fibres overexpressing either MLTK $\alpha$ -tdTomato or MLTK $\beta$ -tdTomato is significantly increased compared with untransfected fibres. Overexpression of the tdTomato control does not result in increased cross-sectional area (figure 6.1 D, E and F). This indicates that overexpression of either MLTK $\alpha$ -tdTomato or MLTK $\beta$ -tdTomato can induce hypertrophic growth in mouse skeletal muscle.

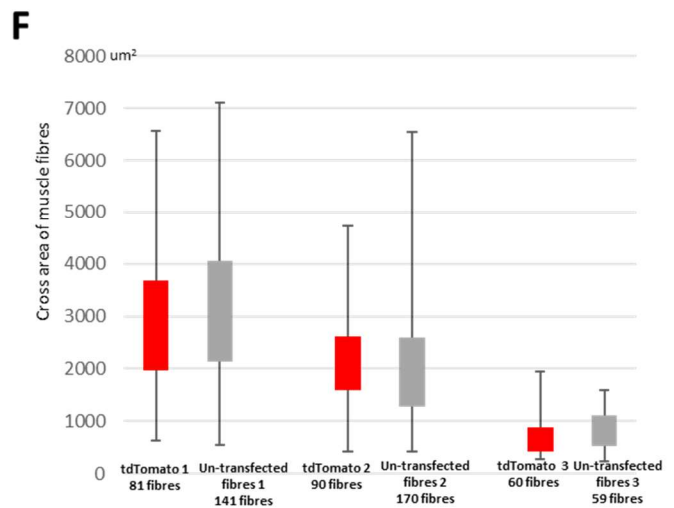
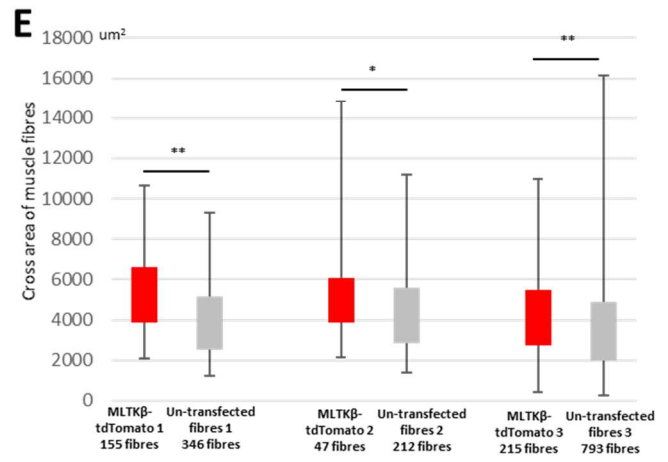
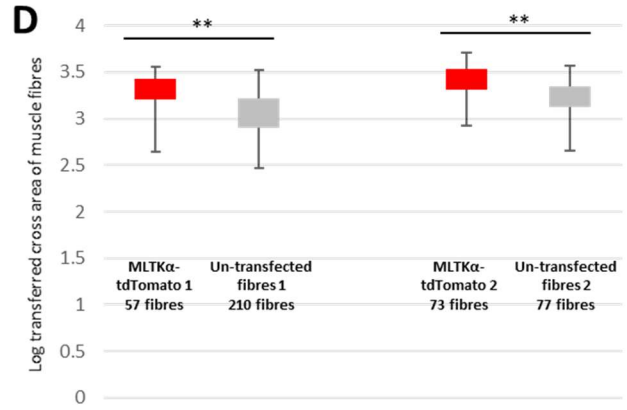
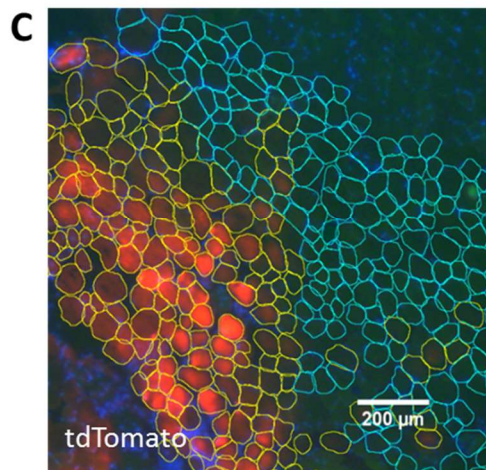
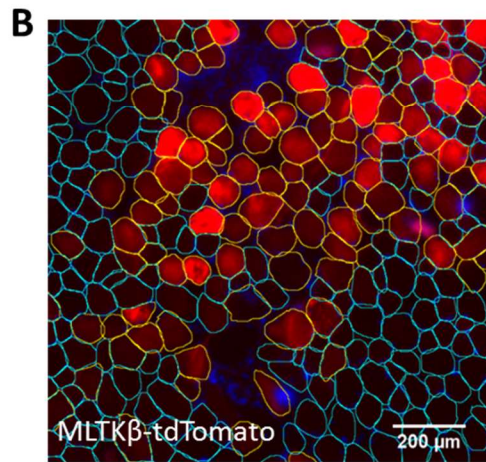
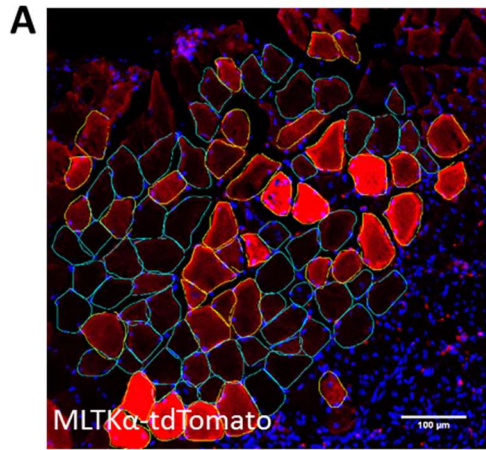


Figure 6.1: Overexpression of MLTK proteins in mouse skeletal muscle increases fibre cross-sectional area.

(A), (B) and (C) represent fibres expressing MLTK $\alpha$ -tdTomato, MLTK $\beta$ -tdTomato and tdTomato respectively for 7 days. Yellow circles indicate successfully transfected fibres showing red fluorescence. Blue circles label untransfected fibres. (D)-(F), Box-and-whisker diagrams describe fibre size (cross-sectional area) comparison between (D) MLTK $\alpha$ -tdTomato, (E) MLTK $\beta$ -tdTomato, or (F) tdTomato overexpressing fibres and untransfected fibres. Red boxes represent the cross-sectional area between upper and lower quartiles of MLTKs-tdTomato transfected fibres. Grey boxes represent the cross-sectional area between upper and lower quartiles of un-transfected fibres. The number of measured fibres was labelled in the figure. Error bars represent variability outside the upper and lower quartiles. \* represent  $P \leq 0.05$  and \*\* represents  $P \leq 0.001$ . Electroporations shown in this figure used 5-8 weeks old mice sacrificed after 7 days (or 19 days, MLTK  $\beta$  -tdTomato 3 and its control) of expression of target proteins. The electroporated EDL/TA muscles were dissected, sectioned or prepared as cross sections to obtain fluorescence images.

### 6.2.2 *In vivo* overexpression of MLTK $\beta$ -tdTomato causes changes in muscle fibre morphology

The results above demonstrate that overexpression either MLTK $\alpha$ -tdTomato or MLTK $\beta$ -tdTomato induces hypertrophic growth in mouse skeletal muscle. Additionally, overexpression of either of these proteins caused morphological changes in some transfected fibres (arrows in figure 6.2A and B label some of these fibres). Fluorescence intensity in the centre of the fibre is not strong as in the periphery. This ring-like appearance gives such fibres the classification of “ring fibres” (figure 6.2 A and B, yellow arrows label “ring fibres”). To test whether the number of ring fibres and the number of MLTK $\beta$ -tdTomato overexpression fibres fit a linear law, these two sets of data were counted in four different transfection areas. The result shows that these two set of numbers follow the linear law, which indicates that the appearance of ring fibres positively correlates with the number of MLTK $\beta$ -tdTomato overexpression fibres (figure 6.2 E). Ring fibres have been reported in denervated muscle and central core disease. In both instances, disorganized filaments are contained within the fibres<sup>81</sup>. Myosin and desmin are key structural components of the myofibril and maintain the mechanical integrity of the contractile apparatus in muscle tissue<sup>31,82</sup>. To test whether the “ring fibres” observed in muscles overexpressing MLTK proteins also contain disorganized filaments, cross sections containing fibres overexpressing MLTK $\beta$ -tdTomato were immunostained with desmin or myosin antibodies and FITC conjugated secondary antibody. The results demonstrated that the “ring fibres” associated with MLTK overexpression also show evidence of disorganised filaments from both desmin and myosin antibody staining. This indicates that overexpression MLTK $\beta$ -tdTomato may affect muscle fibre morphology by changing the organisation of filaments.

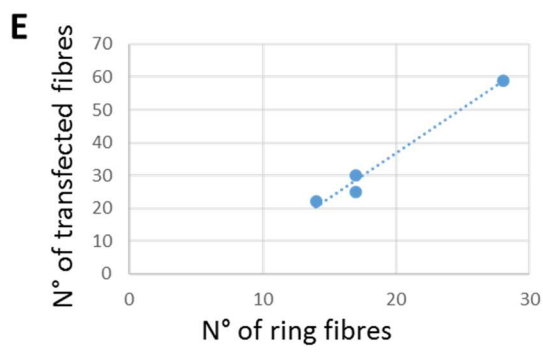
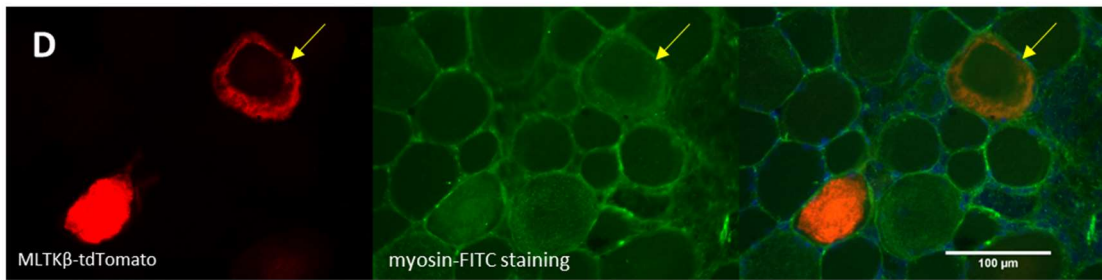
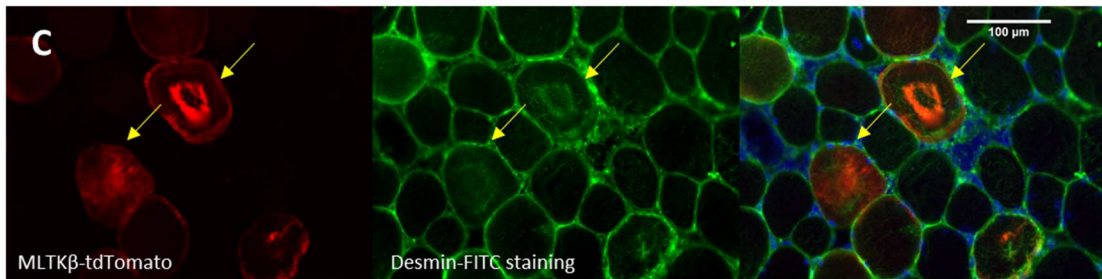
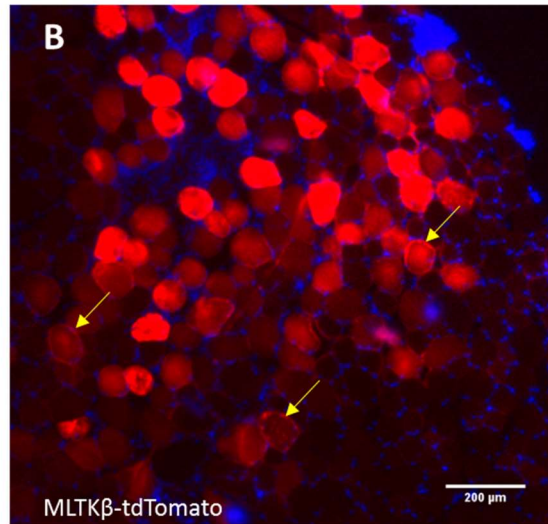
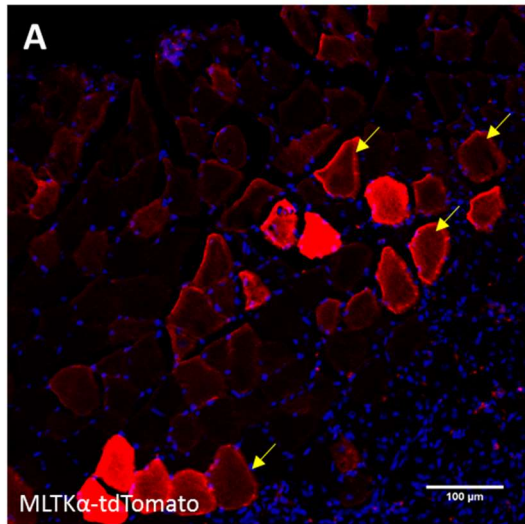


Figure 6.2 overexpression of MLTK $\beta$ -tdTomato causes muscle fibre morphology changes in mouse skeletal muscle.

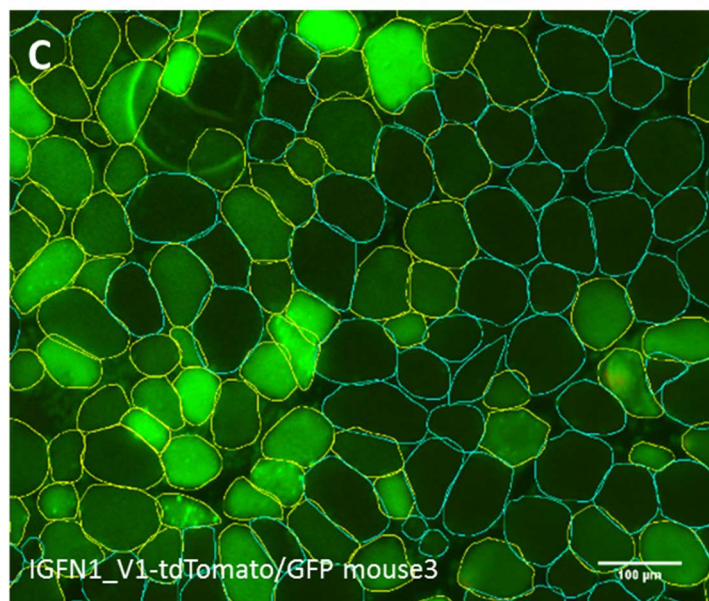
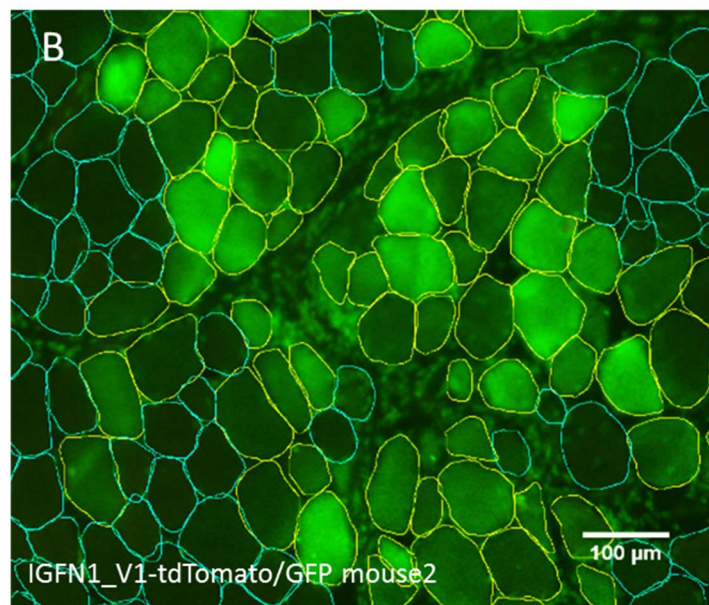
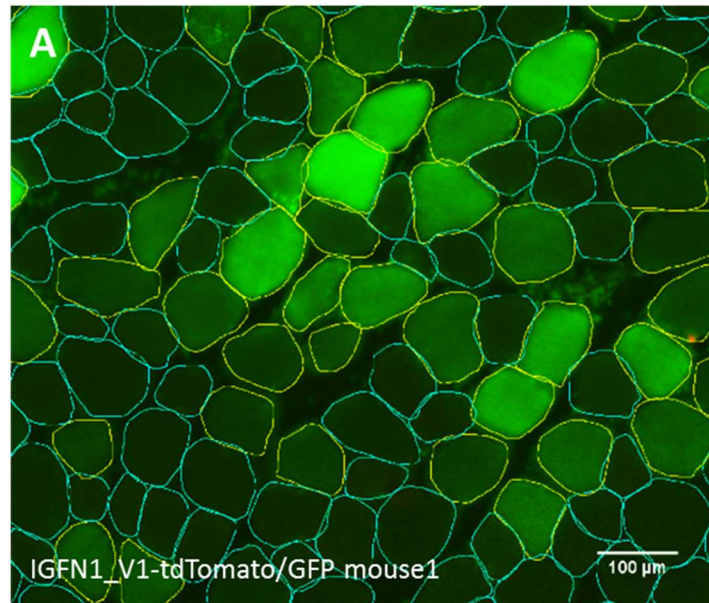
(A) and (B), Cross sections of fibres expressing MLTK $\alpha$ -tdTomato or MLTK $\beta$ -tdTomato respectively. (C) and (D), immunostaining of cross sections of skeletal muscle overexpressing MLTK $\beta$ -tdTomato with desmin (C) or myosin (D) antibodies and FITC conjugated secondary antibody. Arrows in these figure are used to label “ring fibres”. (E), the scatter chart compares the number of ring fibres and the number of transfected fibres. The line shows that the relation of the two is approximately linear.

### 6.2.3 overexpression of IGFN1\_V1-tdTomato in mouse skeletal muscle

To investigate more about the correlations between IGFN1 expression level and muscle fibre size changes, DNA constructs encoding IGFN1\_V1-tdTomato and GFP were injected into mouse EDL/TA muscle and transfected via electroporation to examine the effects of IGFN1\_V1-tdTomato overexpression. Because IGFN1\_V1-tdTomato expression is not easy to observe in cross sections, GFP acts as an extra fluorescence marker to label the transfected fibres. The details of sample preparation are same as in section 6.2.1, with mice left to express the construct for 7 days before being sacrificed and dissected. Three sibling mice were used to compare fibre cross sectional area between fibres overexpressing IGFN1\_V1-tdtomato and un-transfected fibres within the same region of muscle.

The results show that overexpression of IGFN1\_V1-tdTomato caused inconsistent fibre size changes in mouse skeletal muscle. In mouse 1, IGFN1\_V1-tdTomato overexpression significantly increased muscle fibre size compared with untransfected fibres, and there was no significant fibre size difference between IGFN1\_V1-tdTomato transfected fibres and un-transfected fibres in mouse 2. Overexpression IGFN1\_V1-tdTomato statistically decreases muscle fibre size in mouse 3.

To eliminate the possibility that the inconsistent results were caused by effects of GFP overexpression, GFP alone was electroporated into right hind limbs of three mice whose left hind limbs were used to overexpress both IGFN1\_V1-tdTomato and GFP. The results show that overexpression of GFP alone does not affect fibre size in any of the three mice, indicating that the inconsistency of fibre size changes observed in IGFN1\_V1-tdTomato overexpression experiments does not result from effects of GFP overexpression.



D

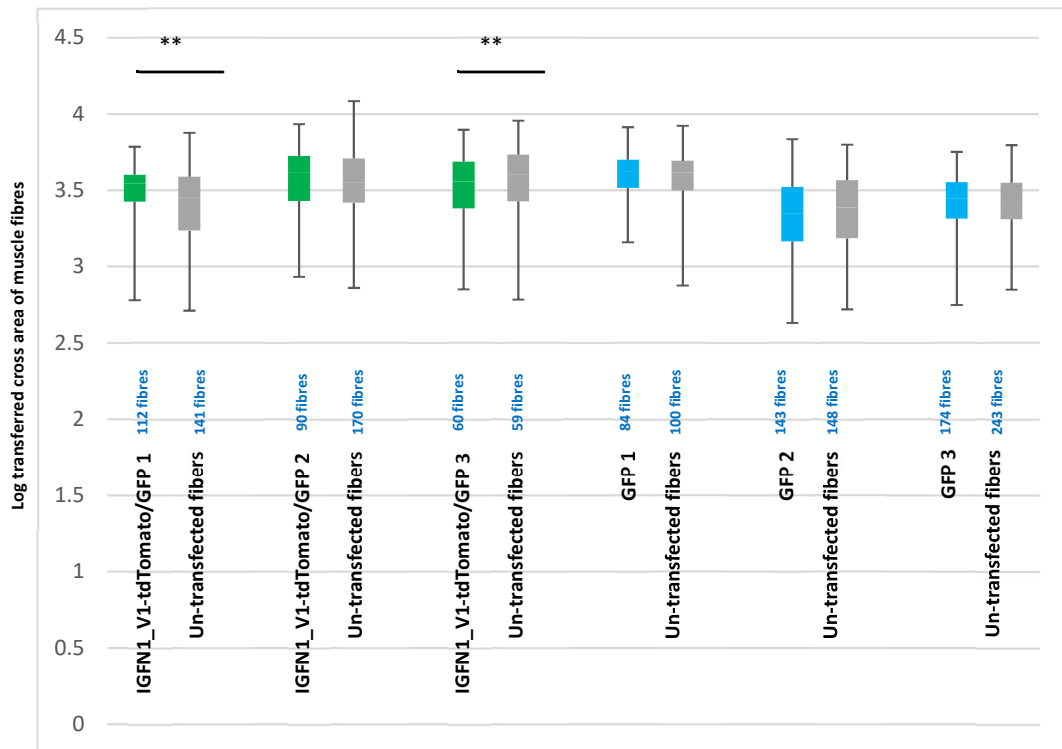


Figure 6.3: Overexpression of IGFN1\_V1-tdTomato and GFP in skeletal muscle.

(A)-(C), Overexpression of IGFN1\_V1-tdTomato and GFP in mouse EDL/TA muscles via *in vivo* electroporation, (A), (B) and (C) represents individual electroporations on three sibling male mice. Yellow circles indicate successfully transfected green fluorescent fibres. Blue circles label untransfected fibres. (D) Box-and-whisker diagrams describe fibre size (cross-sectional area) comparison between IGFN1\_V1-tdTomato/GFP co-transfected or GFP transfected fibres and un-transfected fibres. Green boxes represent the cross-sectional area between upper and lower quartiles of IGFN1\_V1-tdTomato and GFP co-transfected fibres. Blue boxes represent the cross-sectional area between upper and lower quartiles of GFP transfected fibres. Grey boxes represent the cross-sectional area between upper and lower quartiles of un-transfected fibres. The number of measured fibres is labelled in the figure. Error bars represent variability outside the upper and lower quartiles. \*\* represents  $P \leq 0.001$ .

### 6.3 CONCLUSIONS

This chapter aims to study the effects of MLTK $\beta$  and IGFN1\_V1 overexpression on muscle fibre morphology in skeletal muscle. Results show that overexpression either MLTK $\alpha$ -GFP or MLTK $\beta$ -GFP induces fibre size increases, indicating that MLTK is functionally related to muscle hypertrophic growth.

Meanwhile, “ring fibres” were found in muscles overexpressing MLTK $\alpha$ -tdTomato and MLTK $\beta$ -tdTomato. The number of ring fibres positively correlates with the number of MLTK $\beta$ -tdTomato overexpression fibres. Desmin and myosin antibody immunostaining of cross sections of muscle overexpressing MLTK $\beta$ -tdTomato shows that the myofibril structure has been changed in these ring fibres. Previous study utilizing transgenic overexpression of MLTK $\beta$  in mouse heart tissue results in cardiac hypertrophy, the heart shows fibrosis and disorganized myofibril<sup>5</sup>. All these evidence suggest that the overexpression of MLTK $\beta$ -tdTomato affects the morphology of muscle fibres by changing the orientation of filaments.

Overexpression of IGFN1\_V1-tdTomato and GFP in mouse skeletal muscle caused inconsistent fibre size changes in three sibling mice. GFP control overexpression in the same mice showed that overexpression of GFP alone does not affect muscle fibre size, which proves that the inconsistency is not the result of GFP expression. The cause of the inconsistent IGFN1\_V1-tdTomato overexpressed fibre size changes in different mice are still unclear.

IGFN1 proteins consist of immunoglobulin (Ig) and fibronectin type III domains (Fn3)<sup>4</sup>, these globular domains are the key components of a group of muscle proteins associated with the contractile apparatus of muscles, such as titin<sup>83</sup>, this indicates that the function of IGFN1 may relate to muscle contractility. It is possible that the muscle fibre size regulation by IGFN1\_V1

is stimulation dependent. The stimulation includes mechanical force and exercise. In IGFN1\_V1-tdTomato overexpression experiments, some mice may be running more, and other mice running less, during their daily life, which may lead to different amount of mechanical stimulation in each mouse. This may result in the inconsistent IGFN1 overexpression fibre size changes observed in different mice. In order to test this hypothesis, a future experiment may control for this variable using a certain regimen of exercise or denervation in the IGFN1\_V1-tdTomato overexpressing mice to test whether the IGFN1 induction of muscle fibre size changes is stimuli dependent.

Because IGFN1 V1-tdTomato expression is not easy to observe in cross sections, GFP acts as an extra fluorescence marker to label the transfected fibres. This experiment assumed that all fibres expressing GFP are also expressing IGFN1\_V1 at significant levels. In fact, the electroporation may not consistently perform at the same transfection efficiency in different mice, and IGFN1\_V1-tdTomato [ $\sim 189\text{kDa}$ ] is a large protein compared to GFP [ $\sim 27\text{kDa}$ ], which makes GFP expression easier than IGFN1\_V1-tdTomato expression. These reasons may result to IGFN1\_V1-tdTomato expression level difference in three mice. If muscle fibre size changes are dependent on IGFN1\_V1-tdTomato expression reaching a certain level, variance in IGFN1\_V1-tdTomato expression may lead to inconsistent fibre size changes.

Due to the technical restrictions, such as the fact that IGFN1\_V1-tdTomato cannot be easily observed in muscle cross sections and the transfection efficiency cannot be controlled, this experiment was not explored further.

# Chapter 7

## RESULTS

### 7. CRISPR/Cas mediated IGFN1\_V1 gene editing *in vitro* and *in vivo*

## 7.1 INTRODUCTION:

Overexpression of IGFN1\_V1 in mouse skeletal muscle induced inconsistent fibre size changes, and therefore was not able to provide any clear functional insights into the role of IGFN1\_V1. In order to explore the effects of IGFN1 deficiency, CRISPR/Cas9 technology was used to generate a knockout C2C12 myoblast model. In addition, *in vitro* delivery of the CRISPR/Cas components into mouse skeletal muscle was attempted to try and knock down IGFN1\_V1 in muscle fibres.

## 7.2 RESULTS

### 7.2.1 IGFN1 CRISPR/Cas functional characterization

Clustered regularly interspaced short palindromic repeats/CRISPR-associated proteins (CRISPR/Cas) were found in bacteria and archaea functioning as an adaptive immune system against the genomic integration of foreign DNA<sup>84</sup>. CRISPR/Cas technology is an efficient tool to perform genome engineering, and this technology was selected to knock out IGFN1 *in vitro* and attempt to knock IGFN1 expression down *in vivo*.

Two plasmids were generated to perform the IGFN1 knock out by GeneCopoeia Inc. The first plasmid is used to express Cas9 protein and sgRNA, which includes guide RNA and a region complementary to the genomic target sequence in IGFN1. The sgRNA guides Cas9 protein to the target sequence and the Cas9 nuclease then generates a double-strand break (DSB) in the IGFN1 gene (figure 7.1 A and B). DSBs can be repaired by either non-homologous end joining

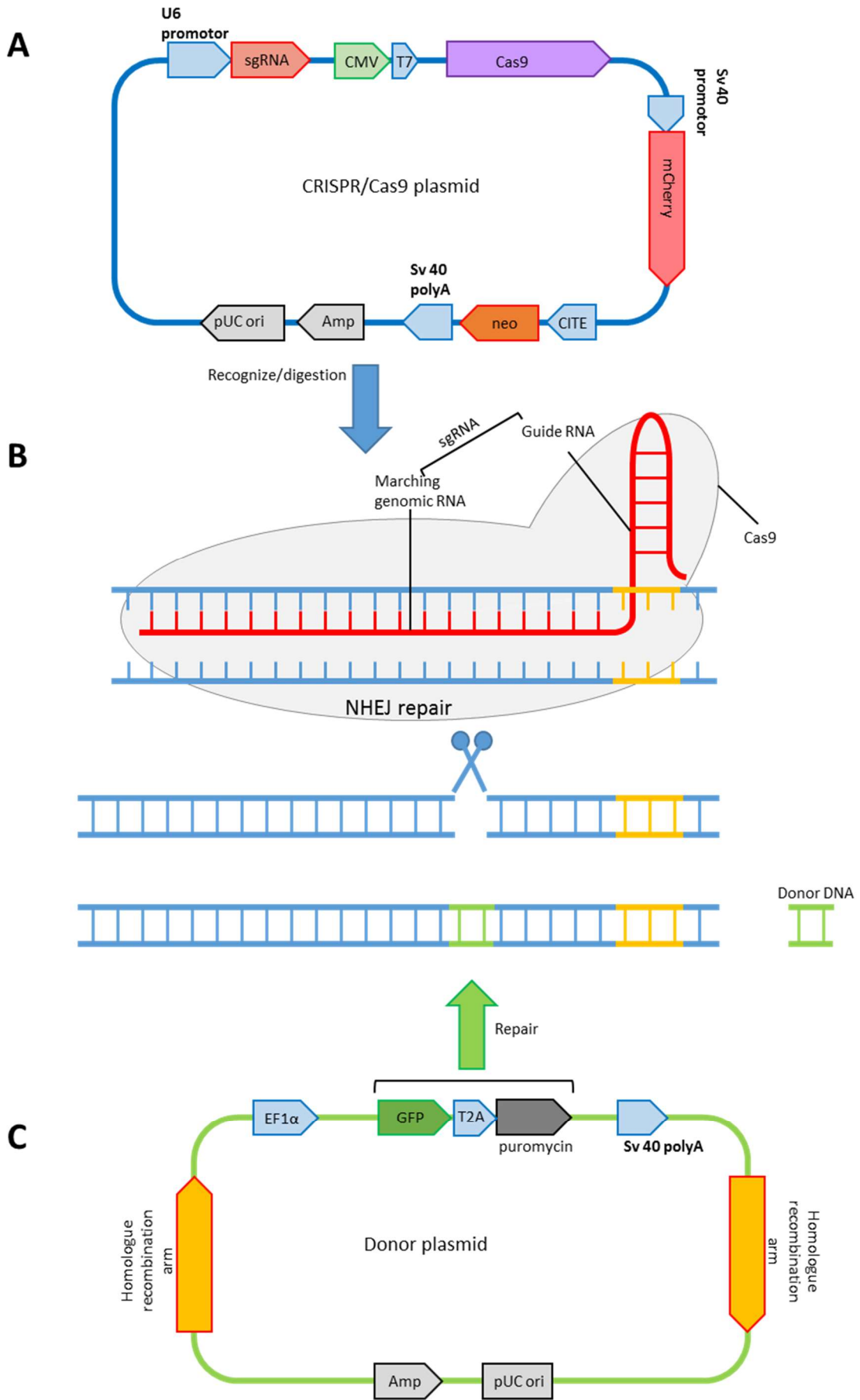
(NHEJ) (figure 7.1D) or by homologous recombination (HR) (figure 7.1E). The second plasmid provides a homologous repair template to promote repair via the HR pathway, and also contains a puromycin selection marker and an eGFP reporter gene (See fig 17.E). Therefore, puromycin selection is expected to enrich for cells that have IGFN1 mutated through homologous recombination. These cells will also show eGFP fluorescence.

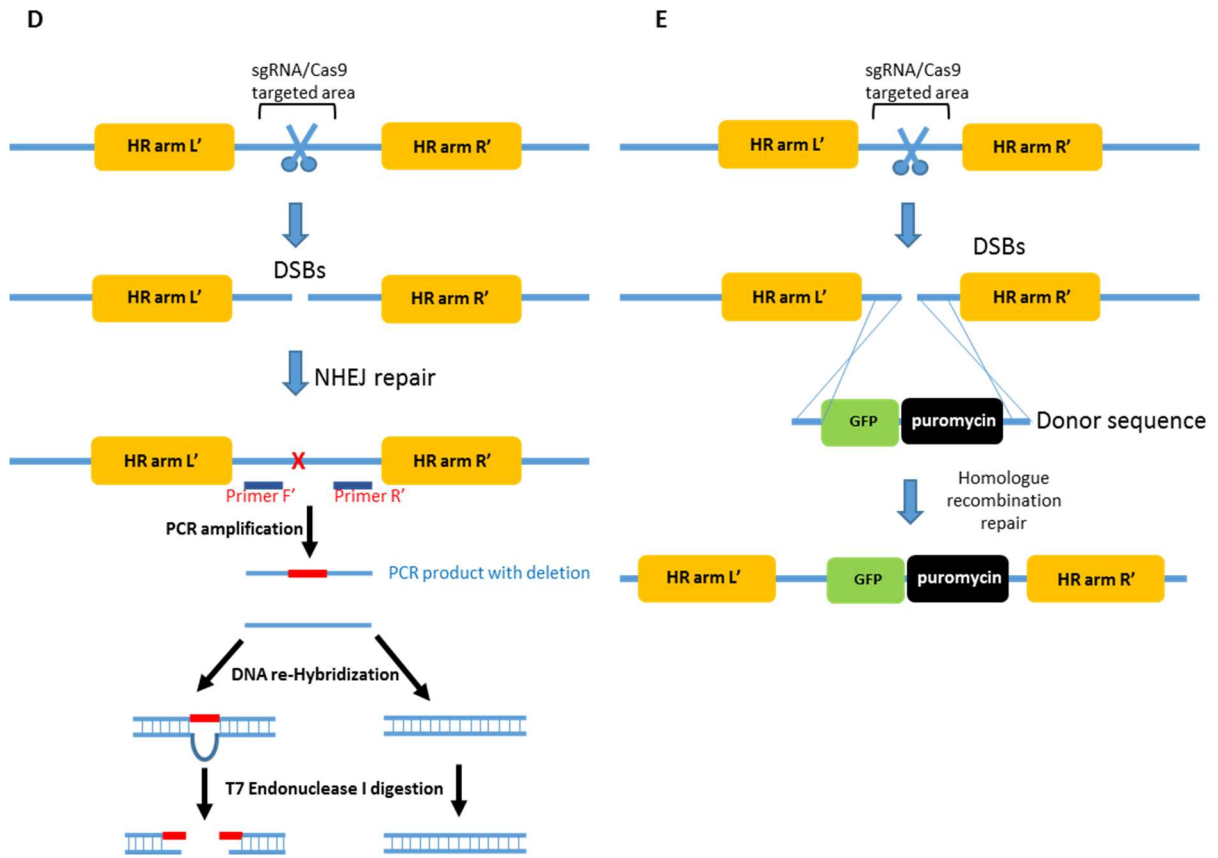
In this experiment, the IGFN1 CRISPR/Cas was designed to target sequence within exon 13 of *Igfn1*. The reason for targeting this exon is because it is common to both of *Igfn1* longest isoforms, *Igfn1* and *Igfn1\_v1*. Moreover, the number of bases in exon 13 is not a multiple of 3, meaning that even if an alternative splicing process eliminates this exon, the downstream sequence will be frame-shifted and cannot be translated into the correct IGFN1 sequence (figure 7.1H and I).

Before the IGFN1 knock out cell line selection, the targeting efficiency of the vector was tested using a mismatch cleavage assay. For this assay, 3T3 cells were used because they have a higher transfection efficiency than C2C12 cells, and are therefore better suited for an initial test of the efficacy of the vector. 3T3 cells were grown in a T25 flask to ~90% confluency before transfection. 12ug of IGFN1 CRISPR/Cas plasmid was transfected into 3T3 cells using GenJet in vitro DNA transfection reagent. Cells were harvested after 48 hours post-transfection. This assay is based on the NHEJ repair pathway, which is error prone and will generate insertions or deletions randomly during the repair of the DSB. CRISPR/Cas transfected cells will contain a mix of non-targeted (untransfected cells plus transfected cells in which targeting did not occur) and mutated alleles. PCR from the cell lysate will therefore contain a mixture of WT and mutated PCR products. The target region was amplified by PCR. The PCR products were subjected to DNA re-hybridization followed by T7 endonuclease I

(T7ENI) digestion. When mutated PCR product combines with non-mutated PCR product, it will form a mismatch bubble that will be detected and cleaved by T7ENI, resulting in the formation of cleavage products (figure 7.1D).

The results of the IGFN1 CRISPR/Cas mismatch cleavage assay is shown in figure 7.1G. The expected PCR product is ~852 bp. T7ENI digestion should produce bands of ~505 bp and ~347 bp (sites of the CRISPR target sequence are shown in green box of figure 7.1F). In this assay, only IGFN1 CRISPR/Cas treated 3T3 cells showed two digestion products (see red arrows). No digestion bands were seen in the control untransfected 3T3 cells. The intensity of each band was measured by ImageJ. The result shows that nearly 54% of PCR product was digested by T7ENI. These results indicated that the IGFN1 CRISPR/Cas can efficiently mutate IGFN1 in the designed target area.

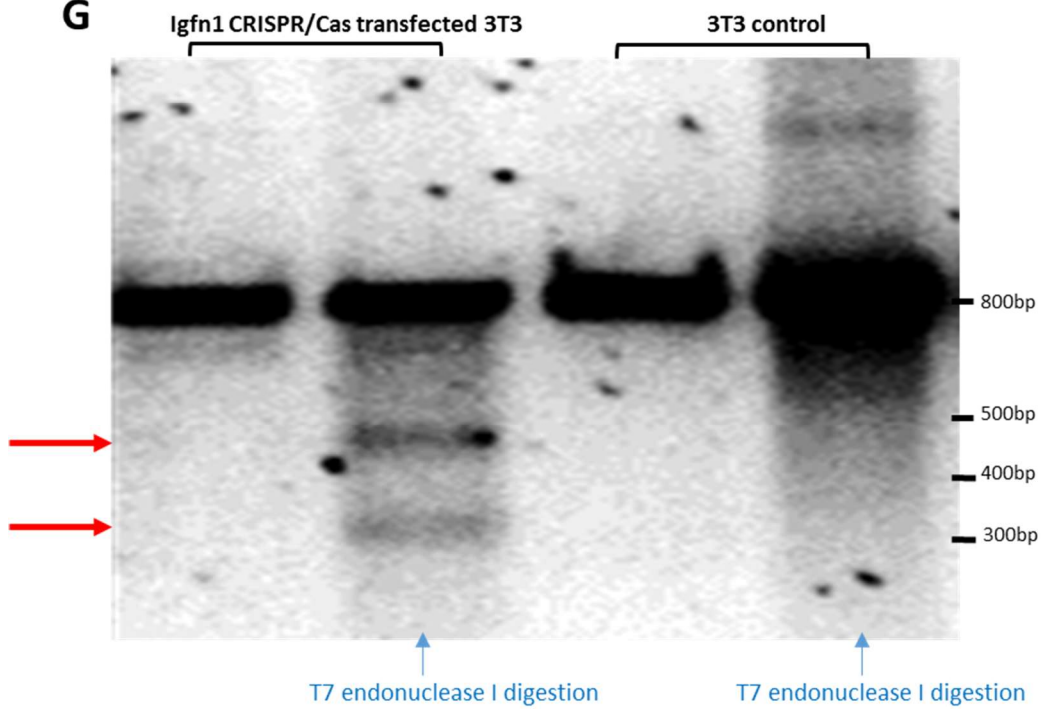




**F**

```
cgggcagctgataagtgtagcgattgtcaattcttgcaagtagcaaactatataatggcttagcaaggatgagtgatgtataaatg
actacattttgtgcatccctggagacattctctgaacatttctggatgattgaatgagctcatagcatgacctctctgctaacacaga
ggctctgtaacaactctctccaagcacaactgtatcagcaatctcagatgtctctgcatatagggcatagtttccactcatgggaa
gtggctggacatccctagaacgtatattccagctacctcatgacctaccctccacatccacgctctgctctgacctggctcaciaa
ccccacatctttatggttctaggatcatgtgtctttgacctggccagtaaccagattgaggctaggataggaggtctttggaccaca
ctgaggccctgaaccatccttctggttcaggatggtgagatgattccctacgggtgtgataaccagaccgaagcactgtctgagac
ggctggggaagcgctaccacttcagatccaggacctgcgccctgaggatgctggccttaccagggtcatggtggaggatgctgt
ggtctctctacagagctagaatccagaagtgagtattcttaccagaggtctgcagaggggaggggagggggtccatgctgtg
ttatggagtgggatacatgcccaggtgcattgcaaaagacaactaggaagagggatacaccagatcctcctgttggtaccaca
gctggaactctacagagtgattgagggacacagtcatatgatgacatgcctctgcccaca
```

**G**



H



I

```

GCCTTAAGCTAGACATTAGTCCCGGGCCTCAGCTTCTTAATTTTTGAAATAAAGGATCAGAAGAGCTACCTCATAGAATACTGCAATGCCAAA
TGACACTGTGCATGCTTGTCTGATCCTGGGACCTGGCTCCTCCACCTGTCTCTCTTCTCCTTGCTGCCCTGGTCTGTCTCCTGGCCTTATG
CCTGTCTCTATAGCTGCTCATGTGCCTAGCATGTTCACTCTGACAGCCATGTGGTTAATTCTCTCATCTCAOCCAAGTGCTTCTGTGAGCT
CCCGCTTCAACCTGGTGGCTTCTGAGCCCATCAOCCOCTTATCCCGCTTTGTTCTTCTTAGTTTTATTTTTCCATATACAAATTAATACTTAC
TTATGCTGCTTATTTTTTCTTCTCTCCTATGGGGTTTTAGCTTCTCAGGGCAGGAATCCTTGTGTTATCGTAATATCTCAGGTACCTGAAA
TAGTGTCTGGCACACAGCGGGCAGCTGATAAGTGTAGCGATGTCAATCTTTGCAAGTAGCAATCTATATATGGCTTAGCAAGGATGAGTG
TATGTATAAATGACTACATTTTGTGCATCCCTGGAGACATTTCTCTGAACATTTTCTGGATGATTGAATGAGCTCATAGCATGACCTCTCCTGC
TAACACAGAGGTCTGTGTAACAACCTCTTCCAAGCACAACTTGTATCAGCAATCTCAGATGTCTCTGCATATAGGGCATAGTTTTCCAACCTCA
GGGAAGTGGCTGGACATCCTTAGAACGTATATTTCCAGCTACCTCATGACCCATCCCTCCACATCCACGGCTCTGCTCTCTGCCCTGGTCTACA
ACCCACATCTTTTATGGTCTTAGGATCATGTTGTCTTTGACCTGGGCCAGTAACAGATTGAGGCTAGGATAGGAGGCTCTTTGGACCCACTG
AGGCCCTGAACCATCCTTTCTGGATTCAGGATGGTGAGATGATTCCCTACGGTGTTGATAACCAGACCAAGCACTGTCTGAGACGGCTGGGAAGC
GCTACCCTTCCAGATCCAGGACCTGGGCTGAGGATGCTGGCCTTACCAGGTCATGGTGGAGGATGCTGTGGCTTCTCTACAGAGCTAGAATCCAG
AAGTGAGTATTCTCATCCAGAGGCTCGCAGAGGGGAGGGGAGGGGTCATGCTGTGTTATGGAGTGGGATACATGCCACAGGCTGCATTGCCAAAAG
ACAACAGGAAGAGGGATACACCCAGATCCTCCTGTTGTACCCAGCTGGACTCTACAGAGTGATTGAGGGACACAGTCATATGACATGCTCTGCC
ACAGGCCCTCTGTGCAATATTTCAGATCAGACCCAGACTATGCCCTTTGCTACATCACCCCTCTGTATAAATGTCATCTCTCCACAATCCCAAGCAA
GAATTTCAACCTGGGCCAGACAGGCCACGCAGCCAGGCTTCTTAGTCTGCTTCTGTGTTACTTCTTCTTGTGCCCTCTTTGAACCTGTCTCTGT
ATCCACAGGCTCCTGTTTCTACACCAGCTATAGAGCACTGACCAGGAGCCTTAGGAGGACAAGGAGAGACCTAGAGGAAGAAGCAGGTCATAAAGAAC
AAGGTTGAACCAAGCCTGAAGAACAGGAAGGGAAGGTCACCCAGCAGGCTAGGTTACTAGGATTGGCTTTGAAAGCCAGAAACATGTGTCAAGG
GCAGTGGATCATGGCCTGGGAGTGAAACCTCTTAGCTGCCAAGTATGAGCAAGTCAATGTTGTTTTTATACCAAGGCTAGCTCATTCTAGGCA
AATACCGGTCTCCAGTCTTTATTTTATTTGAGAAATGCTCTCTAAAGCTGTCCAGGCTGGTCCGAAACACACTGTGCTACAAGCTGGCCTTGAACCT
GTAAGTGTCCCTCTGACCTCCTCAGAAAGCTGGGATTATCAATTTATATACACTGCTACACCTAGATTTTTTAATTTCTAAGCCTCATCTCTTGTGTA
AAAAGAGAATTAAGTTCTCTCAGCGATCATAATATGATTACAACCTACATTTATGTGTGTGTGAGGGTACCAATGCTTTCAGTCTTACTAA

```

Figure 7.1: IGFN1 CRISPR/Cas functional characterisation by mismatch cleavage assay. (A), A diagram of CRISPR/Cas plasmid. (B), A schematic diagram of CRISPR/Cas technology (C), diagram of homologous recombination donor plasmid. (D), schematic diagram of the NHEJ repair pathway and T7 Endonuclease I (T7ENI) mismatch cleavage assay. (E), schematic diagram of the homologous recombination repair pathway. (F) PCR amplification of sequence containing the DSB site. Yellow boxes indicate primer sites. The green box highlights the CRISPR targeting sequence. (G), T7ENI digestion result performed by DNA electrophoresis. PCR amplification product size is ~852bp, two mismatch cleavage products sizes are ~505bp and ~347bp (labelled with red arrows). (H), IGFN1 CRISPR/Cas targets exon 13 of *Igfn1*. The blue boxes represent the exons. (I), The sequence of exon 13 and its flanking sequence. The region highlighted in yellow is the sequence of exon 13, the red-letters represent the IGFN1 CRISPR/Cas targeting sequence, and the blue-letters are the homologous recombination sequence.

### 7.2.2 IGFN1 CRISPR/Cas cell lines generation

Once the effectiveness of the IGFN1 CRISPR/Cas vector was confirmed, IGFN1 CRISPR/Cas and homologous recombination donor plasmids were both transfected into C2C12 cells to generate IGFN1 KO cell lines. 48 hours after transfection, puromycin was added into the growth medium to select for colonies expressing the homologous recombination cassette for 7 days. Clonal selection by dilution was undertaken to generate colonies from single cells. 38 colonies were selected, 6 of them were lost due to contamination and the rest were expanded and frozen for further analyses.

PCR amplification was used to test the selected clones. If the *igfn1* gene was repaired by the homologous recombination pathway, the *igfn1* sequence will contain the insertion cassette of the homologous recombination template. To test whether the template was inserted into the right place, forward primers were placed on the *igfn1* genomic sequence before (or after) the homologous recombination arm1 (or arm2) and the reverse primers were placed within the homologous recombination cassette (figure 7.2A).

The correct size of PCR products indicated that the homologous recombination sequence in the donor plasmid was inserted into the right position. In this experiment, several colonies, 2, 8, 11, 12, 13, 14, 15, 19, 21, 24, 25, 26, 27, 28, 29, 31, 32,33 and 38, produced the expected PCR products for the left and right side of the cassette, indicating insertion of the cassette through complete homologous recombination (figure 7.2C).

Because *igfn1* has two alleles in C2C12 cells, the previous test could only prove that at least one *igfn1* allele contained the donor sequence, and was therefore disrupted. To test whether both alleles were disrupted by insertion of the donor sequence, primer pair 3 was designed.

The forward primer was designed on homologous arm1 and reverse primer was selected on homologous arm2 (figure 7.2B). There were two possible sizes of PCR product. One would be amplified from an IGFN1 allele containing the donor sequence, producing a ~3345 bp product (which cannot be amplified in the 30s extension time of the PCR program). Another would be amplified from an IGFN1 allele which did not contain the donor sequence, producing a ~852 bp product. If both alleles are mutated by insertion of donor sequence, no 852 bp PCR product could be produced. In this experiment, a 852 bp PCR product showed in all the colonies except clone 19, which makes it likely that both alleles of IGFN1 gene in clone 19 have been undergone homologous recombination, and only one of the two alleles of IGFN1 gene have undergone homologous recombination in clone 2, 8, 11, 12, 13, 14, 15, 19, 21, 24, 25, 26, 27, 28, 29, 31, 32, 33 and 38 (figure 7.2C).

In this case, even without repair via homologous recombination, there was still a chance that IGFN1 CRISPR/Cas could mutate other *igfn1* alleles with indels (via the NHEJ repairing pathway). To test this, PCR products generated from primer pair 3 were sent for sequencing. The results showed that only 7 clones contain mutations generated by NHEJ in the second allele.

Clone 2, 11, 12 and 14 showed the same 13 bp deletion in the second IGFN1 allele, meaning they were possibly derived from the same colony during the isolation of single cells by dilution. Clone 28 has a 1 bp deletion in the target sequence of second IGFN1 allele (figure 7.2D). Clone 33 shows a 3 bp deletion in the target sequence and a 1 bp insertion in the deletion point. All these mutations could cause a frameshift in IGFN1 protein translation resulting in a premature stop codon. This may then lead to nonsense-mediated mRNA decay to achieve an IGFN1 gene knockout.

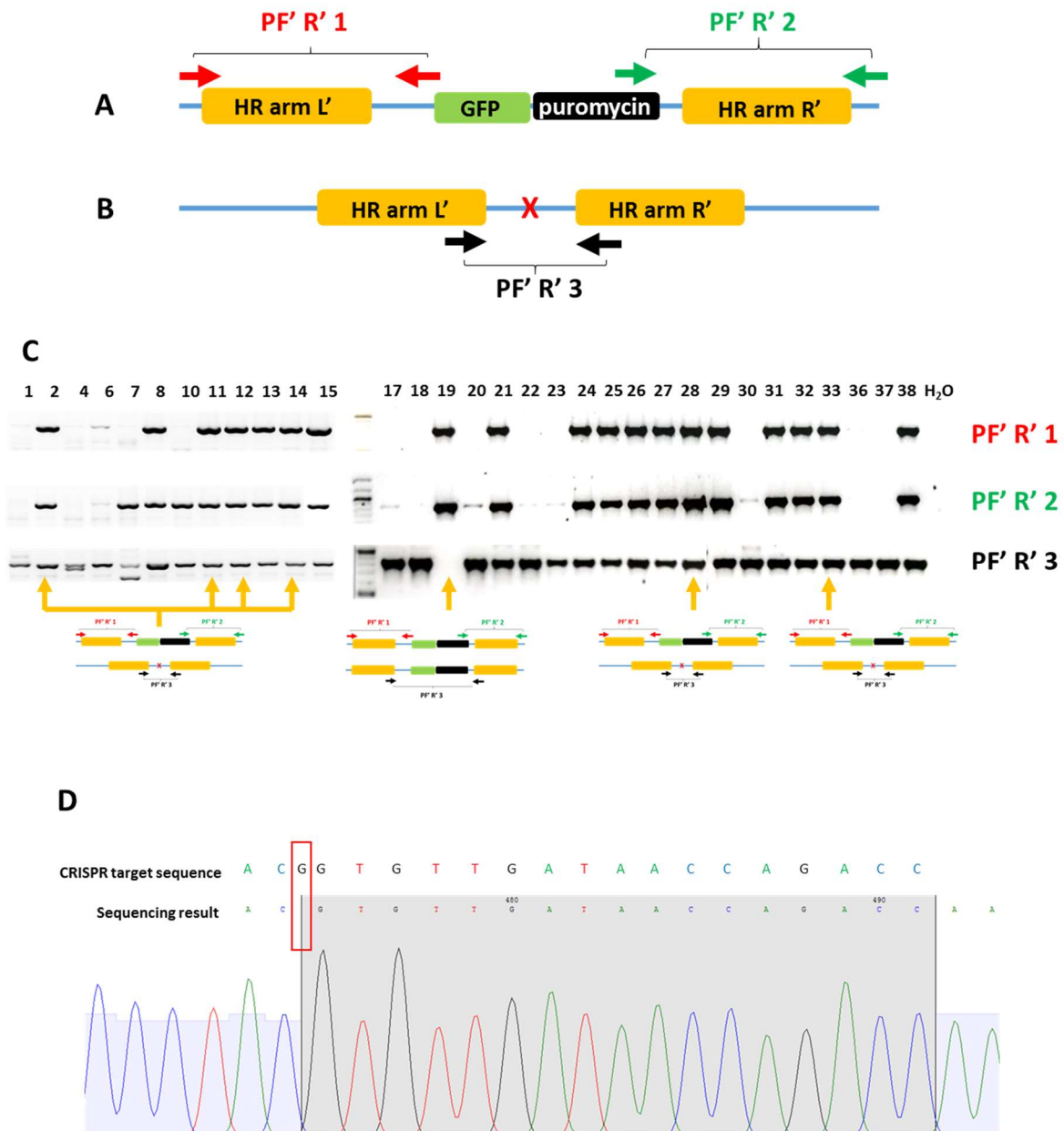


Figure 7.2 PCR screening for IGFN1 knockout cell lines.

(A), locations of primer pair 1&2 in the homologous recombination cassette. (B), locations of primer pair 3 in the native chromosome. (C), electrophoresis results of PCR products amplified from the three primer pairs. All PCR products were sequenced. The successfully mutated clones are labelled with yellow arrows and a structure diagram of the mutation site. (D), Example sequencing result (clone 28), the red square labels were detected sequence differs from expected WT sequence indicating repair via the NHEJ pathway. PF'R' represents primer forward and reverse.

### 7.2.3 RT-PCR confirms IGFN1 gene knockout in C2C12 cells

To test whether the mutations identified led to *Igfn1* nonsense-mediated mRNA decay in KO cell lines, RT-PCR was used to test *Igfn1* transcript levels. Primers were designed at the N' terminal of IGFN1 to span the 11<sup>th</sup> and 12<sup>th</sup> exon junction upstream of the CRISPR/cas9 targeted exon (figure 7.3A). The annealing temperatures of these primers are all between 58 °C and 60 °C. The sequences of these primers are GGTATCGTCGACTTCCGGG (forward primer) and GTCAAACGTAGCGACCCCT (reverse primer). The primer sequences used for the housekeeping gene hypoxanthine-guanine phosphoribosyl transferase (HPRT) were selected from the literature and have been widely used in many publications, e.g., (Luther et al., 2000), which are GTTGGATACAGGCCAGACTTTGTTG (forward primer) and GATTCAACTTGCGCTCATCTTAGGC (reverse primer). Primers were tested by PCR on C2C12 cDNA to confirm that only the target sequence (~ 141 bp) can be specifically amplified (figure 7.3B). Template cDNA was converted from mRNA which was extracted from proliferating C2C12 and knockout cell lines. The cDNA concentration of each sample was measured, diluted to the same concentration and mixed with primers and SYBR Green Master Mix to form RT-PCR reactions on an optical 96 well plate. Each reaction was performed in triplicate and plates were run and analysed on the StepOnePlus machines using a Fast PCR protocol. The principle of RT-PCR calculation is the same as previous RT-PCR experiments (chapter 5 result 5.2.2). The equations shown below were used for calculations.

$$\text{Fold Change} = 2^{-\Delta(\Delta C_T)}$$

$$\Delta C_T = C_{T_{\text{target}}} - C_{T_{\text{HPRT}}}$$

$$\Delta(\Delta C_T) = \Delta C_{T_{\text{stimulated}}} - \Delta C_{T_{\text{control}}}$$

Here, target represents knockout (KO) cell lines.  $\Delta CT_{\text{stimulated}}$  is  $C_{T_{\text{KO cell lines}}} - C_{T_{\text{HPRT}}}$ ,

$\Delta CT_{\text{control}}$  is  $C_{T_{\text{C2C12}}} - C_{T_{\text{HPRT}}}$ .

The RT-PCR results show that the expression level of Igfn1 in clone 14, clone 19, clone 28 and clone 33 are 58.8, 9.8, 18852.6 and 137.3 times lower than in WT C2C12 cells respectively.

This result indicates that the CRISPR/cas9 mutation of the target sequence results in nonsense-mediated mRNA decay and thus gene expression is disrupted at the mRNA level.

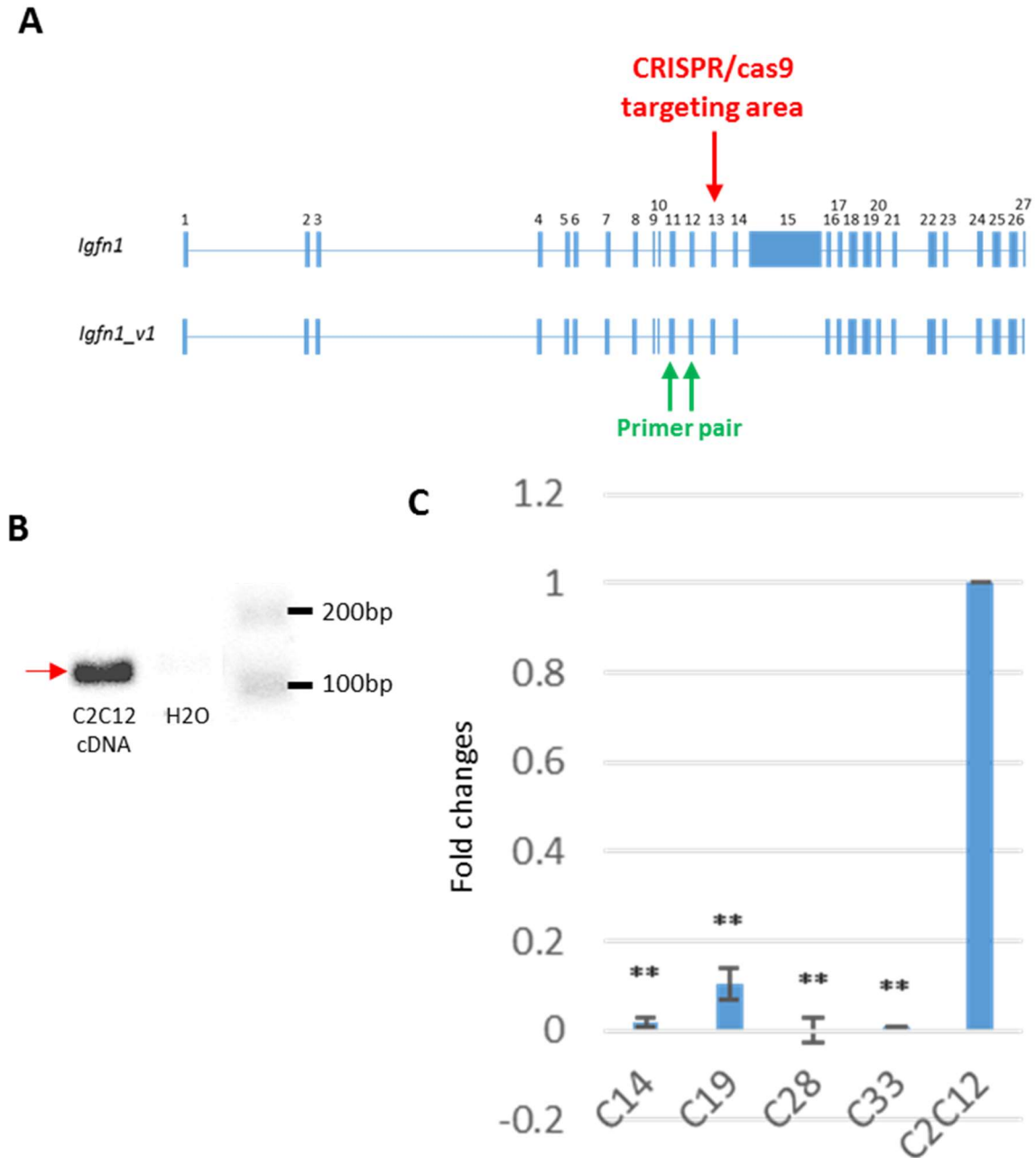


Figure 7.3: Real-time PCR quantification of Igfn1 expression in Igfn1 knockout cell lines. (A), Genomic structure of Igfn1 isoforms. Green arrow labels the CRISPR/Cas9 targeted exon, the blue arrows label the primer locations. (B), Standard PCR test of RT-PCR primers shows specific amplification of the target sequence from cDNA. (C), Real-time PCR quantification of Igfn1 expression in Igfn1 knockout cell lines and WT C2C12 control. Error bars represent the standard deviation of three technical replicates. \*\* represents t-test between KO clone and C2C12 control,  $P \leq 0.001$ .

#### 7.2.4 Validation and characterization of IGFN1 knockout cell clones

To explore how the loss of IGFN1 expression may affect the morphology of C2C12 myoblasts, phalloidin was used to stain the actin cytoskeleton in each knockout clone. The functions of the actin cytoskeleton relate to cell motility, cell division and the formation and maintenance of specialized structures in differentiated cells<sup>85,86</sup>. The staining results show that there was no visible difference between the actin cytoskeletal structure of IGFN1 knockout clones and the C2C12 control (figure 7.4A). Cell size was also measured. Although the size of cells from clone 19 and 33 were significant decreased, other clones did not show a significant difference compared to C2C12 cells (figure 7.4B, table 7.1).

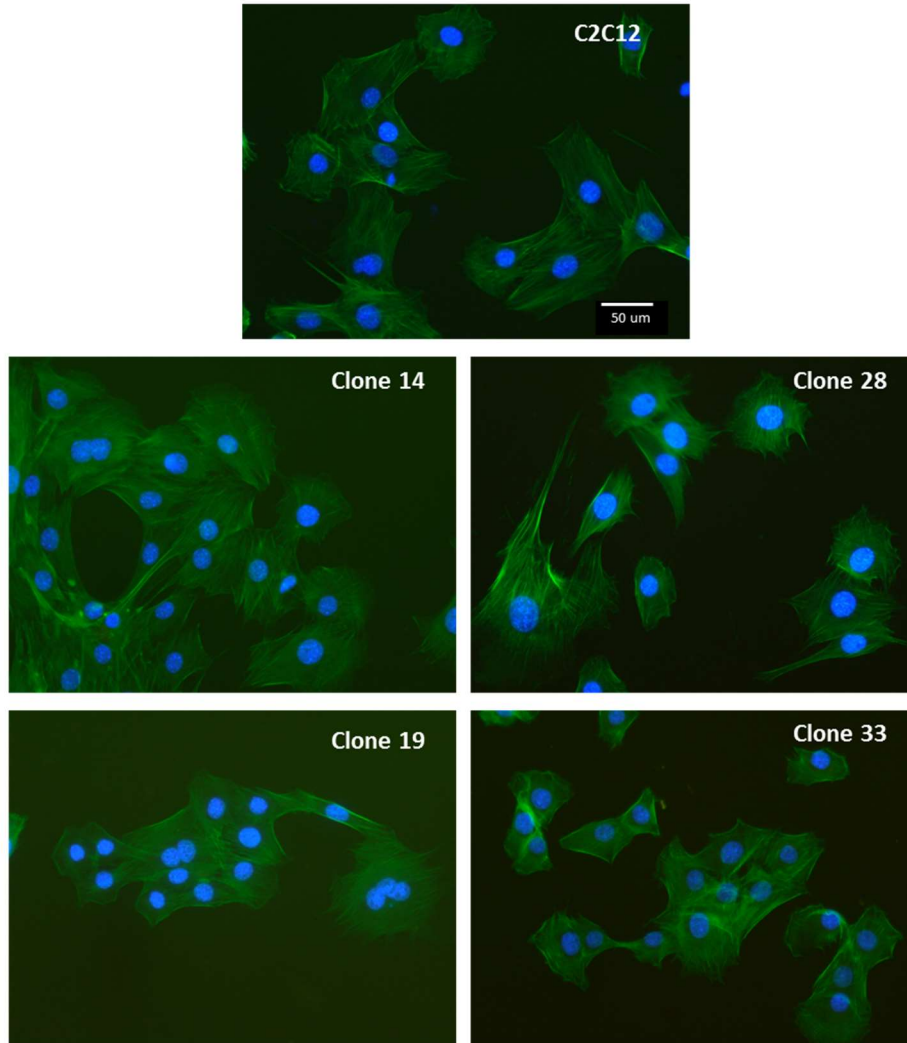
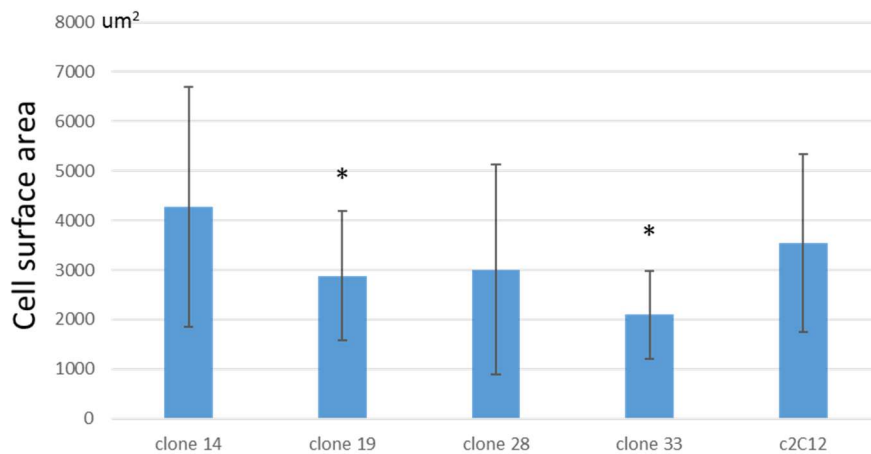
**A****B**

Figure 7.4: Characterization of morphological changes to IGFN1 knockout myoblasts. (A), green phalloidin staining shows the actin cytoskeletal structure in IGFN1 knockout clones and the C2C12 control. (B), cell area measurement of IGFN1 knockout clones and the C2C12 control. Details of cell size average, P value and the numbers of independent experiments in table 7.1. \* represents  $P \leq 0.01$ , t-test. Error bars represent the standard deviation of more than 3 independent experiments. The images in are at the same magnification.

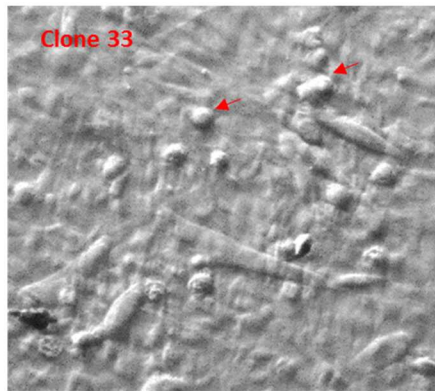
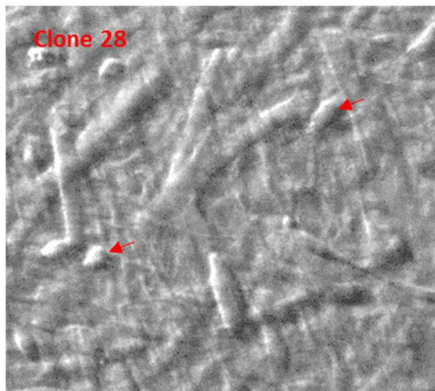
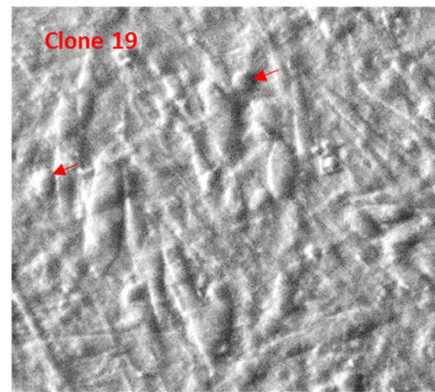
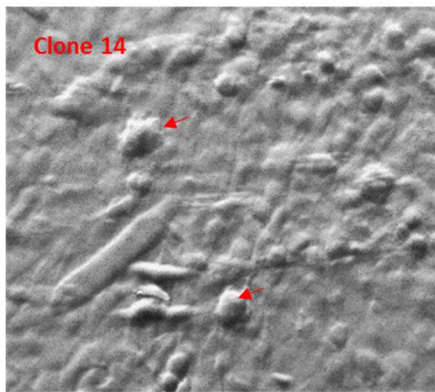
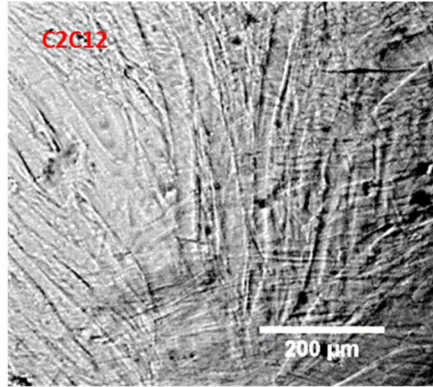
	size average	P value(compare with C2C12)	Number of cells
clone 14	4410.581881	0.18896	66
clone 19	3364.362745	0.33908	47
clone 28	2800.561383	0.67122	29
clone 33	2148.868015	0.00005	90
c2C12	3599.284385		45

Table 7.1: Cell size measurement of IGFN1 knockout clones.

Muscle fibres result from the fusion of many myoblasts during muscle differentiation or myogenesis. To examine the effect of IGFN1 reduction in C2C12 cell differentiation, all the IGFN1 knockout clones and C2C12 control cells were differentiated in differentiation medium containing 2% serum for 7 days, followed with 4% PFA fixation and staining with an  $\alpha$ -actinin antibody and TRITC conjugated secondary antibody. The selected knockout clones showed abnormal morphology during cell differentiation compared to C2C12 cells. The bright-field microscopy images show that C2C12 cells form long and well-arranged myotubes, but all the IGFN1 clones form short myotubes and globular differentiation patterns (figure 7.5A).  $\alpha$ -actinin expression is upregulated during muscle differentiation <sup>75</sup>, and thus was used as a differentiation marker to illustrate how well these IGFN1 knockout clones differentiate. Staining with  $\alpha$ -actinin antibody and TRITC secondary antibody shows that the C2C12 differentiated myotubes express large amounts of  $\alpha$ -actinin in the well-arranged myotubes. Only few short myotubes show  $\alpha$ -actinin expression in all the IGFN1 knockout clones, and a large amount of globular differentiation bodies contain high levels of  $\alpha$ -actinin expression in all the IGFN1 knockout clones. Some of the globular differentiation bodies contain more than

one nucleus, which indicates that these globular differentiation bodies may have formed from the fusion of myoblasts (figure 7.5B arrows show the globular differentiation). To eliminate the possibility that all these phenotypes were an artefact of the clonal selection process, C2C12 cells were transfected with IGFN1 homologous recombination plasmid to generate puromycin resistant C2C12 cells, which were differentiated in 2% serum differentiation medium for 7 days prior to immunostaining as previously for  $\alpha$ -actinin. The results show that only few myotubes appear in puromycin resistant C2C12 cells with strong red fluorescence, but these myotubes do not have the same short morphology as IGFN1 knockout clones. Only a few of the globular differentiation bodies form in puromycin resistant C2C12 cells, and a small number of globular differentiation bodies may also be found in C2C12 controls (figure 7.5B). These results indicate that puromycin treatment may have an inhibitory effect cell fusion and myotube formation, with only a few myotubes appearing after 7 days in differentiation medium, but it does not affect the length of myotubes and does not result in a global inability to differentiate. To confirm that the short myotubes and globular differentiation patterns are not an artefact in these four IGFN1 knockout clones due to the process of clonal selection, C2C12 cells were transfected with both IGFN1 CRISPR/Cas and homologous recombination donor plasmid and treated with puromycin for 7days. Instead of selecting single IGFN1 knockout clones, all the puromycin resistant cells were mixed and differentiated for 7days. The results in this mixed population show the same phenotypes, short myotubes and globular differentiation patterns, as all four IGFN1 knockout clones (figure 7.5B). Taken together, knockout of IGFN1 in C2C12 cells appears to cause abnormal cell differentiation by causing the formation of short myotubes and globular differentiation patterns, which indicates that IGFN1 may be functionally related with regulation of muscle myogenesis.

**A**



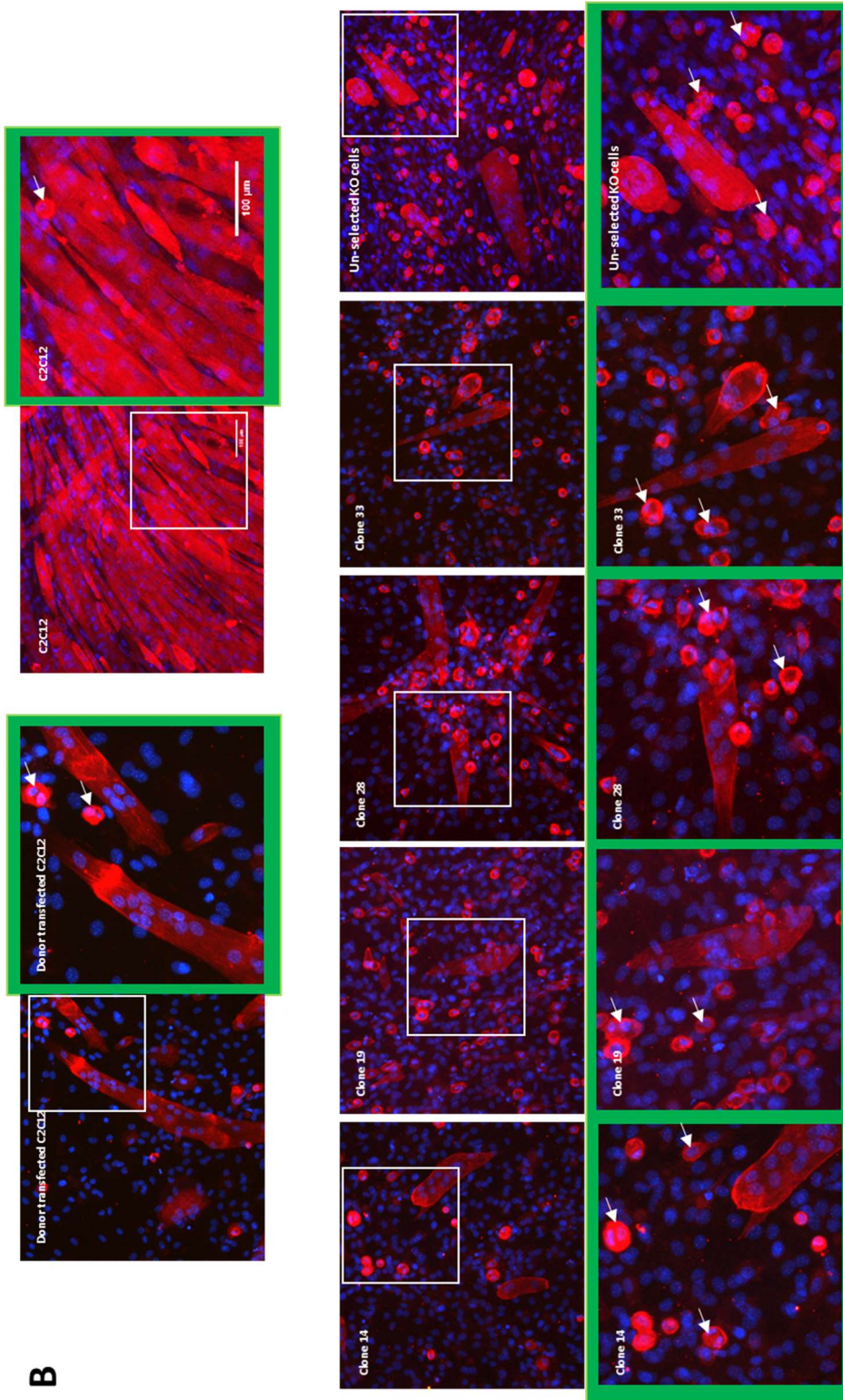


Figure 7.5: Characterization of morphological changes in IGFN1 knockout clones during cell differentiation.

(A), bright field microscopy images of IGFN1 knockout clones and C2C12 controls after 7 days in differentiation medium. Red arrows indicate examples of globular staining of knockout clones and C2C12 cells after 7 days in differentiation medium. Images labelled by green squares are inset images magnified from the areas labelled with white squares. Arrows indicate examples of globular differentiation. The images without green squares are at the same magnification. The images with green squares are at the same magnification.

### 7.2.5 Knocking down IGFN1 in mouse skeletal muscle

Previous results show that the knockout of IGFN1 in myoblasts (C2C12) caused abnormal differentiation. Because the IGFN1 CRISPR/Cas constructs showed high efficiency during *in vitro* experiments, these were also used to study the function of IGFN1 in mouse skeletal muscle. The IGFN1 CRISPR/Cas plasmid was co-injected along with a tdTomato expression plasmid into mouse EDL/TA muscle and transfected via *in vivo* electroporation (all the mice used in this experiment are male and between 5-8 weeks old). Expression of tdTomato plasmid was assumed to indicate the fibres into which the CRISPR/Cas plasmid was transfected. Because muscle fibres contain multiple nuclei, in order to mutate as many nuclei as possible the constructs were left to express in the muscle for 21 days or more. Then the mice were sacrificed and the electroporated muscles were dissected. Tissue samples were briefly fixed in PFA and snap frozen in liquid nitrogen-cooled isopentane prior to cryostat sectioning. Images were obtained from cross sections by fluorescence microscopy. Red fluorescence in figure 7.6A arises from expression of tdTomato in fibres and was presumed to indicate fibres also containing the IGFN1 CRISPR/Cas plasmids. The red fluorescence signal remains strong, which indicates that the transfected plasmids have not been eliminated by the 21<sup>st</sup> day after injection.

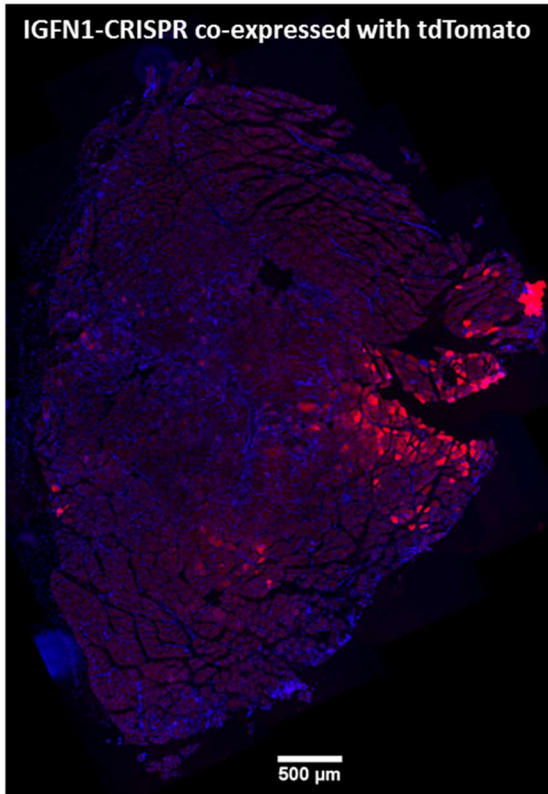
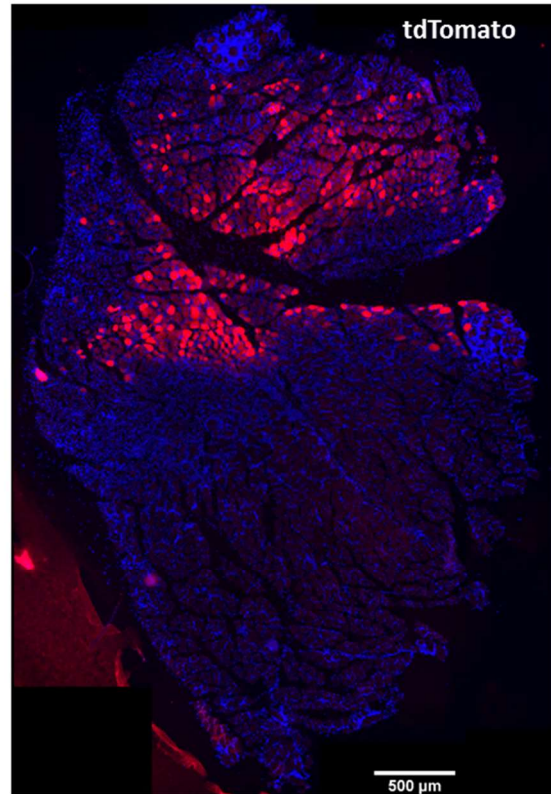
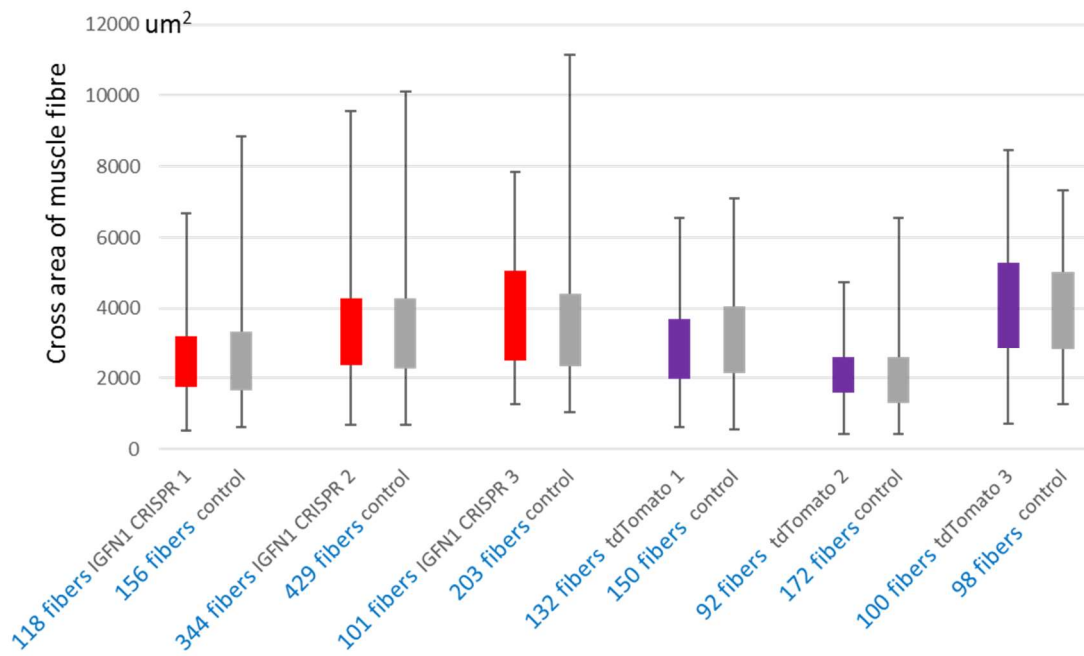
To analyse the effect on muscle fibre size, the cross-sectional area of IGFN1 CRISPR/Cas+tdTomato transfected fibres were measured and compared with un-transfected fibres in the same region of the muscle (measurements for this analysis were performed on mice left to express the constructs for 37days after electroporation, so that any potentially confounding effect of the electroporation protocol, such as focal degeneration, could be eliminated). The results show that there were no significant fibre size changes between

transfected and un-transfected fibres in three independent mice (figure 7.6C), which suggests that knockout IGFN1 in mouse skeletal muscle was either unsuccessful or it may not affect muscle fibre size.

To analyse whether the attempted IGFN1 knockout may cause other fibre morphology changes, Hematoxylin and eosin (H&E) staining was performed (figure 7.6D and E). Transfected areas were labelled in figure 7.6D and E with green squares, and they are magnified as figure 7.6F and G. No morphological changes are found in fibres expressing IGFN1 CRISPR/Cas and tdTomato plasmids compared to fibres expressing tdTomato alone. Regenerating fibres with central nuclei are found in both IGFN1 CRISPR/Cas + tdTomato transfected mice and tdTomato only control mice, which indicated that 21days after electroporation may not be enough time for muscle to recover from the damaged caused by the electroporation protocol. The H&E result for 37days after electroporation shows fewer regenerating fibres (figure 7.6I and J), and these samples were used to measure cross-sectional area of IGFN1 CRISPR/Cas transfected fibres.

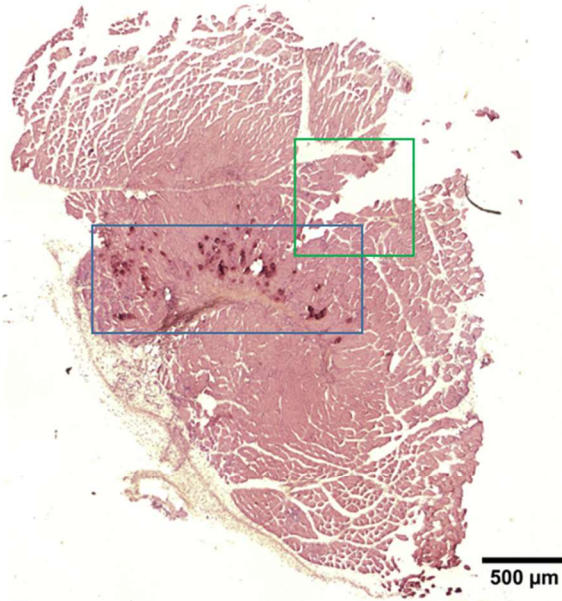
A number of dead fibres close to tendons appear in some of IGFN1 CRISPR/Cas + tdTomato transfected mice (note that not all the IGFN1 CRISPR/Cas + tdTomato transfected mice contain dead fibres). A previous study found that gene transfer by electroporation could possibly cause muscle damage<sup>87</sup>, which is the likely explanation for the dead fibres in IGFN1 CRISPR/Cas and tdTomato transfected mice.

Taken together, my results suggest that the presumed knockout of exon 13 from the *Igfn1* locus in mouse skeletal muscle did not affect fibre morphology.

**A****B****C**

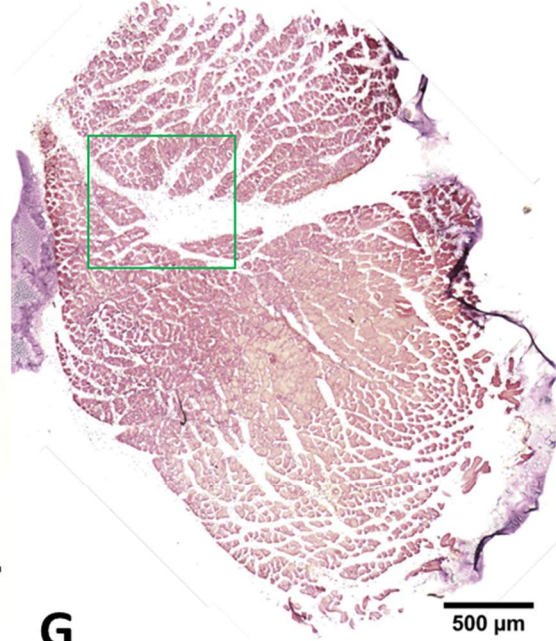
**D**

IGFN1-CRISPR co-expressed with tdTomato



**E**

tdTomato



**F**

IGFN1-CRISPR co-expressed with tdTomato



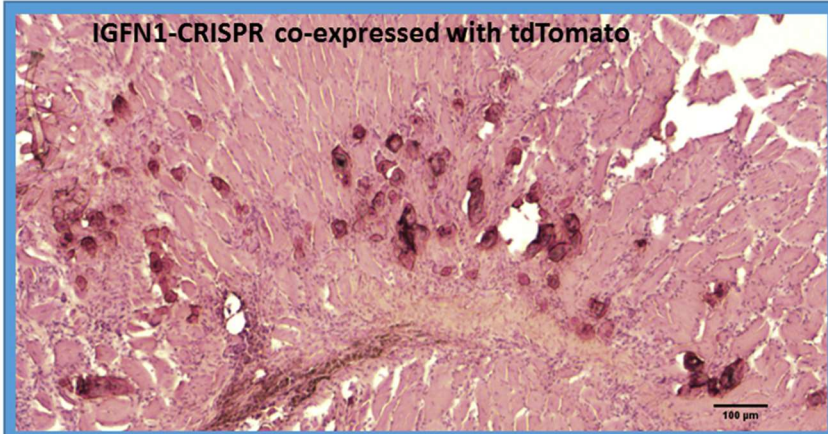
**G**

tdTomato



**H**

IGFN1-CRISPR co-expressed with tdTomato



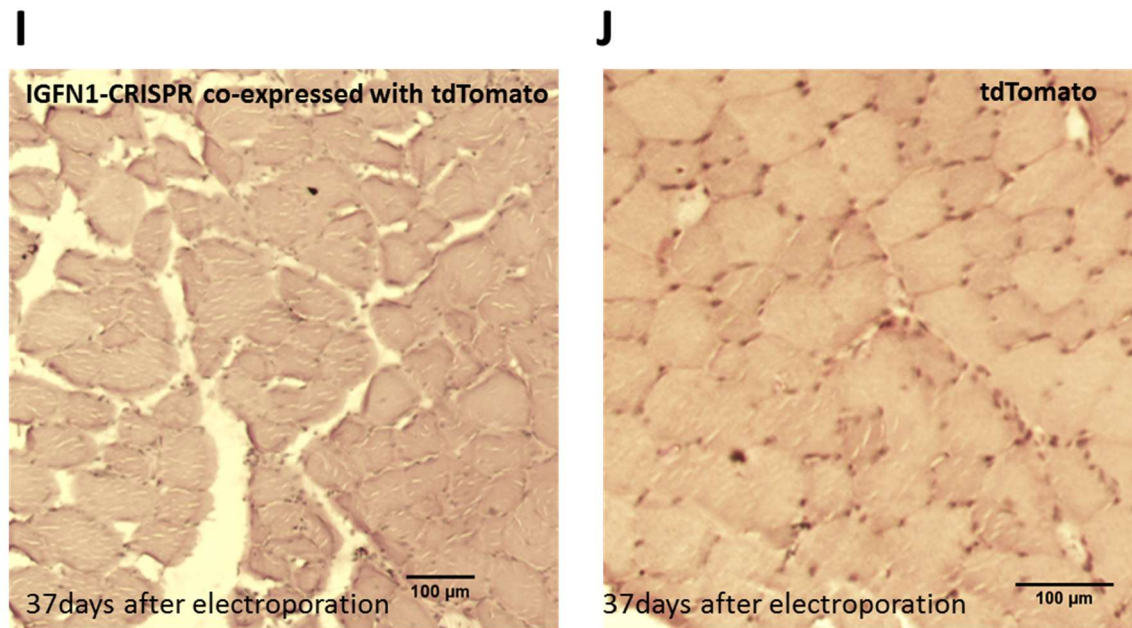


Figure 7.6: Attempt at *In vivo* knockout of IGFN1 by electroporation of IGFN1 CRISPR/Cas plasmid in mouse EDL/TA muscle.

(A) and (B) represent fluorescence microscope images of IGFN1 CRISPR/Cas and tdTomato transfected muscle and tdTomato only transfected muscle respectively. (C), Box-and-whisker diagram described fibre size (cross-sectional area) comparison between red fluorescent fibres (assumed to be expressing both the tdTomato and IGFN1 CRISPR/Cas constructs) and fibres without fluorescence. Red boxes represent the cross-sectional area between upper and lower quartiles of IGFN1 CRISPR/Cas and tdTomato co-transfected fibres. Violet boxes represent the cross-sectional area between upper and lower quartiles of tdTomato transfected fibres. Blue boxes represent untransfected fibres in same region of a single muscle. The number of fibres measured was labelled under the samples. Error bars represent variability outside the upper and lower quartiles. (D) and (E) are H&E staining results of IGFN1 CRISPR/Cas and tdTomato transfected muscle and tdTomato only transfected muscle respectively (21days after electroporation). (F) and (G) are the magnified images of the area within the green square in (D) and (E) respectively. (H) is the magnified image of area within the blue square in (D). (I) and (J) are H&E staining results of IGFN1 CRISPR/Cas and tdTomato transfected muscle and tdTomato only transfected muscle respectively (37days after electroporation).

### 7.3 CONCLUSION:

This chapter aims to provide insights into the function of IGFN1 in skeletal muscle by knockout of the *igfn1* gene *in vivo* and *in vitro*. The method used to knockout IGFN1 expression is CRISPR/Cas technology. The IGFN1 CRISPR knockout efficiency was tested by a mismatch cleavage assay, with the results showing that a nearly 54% mutation efficiency was found in IGFN1 CRISPR/Cas plasmid transfected 3T3 cells, which indicates that the IGFN1 CRISPR/Cas can efficiently mutate IGFN1 in the designed target area.

To study the function of IGFN1 in myoblasts and in differentiating myotubes, IGFN1 knockout clones were generated by transfecting IGFN1 CRISPR/Cas and homologous recombination donor plasmids into C2C12 cells. In this work, 4 IGFN1 KO clones were selected and confirmed to result in a frame shift in IGFN1 protein translation, in turn resulting in a premature stop codon and leading to nonsense-mediated mRNA decay to achieve the IGFN1 knock out. The RT-PCR result shows that the expression level of *igfn1* was highly reduced in all four IGFN1 knockout clones.

Attempts were made to characterize whether IGFN1 knockout caused morphological changes in C2C12s at the undifferentiated myoblast stage. Phalloidin staining results showed that no distinct differences in the actin cytoskeleton between knockout clones and the C2C12 control. The cell size measurement result shows that except for a decrease in cell sizes in clone 33, the other three clones do not have significant size differences compared with the C2C12 control. Because only one knockout clone shows cell size differences, and the other three clones show

no significant size changes, this indicates that cells size reduction showed in clone 33 may not cause by IGFN1 knockout and instead may be an artefact of the clonal selection process.

To characterize whether disruption of exon 13 of the *Igfn1* gene caused morphological changes during C2C12 differentiation, all the IGFN1 knockout clones and the C2C12 control were treated in differentiation medium for 7days. All the IGFN1 knockout clones show abnormal morphology during cell differentiation compared with C2C12 cells. These abnormalities appear as short myotube formation and globular differentiation bodies seen in bright-field images. Using  $\alpha$ -actinin as a differentiation marker, both short myotubes and globular differentiation bodies showed highly expression levels of  $\alpha$ -actinin expression. Given that some of the globular differentiation bodies contain more than one nuclei, it is possible that these globular differentiation bodies may be formed by the fusion of myoblasts, and they may able fuse to make a short tube. All these results suggest that IGFN1 may implicated in skeletal muscle myogenesis.

It is also possible that the phenotypes arising in IGFN1 KO clones results from off targeting effects. Blasting the CRISPR/Cas targeting sequence to the mouse genome, excluding *Igfn1*, only a sequence from an intron of gene *Apobec3* partially matches the CRISPR/Cas targeting sequence. Four mismatches showed between gene *Apobec3* and CRISPR/Cas targeting sequence showing as two mismatches each end. Based on the fact that this alignment shows in the non-coding intron sequence and contains 4 bases mismatches, it is unlikely to cause off target effects on this gene. To test for putative off target mutations in this region, PCR amplification and sequencing of this area can be performed in the future.

To study the function of IGFN1 in skeletal muscle, IGFN1 CRISPR/Cas plasmid was transfected into mouse TA/EDL muscle by electroporation. There was no significant difference in cross-sectional area between IGFN1 CRISPR/Cas plasmid transfected fibres and un-transfected fibres in three independent IGFN1 CRISPR/Cas plasmid transfected mice. H&E staining results showed no morphological differences between IGFN1 CRISPR/Cas plasmid transfected fibres and tdTomato control transfected fibres.

In order to show that the CRISPR/Cas plasmid causes IGFN1 mutation in skeletal muscle, genomic DNA was extracted from IGFN1 CRISPR/Cas transfected muscle, then used as a template to amplify the CRISPR target region by PCR. PCR products were sent for sequencing, but all sequencing results returned as un-readable. The cause of this result is still unclear and a more sensitive method such as next generation sequencing may be required in order to detect mutagenesis. Because the mutation efficiency of IGFN1 CRISPR/Cas was so high in 3T3 cells and in C2C12 cells, it might be predicted that the IGFN1 CRISPR/Cas may also achieve a good mutation efficiency in skeletal muscle. If this hypothesis is true, all these results suggest that knockout IGFN1 in skeletal muscle may not affect the morphology of muscle fibres.

It is also possible that CRISPR/Cas did at most only partially affected IGFN1 expression in skeletal muscle. Skeletal muscle fibres contain multiple nuclei, and even though it seems likely that the CRISPR/Cas plasmid is expressed in the muscle throughout the experiment (37days), CRISPR/Cas may still not be able to knock out IGFN1 in all the nuclei along the muscle fibre. Additionally, skeletal muscle is typically quiescent, and is not actively dividing. This may mean that the DNA is in a less accessible state than in proliferating cells, which would also contribute towards inefficiencies in *in vivo* genome editing in muscle. Thus, the IGFN1 produced from a

reasonable population of un-mutated nuclei may be sufficient to maintain normal fibre morphology. To identify the level of IGFN1 expression in CRISPR/Cas targeted muscles, WB was performed. However, all the available IGFN1 antibodies were not sensitive or specific enough to clearly identify the target proteins from the background in skeletal muscle.

# Chapter 8

## RESULTS

### 8. Characterization of an MLTK deficient mouse

## 8.1 INTRODUCTION

Previous studies have examined an MLTK deficient mouse strain created using Gene-trap technology and generated by the Texas A&M Institute for Genomic Medicine (TIGM). RT-PCR tests showed the absence of *Mltk* transcript expression in bone marrow-derived macrophages from these mice <sup>88,89</sup>. This chapter describes experiments examining the effect of MLTK deficiency in skeletal muscle using skeletal muscles from these MLTK deficient mice, including H&E staining, cross sectional area measurement, fibre type proportion analysis and RT-PCR testing *Mltk* expression levels in skeletal muscle.

## 8.2 RESULTS

### 8.2.1 H&E staining analysis indicates MLTK deficiency causes phenotypic changes in mouse skeletal muscles

The MLTK deficient mouse was generated by the Texas A&M Institute for Genomic Medicine (TIGM) using gene trap technology, which inserts a trapping cassette into the 5' terminal of the MLTK gene upstream of the initiator ATG to lead to null alleles. Based on the introduction from TIGM website, the knockdown efficiency is higher than 96%.

Two MLTK deficient mice (between 4-5 weeks) were sacrificed, fixed in 10% formaline and shipped from the Stem Cell Biology and Developmental Genetics group in Tufts University. To test whether MLTK deficiency causes skeletal muscle morphology changes, skeletal muscle histology analysis was performed by incubating the left hind limbs from two MLTK deficient mice and two control mice in 9% formic acid for ~ 24 hours, followed by incubations in a series

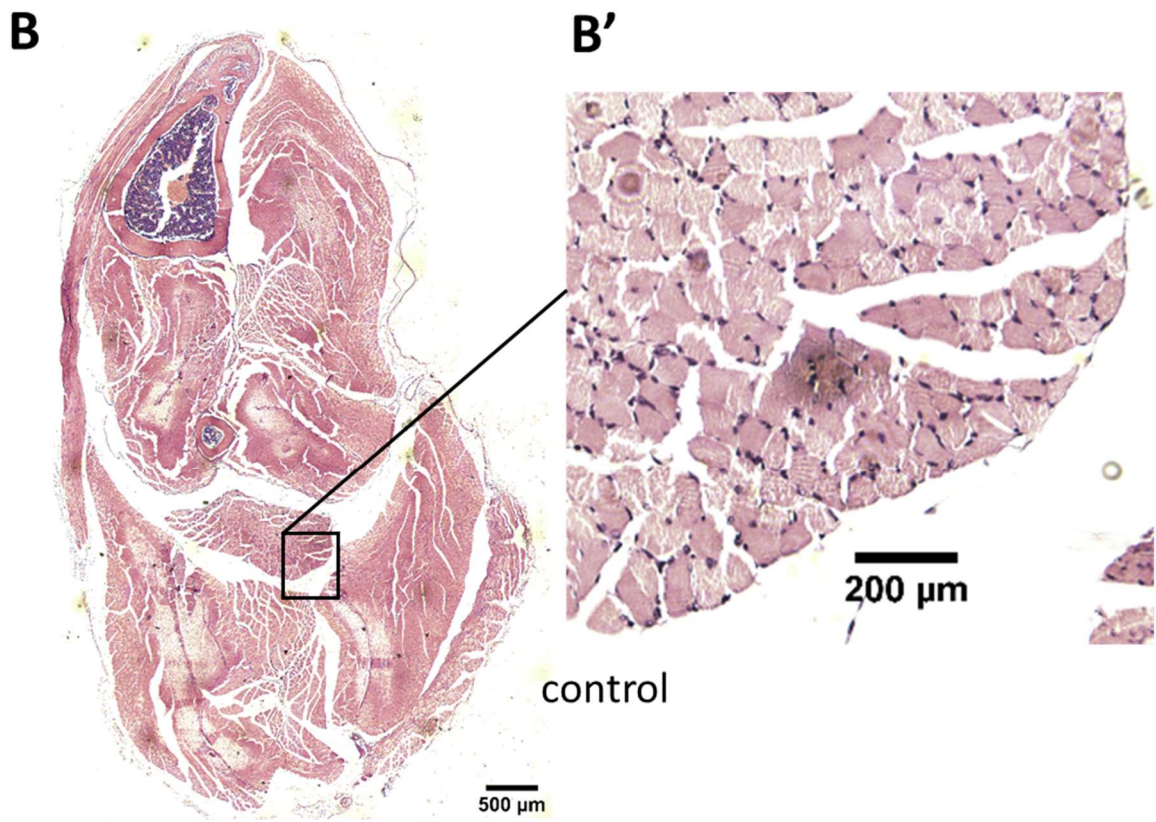
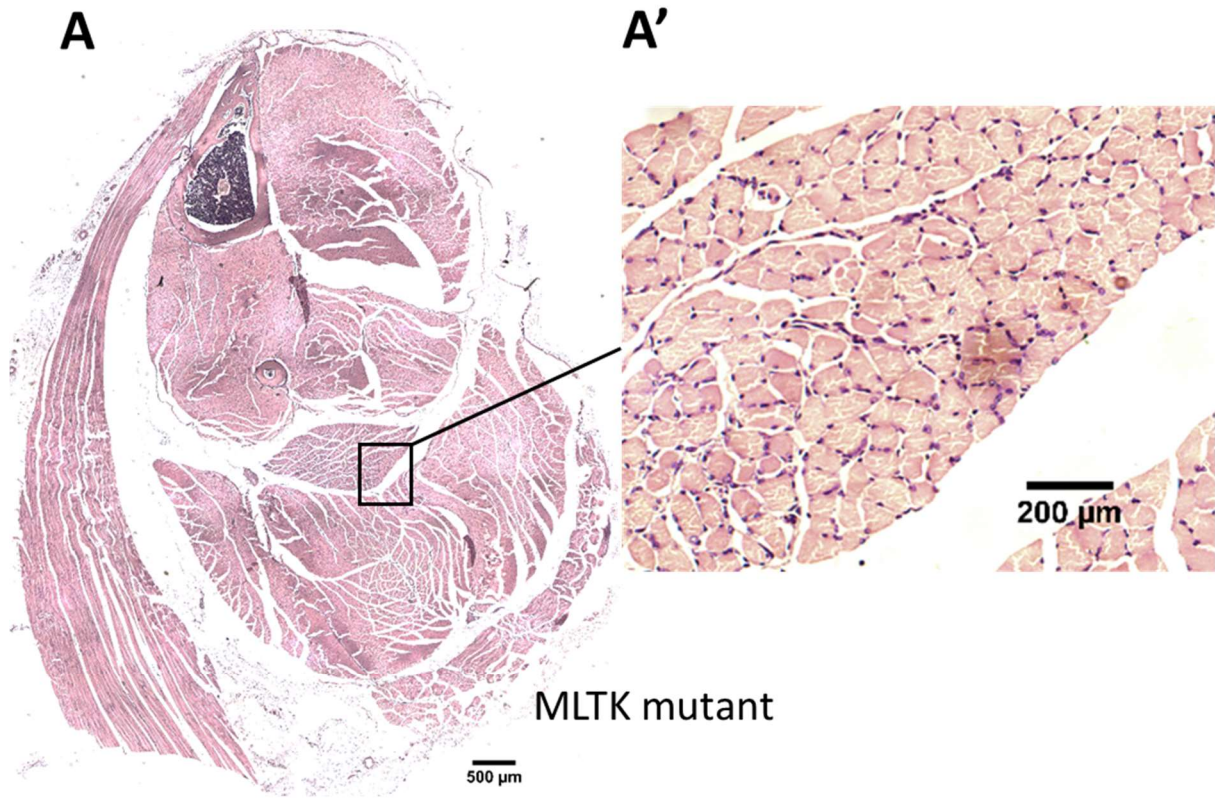
of ethanol dilutions, xylene and wax. Samples were then ready to prepare cross sections for histological analysis.

The H&E staining results show that the soleus muscles from both MLTK deficient mice contain more nuclei than control mice (figure 8.1 A' and B' are soleus cross section images from MLTK deficient mouse 1 and control mouse 1). To confirm whether the increased number of nuclei was statistically significant between MLTK deficient mice and control mice, fifty fibres were selected from same region of soleus in each mouse, and the number of nuclei around every single selected fibres was counted and averaged (table 8.1). The results show that both MLTK deficient mice contain more nuclei in soleus fibres than control mice.

A study has shown that the number of nuclei is proportional to fibre volume in mouse soleus muscle <sup>90</sup>, which indicated that the increased number of nuclei may be due to increased fibre size in MLTK deficient mouse soleus. To test this, the fibre cross sectional area from soleus muscle was measured in MLTK deficient mice and control mice (age between 4-5 weeks, same strains and gender but not siblings). The results show that the cross sectional area of fibres in the soleus muscle compared between MLTK mutant mice and control mice are not significantly different (figure 8.1 C), which indicates the elevated number of nuclei associated with MLTK mutation doesn't affect muscle cross area.

	number of nuclei/fibre	t-test with control 1	t-test with control 2	N=sample number
MLTK mutant 1	7.02	1.26517E-11	1.555E-06	50
MLTK mutant 2	6.84	1.55471E-06	6.162E-07	50
control 1	4.08			50
control 2	5.16			50

Table 8.1: MLTK deficient mice contain more nuclei in soleus fibres than control mice.



C

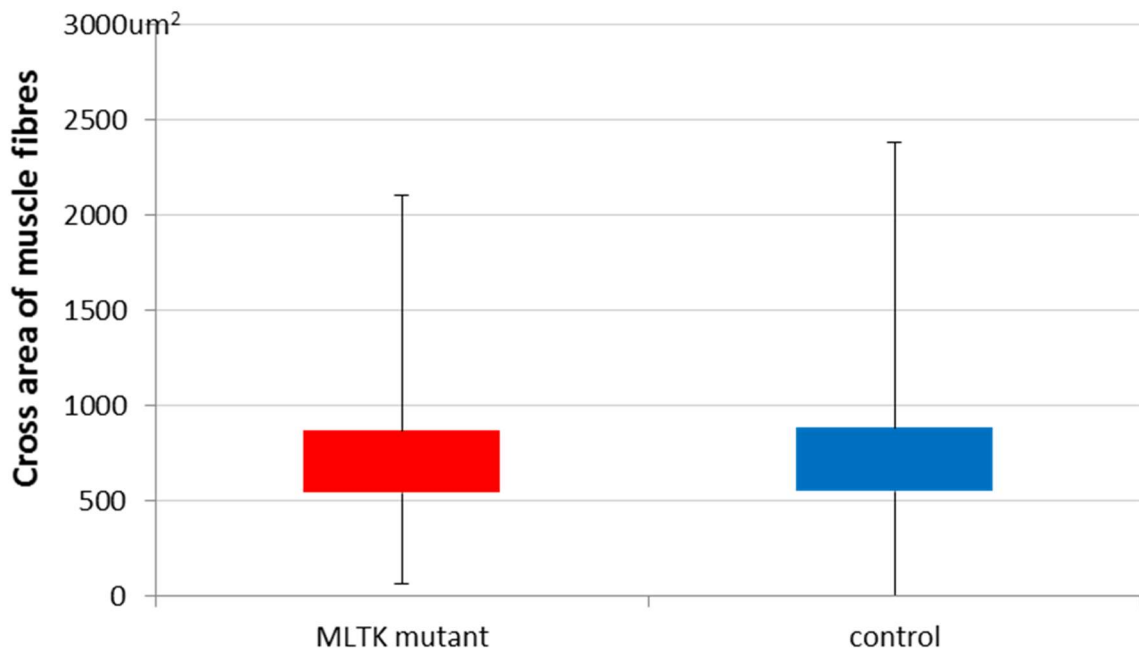


Figure 8.1: characterisation of MLTK deficient mice by H&E staining and cross sectional area measurement.

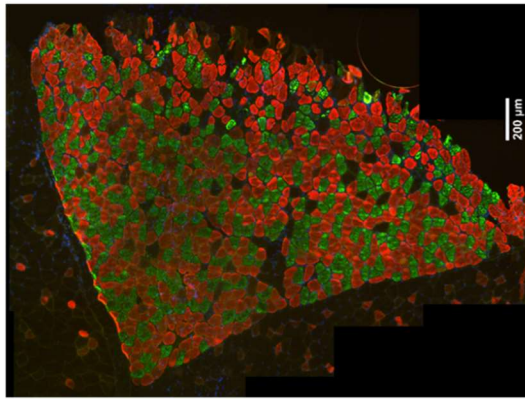
(A) and (B) are examples of H&E staining results from a MLTK deficient mouse and a control mouse. (A') and (B') are images magnified from the area within the square in (A) and (B) respectively. The magnified area is within the soleus. (C), Box-and-whisker diagram depicting a fibre size (cross-sectional area) comparison between MLTK deficient mice and control mice. All the fibres in soleus muscle were measured. Error bars represent variability outside the upper and lower quartiles. Two MLTK mutant mice and two control mice were used for fibre cross sectional area tests, the mean values of soleus fibre cross areas for MLTK mutant mice and control mice are  $719 \text{ um}^2$  and  $755 \text{ um}^2$  respectively. All the mice used in this figure are male and between 4 to 5 weeks old. MLTK deficient mice and control mice are all of the C57BL/6J strain but not siblings.

### 8.2.2 Fibre typing analysis in soleus of MLTK deficient mice

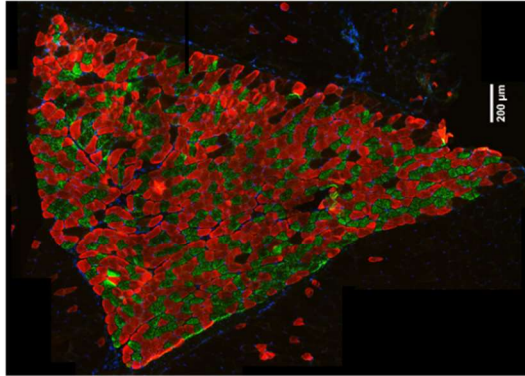
To test whether MLTK deficiency can cause other phenotypic changes in skeletal muscle, the proportions of fast and slow fibres were measured in soleus muscle. Antibodies against type I and type IIA myofibers were used in cross sections from MLTK deficient mice. However, the antibodies are not able to detect any signals from these sections. A likely reason for this failure is that the tissue was processed by paraffin embedding, which can mask the epitope in the sample. To solve the problem, two more MLTK deficient mice were sacrificed, and tissue samples were snap frozen in liquid nitrogen-cooled isopentane prior to cryostat sectioning (these tissues were collected from The Francis Crick Institute, Mill Hill Laboratory. Both mice were male and sacrificed at 11 weeks old). The immunostaining results shows that around 60% of fibres express type IIA myosin, and about 30% of fibres express type I myosin in soleus muscle in both MLTK deficient mice and a control mouse (control mouse is 10 weeks old and not sibling of MLTK deficient mice) (figure 8.2). A study has shown that the relative proportions of fast and slow type fibres are similar from the ages of 1 week to 1 year - about 60-70% of fibres in soleus are fast and about 30-40% are slow<sup>91</sup>. This suggests that MLTK deficiency does not change the proportions of fast and slow fibres in mouse skeletal muscle.

**A**

MLTK mutant3



MLTK mutant4



Control 3

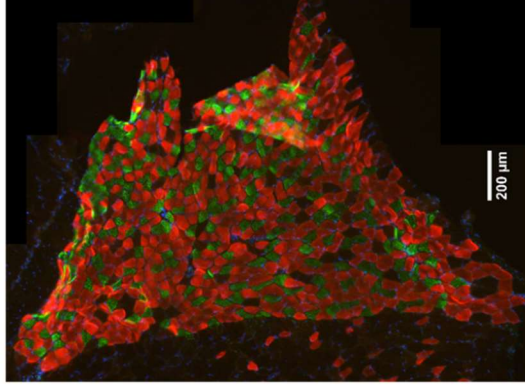
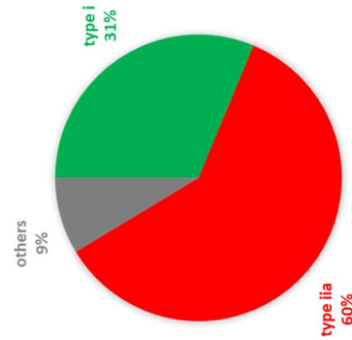


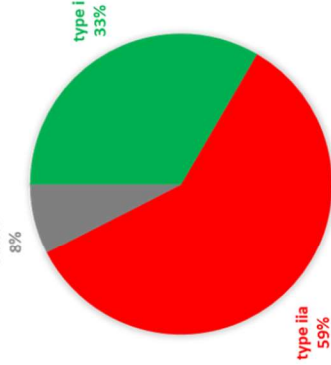
Figure 8.2: Data showing the proportion of type I and type IIA fibres in soleus muscle in MLTK deficient mice and a control mouse. (A), Immunostaining of type I and type IIA fibres. Red fibres are type IIA myosin antibody and TRITC conjugated secondary antibody stained fast myofibres. Green fibres are type I myosin antibody and FITC conjugated secondary antibody stained slow myofibres. (B) Pie charts show the proportion of type I and type IIA fibres in soleus muscle in MLTK deficient mice and a control mouse. The measured fibres are from figure (A). Both MLTK deficient mice are 11 week old, male siblings. The control mouse is 10 weeks old, male, not a sibling with the MLTK deficient mice.

**B**

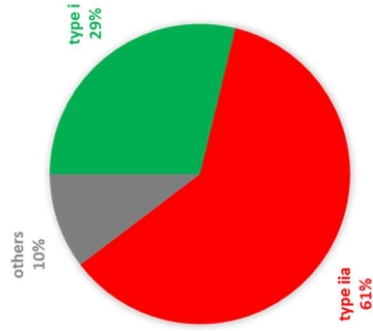
MLTK mutant3



MLTK mutant4



Control 3



### 8.2.3 RT-PCR analysis of MLTK expression in mouse skeletal muscle

To explore the effects of MLTK deficiency in mouse skeletal muscle, H&E staining, fibre cross sectional area measurement and the proportions of fast and slow fibres analysis in soleus muscle were performed. The only effect that could be observed as a result of MLTK deficiency in the mice is that the number of nuclei in soleus muscle fibres was increased in MLTK deficient mice compared with control mice. Until now, the only RT-PCR result demonstrating a knockdown of MLTK expression in the MLTK deficient mouse was from bone marrow-derived macrophages<sup>89</sup>, and no clear evidence to prove that MLTK expression level has been knocked down in mouse skeletal muscle. To address this, RT-PCR testing of MLTK $\beta$  expression levels in skeletal muscle was performed in the presumed MLTK deficient mice and control mouse. MLTK $\alpha$  expression levels were not examined because previous experiments have shown that MLTK $\beta$  is the main isoform in mouse skeletal muscle (see chapter 5). The primers for MLTK $\beta$  and housekeeping gene amplification are the same as the primers used previously (chapter 5 results 5.2.1). The method used to perform RT-PCR analysis is the same as in chapter 5 result 5.2.2. The equations shown below were used for these calculations.

Here,  $\Delta C_T$  stimulated is  $C_{T_{MLTK\text{ deficient}}} - C_{T_{HPRT}}$ ,  $\Delta C_T$  control is  $C_{T_{control}} - C_{T_{HPRT}}$ .

$$\text{Fold Change} = 2^{-\Delta(\Delta C_T)}$$

$$\Delta C_T = C_{T_{\text{target}}} - C_{T_{HPRT}}$$

$$\Delta(\Delta C_T) = \Delta C_{T_{\text{stimulated}}} - \Delta C_{T_{\text{control}}}$$

Figure 8.3 shows that the expression level of MLTK $\beta$  in the MLTK deficient mouse 3 is almost the same as in the control mouse 3, but is 1.6 times lower in MLTK deficient mouse 4 compared to control mouse 3. Additionally, the t-test results (from three technical replicates) do not reveal any statistical difference between MLTK deficient mice and the control mouse.

The RT-PCR results therefore indicate that the expression level of MLTK $\beta$  has not been knocked down in skeletal muscle in these presumed MLTK deficient mice. Previous study showed that MLTK expression in bone marrow-derived macrophages from 4 independent MLTK deficient mice are significantly decreased comparing with control <sup>89</sup>. The macrophages RT-PCR results contradict to the RT-PCR results showed in this section.

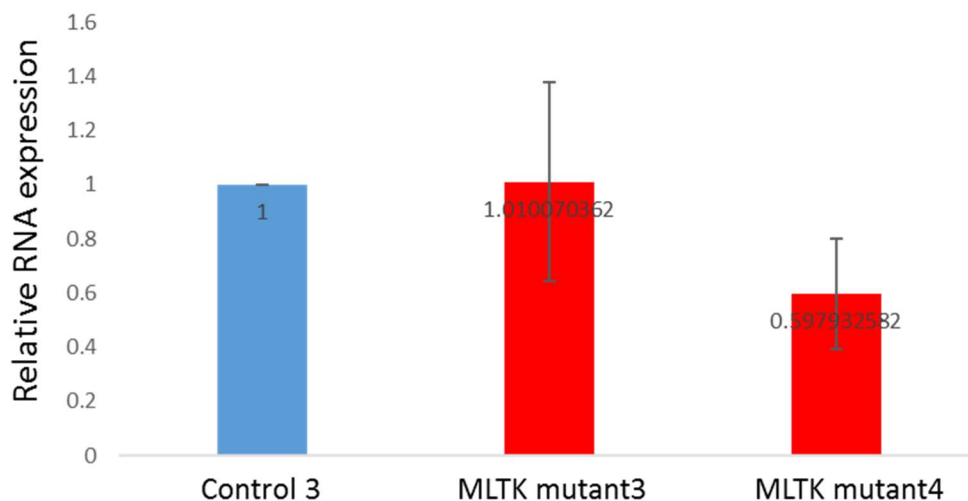


Figure 8.3: Real-time PCR quantification of MLTK $\beta$  expression in MLTK deficient mice and control mouse.

Both MLTK deficient mice are male and 11 weeks old. The control mouse is male and 10 weeks old. The MLTK deficient mice and control mouse belong to the C57BL/6J strain but they are not siblings. Error bars represent the standard deviation of three technical replicates.

#### 8.2.4 Western blot analysis of MLTK expression in mouse skeletal muscle

To test the MLTK protein expression level in MLTK deficient mice, two antibodies against MLTK (Anti-MLTK 14945-1-AP from Proteintech and Anti-MLTK 4-23 <sup>61</sup>) were used to detect

endogenous MLTK $\beta$  expressions in two MLTK deficient mice and a control mouse. The protein lysates were prepared from skeletal muscle of mouse MLTK deficient 3, MLTK deficient 4 and control 3, and diluted to the same concentrations to perform WB analysis. GAPDH antibody was used to confirm that same amount of protein lysates from MLTK deficient 3, MLTK deficient 4 and control 3 were loaded in each lane. To confirm that both MLTK antibodies were efficiently detecting MLTK $\beta$  protein, protein lysate from MLTK $\beta$ -GFP expressing COS7 and normal COS7 control cells were loaded into the same protein gel, the WB results shown a strong band between 70-100kDa in COS7 MLTK $\beta$ -GFP lanes, the molecular weight of MLTK $\beta$ -GFP is 78 kDa, and the same band did not show in COS7 control lanes, which confirmed that both MLTK antibodies efficiently recognized MLTK $\beta$  recombinant protein. The results also showed that MLTK antibodies detected MLTK $\beta$  expression in both MLTK deficient mice, but the expression in MLTK deficient 4 was not as strong as in MLTK deficient 3 and control 3 (figure 8.4). These results indicate that the MLTK “deficient” mice still express MLTK $\beta$  in skeletal muscle.

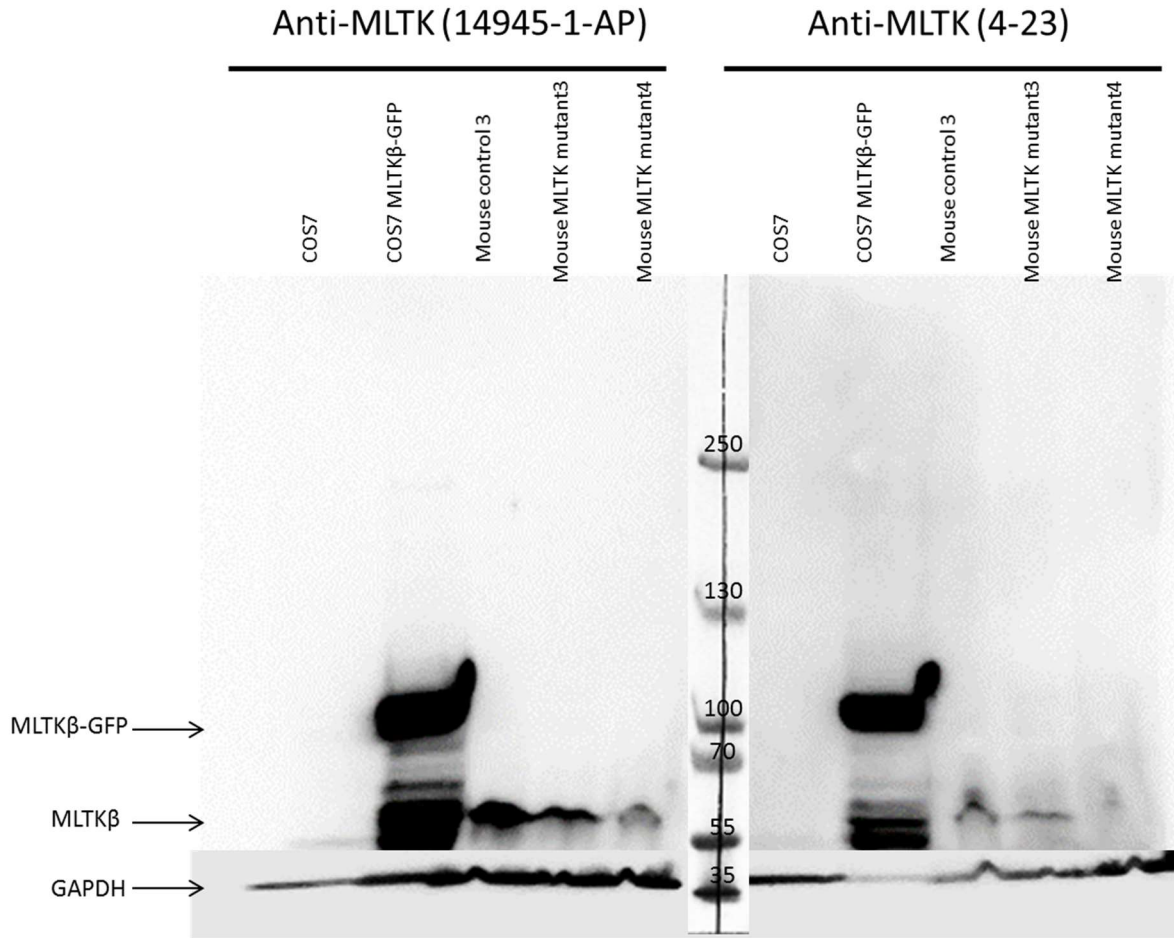


Figure 8.4 Western blot analysis of MLTK expression in mouse skeletal muscle. Two MLTK antibodies were used to detect endogenous MLTK $\beta$  expression in mouse skeletal muscle, the same amount of protein lysates from MLTK deficient 3, MLTK deficient 4 and control 3 were loaded in the protein gel.

### 8.3 CONCLUSIONS

This chapter aimed to characterise the effect of MLTK deficiency on skeletal muscle. The only phenotype observed in the MLTK deficient mice is an increased number of nuclei in soleus muscle in MLTK deficient mice compared to control mice. Both RT-PCR and WB results confirmed that the expression level of MLTK $\beta$  in skeletal muscle is not statistically significantly reduced in MLTK deficient mice, which indicates that the MLTK “deficient” mice cannot be

used to study the effect of MLTK deficiency on skeletal muscle, and the number of nuclei in soleus increases in MLTK deficient mice are not a result of MLTK deficiency. Because the MLTK deficient mouse and its sibling control were located in colonies in the US and The Francis Crick Institute, Mill Hill Laboratory (London), very limited numbers of mice of the desired genotype were available for this study (two MLTK mutant mice from US with 10% formaline fixation and another two mutant mice from Mill Hill laboratory with snap frozen in liquid nitrogen), hence the increased number of nuclei in the soleus of MLTK deficient mice was not further explored.

# Chapter 9

## 9. DISCUSSION

## 9.1 Introduction and aims:

The aims of the work presented in this thesis have been to characterize the function of IGFN1 and MLTK in skeletal muscle.

## 9.2 Subcellular localization of IGFN1 and MLTK:

A previous study identified the localization of IGFN1 protein using two antibodies, Ab-US42 (against the N-terminus of IGFN1) and Ab-Kip2b (against the C-terminus of IGFN1). Both identified that IGFN1 locates to the nucleus and Z-disc <sup>4</sup>. Since these antibodies are not able to distinguish between the specific isoforms of IGFN1, this thesis used ectopic expression of IGFN1-tdTomato and IGFN1\_V1-tdTomato *in vitro* and *in vivo* to study the specific localization of IGFN1 and IGFN1\_V1 isoforms. The constructs encoding IGFN1-tdTomato and IGFN1\_V1-tdTomato were tested in COS7 cells, due to the COS7 cell being an easily transfectable mammalian cell line. Both constructs expressed strong fluorescence in COS7 cells, indicating that the construct was capable of inducing robust expression of the protein isoforms, which was confirmed by western blot (in results 4.2.5). The results demonstrating that these constructs are capable of robustly inducing the expression of the tagged protein isoforms, making the plasmids good tools to study protein localization *in vivo* and *in vitro*.

The thesis identified the localizations of IGFN1-tdTomato and IGFN1\_V1-tdTomato in undifferentiated mouse myoblasts (C2C12). The results showed nuclear, cytoplasmic or nuclear/cytoplasmic localization patterns in proliferating myoblasts transiently transfected with either IGFN1-tdTomato or IGFN1\_V1-tdTomato. The multiple localization patterns indicated that IGFN1 and IGFN1\_V1 may shuttle between the nucleus and cytoplasm. The

stable cell lines generated for constitutive expression of IGFN1-tdTomato or IGFN1\_V1-tdTomato show only cytoplasmic localisation in both proliferating myoblasts and differentiated myotubes (few examples of nuclear localisation were observed in IGFN1-tdTomato stable expressed myoblasts, and this cell line was unable to form myotubes).

The discrepancy between the protein localisation seen between cells transiently expressing the IGFN1 isoforms and cells constitutively expressing the isoforms may be down to a dosage effect. Judging from fluorescence levels, transient expression of the proteins was much stronger than the expression seen in constitutively expressing cells. It may therefore be that the increased dosage of IGFN1 in transiently expressing cells allows for nuclear localisation whereas lower levels remain cytoplasmic. For example, if there is a negative regulator inhibiting the nuclear translocation of IGFN1, increased levels of IGFN1 may have overwhelmed this inhibition. It may also be because that culture reagents are specifically designed to promote cell growth and proliferation, and so it is likely that myoblasts have robust pro-growth signalling. If such signalling is responsible for preventing IGFN1 nuclear translocation, this may make nuclear translocation difficult to achieve if IGFN1 expression is not high. In contrast, in skeletal muscle tissue, nuclear expression is observed consistently. Skeletal muscle is quiescent and thus the signalling environment in skeletal muscle tissue is not specifically engineered to promote growth and proliferation. Therefore, if growth signals do interfere with IGFN1 localising to the nucleus, we might expect this inhibitory effect to be less pronounced in skeletal muscle tissue. Future experiments could test this hypothesis by examining whether IGFN1 localisation alters under pro-atrophic conditions. For example, the cell lines could be tested to see whether IGFN1 is more likely to locate to the nucleus in media deficient in amino acids or other nutrients/growth factors.

In order to prove that the cytoplasmic localization is not artefact, more stably-expressing clones should be generated. Due to the low transfection efficiency in C2C12 cells, only 5% of cells or even less can be transiently transfected with plasmids encoding IGFN1-tdTomato or IGFN1\_V1-tdTomato, and most transfected cells will not integrate the plasmid into the genome. After selective antibiotic treatment for at least 7 days, only a few clones remained in the cell culture plates. The majority of clones were lost during the expansion of the cell population due to some technical reasons such as contamination. As a result, only one stably-expressing clone for each IGFN1-tdTomato or IGFN1\_V1-tdTomato were successfully generated. There is therefore a reasonable possibility that the observed localisations could be influenced by artefacts of the process of clonal selection.

To identify the subcellular localization of IGFN1 and IGFN1\_V1 in mouse skeletal muscle, this thesis ectopically expressed recombinant IGFN1-tdTomato and IGFN1\_V1-tdTomato in muscle by *in vivo* electroporation. The results show that both IGFN1-tdTomato and IGFN1\_V1-tdTomato localise to the Z-disc and nuclei. The difference between IGFN1 and IGFN1\_V1 is an unstructured region existing between the 3<sup>rd</sup> and 4<sup>th</sup> globular domains of IGFN1. The localization results from IGFN1 and IGFN1\_V1 overexpression in muscle indicates that the unstructured region does not cause differences in subcellular localisation between IGFN1 and IGFN1\_V1 in skeletal muscle.

Previous studies found that *Igfn1* is upregulated in atrophic muscle caused by short term denervation<sup>45</sup> or activin A treatment<sup>46,47</sup>. *Igfn1* is downregulated in hypertrophic muscle treated with ActRIIB-Fc<sup>48</sup>. This indicates that the expression level of IGFN1 relates with muscle hypertrophy or atrophy possibly via activin A signalling. Both *in vitro* and *in vivo* approaches

have suggested a dual localisation for IGFN1 isoforms, between the nucleus and the cytoplasm in myoblasts and between the nucleus and z-disc in muscle tissue. One hypothesis for the patterns observed is that when IGFN1 expression reaches sufficient levels, it is able to translocate to the nucleus where it may help mediate altered expression of genes related to hypertrophy or atrophy, such as the genes involving with activin A signalling. If this hypothesis is true, changing the expression level of IGFN1 may result in muscle hypertrophy or atrophy. To address the problem, IGFN1\_V1-tdTomato was overexpressed in mouse skeletal muscle. The overexpressing fibres showed inconsistent fibre size changes in three different mice: in mouse 1, the IGFN1 overexpressing fibres are significantly bigger than non-transfected fibres; mouse 2 showed no fibre size difference between IGFN1 overexpressed fibres and non-transfected fibres; and mouse 3 showed that overexpression IGFN1\_V1-tdTomato significantly decreases muscle fibre size. The cause of these inconsistent fibre size changes is unclear, and the result is not able to address the hypothesis of whether IGFN1 overexpression might mediate hypertrophic or atrophic signalling. However, given the evidence for a dose-dependent change in IGFN1 localisation, it would seem likely that the effects of IGFN1 overexpression vary depending on how much protein is expressed. It is possible that differences in electroporation efficiency in individual mice may have resulted in inconsistent dosages of the IGFN1 isoforms and this may underlie the apparent contradictory results.

There are many studies focused on MLTK and it has been found to be highly expressed in skeletal muscle and heart <sup>51,53</sup>. However, the function of this protein in skeletal muscle has not been substantially investigated. To study the function of MLTK in skeletal muscle, this thesis first investigated the subcellular localization of MLTK *in vivo* and *in vitro*. The constructs for expression GFP- or tdTomato-labelled MLTK $\alpha$  and MLTK $\beta$  were tested in COS7 cells due to

the fact that this cell line is easily transfected. The results showed that MLTK $\alpha$  and MLTK $\beta$  locate to both nuclei and cytoplasm. Greater nuclear expression was observed in MLTK $\beta$ -transfected cells. This result is consistent to the previous study<sup>53</sup>, indicating that that labelling MLTK $\alpha$  or MLTK $\beta$  at C-terminus with fluorescent protein tags does not affect their subcellular localization.

The *in vivo* expression of MLTK $\alpha$ -tdTomato and MLTK $\beta$ -tdTomato confirmed the Z-disc localization of both MLTK isoforms in mouse skeletal muscle. Besides the Z-disc, MLTK $\alpha$ -tdTomato and MLTK $\beta$ -tdTomato were also found at the M-line and in parallel lines along the muscle fibres. The nuclear localization has not been observed in either MLTK $\alpha$ -tdTomato or MLTK $\beta$ -tdTomato expressing fibres. Since the Z-disc is the only location in which both IGFN1 and MLTK localise, this suggests that the interactions between IGFN1 and MLTK happens at the Z-disc. This hypothesis was tested in this thesis by co-expression of IGFN1\_V1-tdTomato and MLTK $\beta$ -GFP in skeletal muscle. The co-expression results confirmed that both IGFN1\_V1-tdTomato and MLTK $\beta$ -GFP co-localised at the Z-disc. Moreover, MLTK $\beta$ -GFP was also found co-located at nuclei with IGFN1\_V1-tdTomato. Immunofluorescence analysis using an MLTK antibody to probe IGFN1\_V1-tdTomato expressing fibres found that endogenous MLTK accumulated in IGFN1\_V1-tdTomato expressing nuclei. These findings suggest that IGFN1\_V1 shuttles between nuclei and the Z-disc, and it is responsible for driving MLTK into nuclei. The reason why elevated expression of IGFN1 drives MLTK into nuclei still unknown. Interestingly, overexpression MLTK $\beta$ -tdTomato alone in muscle does not result in nuclear localisation, whereas co-expression of MLTK $\beta$ -GFP and IGFN1\_V1-tdTomato or overexpression of IGFN1\_V1-tdTomato alone could induce recombinant MLTK $\beta$  or endogenous MLTK into nuclei.

These findings suggest that the nuclei localization of MLTK $\beta$  is sensitive to the expression level of IGFN1\_V1.

### 9.3 The interactions between IGFN1\_V1 and MLTK $\beta$ :

In this thesis, the interactions between IGFN1\_V1-v5 and MLTK $\alpha$ -GFP or MLTK $\beta$ -GFP were confirmed by immunoprecipitation. An additional experiment, performed by a placement student Matthew Winder, used his-tagged IGFN1, IGFN1<sub>(d1-d3)</sub> and IGFN1<sub>(d8-d11)</sub> to pull down MLTK $\alpha$ -GFP and MLTK $\beta$ -GFP produced from COS7 cells. The result showed that both MLTK $\alpha$ -GFP and MLTK $\beta$ -GFP could be pulled down with all his-tagged IGFN1, IGFN1<sub>(d1-d3)</sub> and IGFN1<sub>(d8-d11)</sub> isoforms, which indicates that the interaction site responsible for IGFN1 and MLTK interactions exists in both IGFN1<sub>(d1-d3)</sub> and IGFN1<sub>(d8-d11)</sub> regions. Moreover, as mentioned before, both IGFN1\_V1-tdTomato and MLTK $\beta$ -GFP co-located to the Z-disc, which is additional evidence to confirm the interaction between IGFN1\_V1-tdTomato and MLTK $\beta$ -GFP.

A distinctive phenotype was observed in IGFN1\_V1-tdTomato and MLTK $\alpha$ -GFP or MLTK $\beta$ -GFP co-expressing fibres, namely numbers of patches or clusters of small apparent aggregates around the nucleus. These aggregates were composed of IGFN1\_V1-tdTomato and MLTK $\alpha$ -GFP or MLTK $\beta$ -GFP proteins. This expression pattern was not observed in IGFN1\_V1-tdTomato, MLTK $\alpha$ -GFP or MLTK $\beta$ -GFP single transfections. Usually, newly generated polypeptides need to fold into a distinct three-dimensional conformation and go through further modifications to form a functional protein<sup>76</sup>. If even a small mistake occurs during protein folding, it may result in misfolded proteins which are prone to form aggregates<sup>77</sup>. One estimate is that up to 30% of newly generated proteins are not folded properly<sup>78</sup>.

Overexpression of a large amount of high molecular weight recombinant proteins in muscle cells may therefore generate a significant amount of misfolded proteins. Because IGFN1\_V1 and MLTK proteins are interaction partners, the interactions may still exist between misfolded IGFN1\_V1 and MLTK recombinant proteins, and this may increase the possibility of forming protein aggregations. This may explain why the aggregates are easily observed in the co-expression fibres compared to fibres expressing IGFN1\_V1-tdTomato, MLTK $\alpha$ -GFP or MLTK $\beta$ -GFP alone. Misfolded proteins are usually recognized by ubiquitin E3 ligases, which form polyubiquitinated protein and lead to proteasome-mediated protein degradation <sup>79</sup>. To test whether these aggregations are caused by protein misfolding, future experiments can test whether these aggregates are polyubiquitinated by immunostaining the fibres with a ubiquitin antibody.

#### 9.4 Muscle hypertrophy induced by MLTK overexpression:

A previous study found that cardiac-restricted overexpression of MLTK $\beta$  caused cardiac muscle hypertrophy <sup>5</sup>. Since both cardiac muscle and skeletal muscle contains the same contractile structure, sarcomere, and MLTK locates at the important sarcomere structures such as the Z-disc and M-line, it is possible that MLTK can also induce skeletal muscle hypertrophy. In this thesis, MLTK $\beta$ -tdTomato was overexpressed in skeletal muscle to test this hypothesis. The results showed that overexpression of MLTK $\beta$ -tdTomato significant increased cross sectional area of muscle fibres compared to non-transfected fibres. Moreover, some of the MLTK $\beta$ -tdTomato overexpressing fibres showed ring fibres and desmin and myosin antibody staining showed disorganized myofibrils due to the MLTK $\beta$ -tdTomato overexpression. These ring fibres were also observed in a patient with MLTK mutation in exon

7, which affects the kinase domain in both isoforms of MLTK, leading to a frameshift and a predicted truncated protein. The patient suffered from muscle weakness, impaired ambulant ability and decreased ventilatory capacity <sup>6</sup>. Moreover, cardiac-restricted overexpression of MLTK $\beta$  also caused disorganized myofibrils in mice <sup>5</sup>. These findings indicate that a certain expression level of MLTK $\beta$  is important to maintain muscle health. However, overexpression, deficiencies in expression or the loss of MLTK $\beta$  kinase function can result in disorganized myofibrils.

#### 9.5 Knocking out/down IGFN1 *in vivo* and *in vitro*:

To study the function of IGFN1 at the undifferentiated myoblast stage or during myotube differentiation, IGFN1 expression was knocked out using CRISPR/Cas technology. RT-PCR analysis confirmed that the expression levels of IGFN1 in all the IGFN1 KO clones are significantly reduced. Morphological changes were not observed between IGFN1 KO clones and control cells during the undifferentiated myoblast stage. All the IGFN1 knockout clones show abnormal morphology during cell differentiation compared with C2C12 cells. These abnormalities appear as short myotube formation and globular differentiation bodies seen in bright-field images. These results indicate that IGFN1 is important for regulation of muscle myogenesis.

The same CRISPR/Cas plasmid used to knockout IGFN1 in C2C12 cells was used in skeletal muscle to perform and *in vivo* IGFN1 knockdown. 21 days or longer after injection, there were no significant fibre cross sectional area changes between CRISPR/Cas plasmid transfected fibres and un-transfected fibres. The T7 endonuclease I mismatch cleavage assay showed the

IGFN1 CRISPR/Cas plasmid could perform with high mutation efficiency in 3T3 cells, and it also had a good efficiency during the IGFN1 KO cell line generation. In theory, this IGFN1 CRISPR/Cas plasmid should also perform a good mutation efficiency in skeletal muscle. To test whether IGFN1 CRISPR/Cas can cause *Igfn1* gene mutation in skeletal muscle, genomic DNA was isolated from IGFN1 CRISPR/Cas transfected muscles, and the IGFN1 CRISPR/CAS targeting area was amplified by PCR. All the PCR products were sent out for sequencing, but all the sequencing results returned showing multiple detection peaks in the sequence chromatograms along the whole sequence (figure 9.1A). This is either an artefact, or indicates that more than one IGFN1 sequence exists in the PCR products. In results showing mutagenesis in cell lines, the multiple peaks start from the IGFN1 CRISPR/Cas targeting area as shown in figure 9.1B. The sequence before the targeting area is identical to the wild type *Igfn1*, therefore the sequencing result shows as a single peak. Once the sequencing process reaches the mutation site, the following sequencing base will be disrupted by the mutations, such as insertions or deletions, which will lead to multiple peaks. However, this ideal sequencing result may not be easy to observe in IGFN1 CRISPR/Cas transfected muscles. Because the muscle contains multiple nuclei in each muscle fibre, if mutagenesis is successful it will result in many different mutations in a single fibre, and even more different mutations for the IGFN1 CRISPR/Cas transfected muscles. This may mean that the sensitivity of Sanger sequencing is not enough to identify these mutations. Future experiments can use next generation sequencing to isolate any mutated alleles. Until such mutant alleles are isolated, it is presently not possible to say whether *in vivo* mutagenesis has been successful.

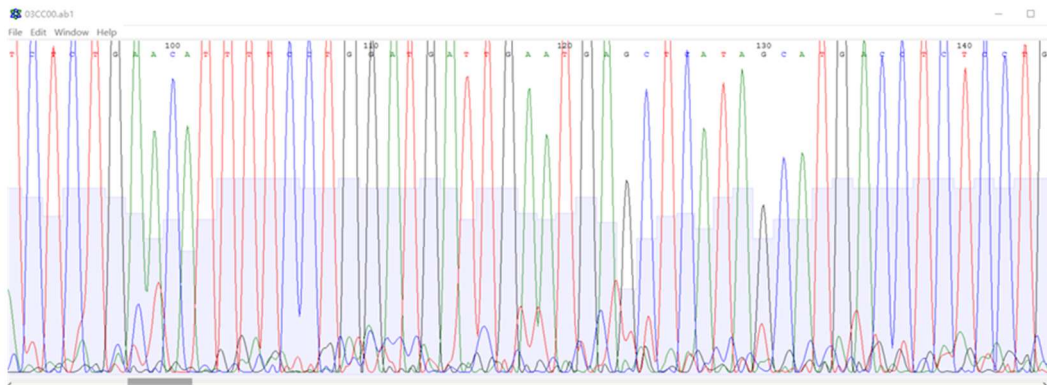
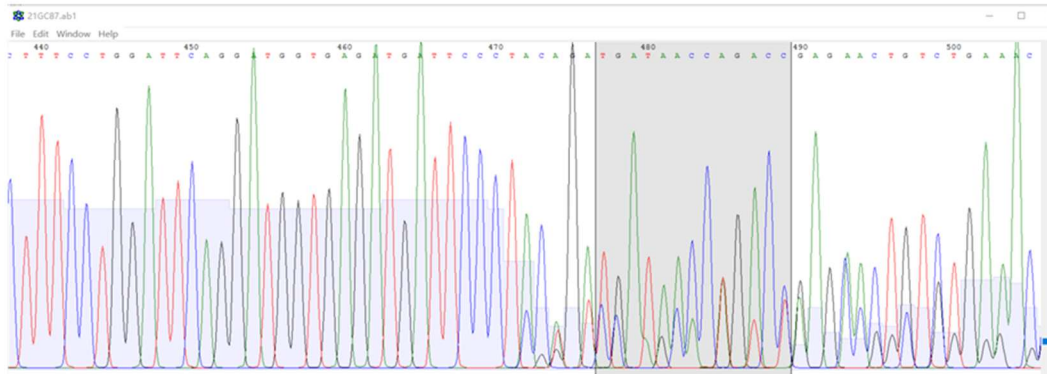
**A****B**

Figure 9.1: Sequence chromatograms of PCR products from *Igfn1* in targeted samples. (A), an example of unclear sequencing results. (B) an example of ideal sequencing result. The result came from a IGFN1 KO clone mixed with cells which do not contain any mutations. The grey area is the IGFN1 CRISPR/Cas targeting area, the mutations should be happening around this area, which is apparent from multiple peaks starting from this area. However, the sequencing results from CRISPR/Cas transfected muscle shows as figure A, with multiple peaks all along the whole sequencing result.

In summary, this thesis confirmed the interactions between IGFN1\_V1 and both isoforms of MLTK by immunoprecipitation and pulldown assays. Given that KY and MLTK both interact with IGFN1, and all three proteins locate in Z-disc <sup>4</sup>, as well as the similar pathology affecting skeletal muscle in both KY and MLTK mutant mice or human <sup>1,6</sup>, all these evidences indicate that IGFN1 and MLTK may be involved in the same pathway.

This thesis shows that overexpressing recombinant MLTK $\beta$  results skeletal muscle fibre cross sectional area increases. MLTK belongs to the MAPKKK family, which are able to activate downstream factors, MAPKKs and MAPKs, in MAPK pathways. There are at least four MAPK pathways in mammals, ERK1/2, JNK, P38 and ERK5 <sup>92</sup>. However, the evidence to determine which MAPK pathways are responsible for MLTK induced increases of muscle fibre size is still lacking. To study this, specific inhibitors for each MAPK pathway (such as, p38 $\alpha/\beta$  inhibitor SB-203580, JNK inhibitor SP-600123 and MEK inhibitor PD-98059) can be used in the future to test whether blocking each MAPK pathway is able to prevent MLTK induced muscle fibre hypertrophy. In addition, mTOR signalling is a major pathway regulating protein synthesis in skeletal muscle, the question whether MLTK induced muscle hypertrophy is mTOR dependent can be also investigated in the future.

In addition, MLTK $\beta$  was confirmed as the primary isoform in skeletal muscle by RT-PCR. Overexpression of recombinant MLTK $\beta$  resulted in disorganized myofibrils. Together with the previous finding that overexpression <sup>5</sup> or reduction <sup>6</sup> of MLTK $\beta$  causes myofibril disorganization in either cardiac or skeletal muscles, this indicates that a certain expression level of MLTK $\beta$  is important for maintaining muscle health.

This thesis also found that IGFN1 protein is important for maintaining morphology of myotubes during myogenesis. Given that IGFN1 interacts with many other muscle proteins,

some of which are important sarcomeric cytoskeletal proteins, such as TTN, FLNC, actin, slow type myosin binding protein C (MYBPC1) and myomesin <sup>4</sup>, it is possible that knocking out IGFN1 expression in myoblast causes the absence of interactions between IGFN1 and these sarcomeric cytoskeletal proteins. This may in turn result in abnormal differentiation patterns. To test this hypothesis, immunostaining IGFN1 KO myotubes with antibodies against TTN, FLNC, actin, MYBPC1 and myomesin will be used to compare sarcomeric cytoskeletal protein distributions in KO cell lines and control.

Furthermore, ectopically expressed recombinant IGFN1 or IGFN1\_v1 in adult mouse muscle fibres shows Z-disc and nuclear localization, whilst MLTK $\alpha$  and MLTK $\beta$  show Z-disc localization without nuclear localization. Moreover, co-expression of recombinant IGFN1\_V1 and different isoforms of MLTK in skeletal muscle results in Z-disc co-localization. Additionally, IGFN1\_V1 co-expression induces a clear nuclear localization for ectopic MLTK $\beta$ , whilst endogenous MLTK $\beta$  was also found accumulated in the nuclei of muscle fibres where IGFN1\_V1-tdTomato alone was overexpressed. These results indicate that IGFN1\_V1 interacts with MLTK $\alpha$  and MLTK $\beta$  at the Z-disc and overexpression possibly drives MLTK $\beta$  into the nucleus.

## Abbreviations:

<b>4E-BP1</b>	factor 4E-binding protein 1
<b>Ab-Kip2b</b>	against the C-terminus of IGFN1
<b>Ab-US42</b>	against the N-terminus of IGFN1
<b>ACVR II</b>	activin receptor II
<b>ALK4 and ALK5</b>	activin receptor-like kinase 4 and 5
<b>BDL</b>	Bile Duct Ligation
<b>BMD</b>	Becker muscular dystrophy
<b>BMK1</b>	Big MAPK1
<b>BSA</b>	bovine serum albumin
<b>CMD</b>	Congenital muscular dystrophies
<b>ddH<sub>2</sub>O</b>	double distilled water
<b>DLK</b>	dual leucine zipper kinase
<b>DMD</b>	Duchenne muscular dystrophy
<b>DMEM</b>	Dulbecco's Modified Eagle Medium
<b>DSB</b>	double-strand break
<b>EDL</b>	Extensor digitorum longus
<b>EDL/TA</b>	Extensor digitorum longus/ Tibialis Anterior
<b>ERK</b>	extracellular signal regulated kinase
<b>FBS</b>	Fetal Bovine Serum
<b>Fn3</b>	fibronectin type III
<b>H&amp;E</b>	Hematoxylin and eosin
<b>Ig</b>	immunoglobulin
<b>IGF1</b>	insulin-like growth factor 1
<b>IGFN1</b>	immunoglobulin-like and fibronectin type III domain containing 1
<b>IP</b>	immunoprecipitation
<b>JNK</b>	c-Jun N-terminal kinase
<b>KY</b>	kyphoscoliosis peptidase
<b>LB</b>	Lysogeny broth
<b>LZK</b>	leucine zipper kinase
<b>MAFbx</b>	muscle atrophy F-box
<b>MAPKKK</b>	mitogen activated protein kinase kinase kinase
<b>MAPKs</b>	mitogen activated protein kinases
<b>MHCI</b>	myosin heavy chain I
<b>MLC</b>	myosin light chain
<b>MLTK</b>	MLK-like mitogen-activated protein triple kinase
<b>mTOR</b>	mammalian target of rapamycin
<b>mTORC2</b>	mTOR complex 2
<b>MuRF1</b>	Muscle RING finger 1

<b>NES</b>	nuclear export signal
<b>NHEJ</b>	non-homologous end joining
<b>NLS</b>	nuclear localization signal
<b>PCR</b>	Polymerase chain reaction
<b>PI3K-Akt</b>	phosphoinositide-3-kinase-Akt
<b>S.O.C.</b>	Super Optimal Broth
<b>SAM</b>	sterile $\alpha$ -motif
<b>SAPK</b>	stress-activated protein kinase
<b>TAE</b>	Tris-acetate buffer
<b>TE</b>	Tris-EDTA buffer
<b>Tg</b>	transgenic
<b>TGF<math>\beta</math></b>	transforming growth factor $\beta$
<b>Y2H</b>	yeast two hybrid

## BIBLIOGRAPHY:

1. Blanco, G. *et al.* The kyphoscoliosis (ky) mouse is deficient in hypertrophic responses and is caused by a mutation in a novel muscle-specific protein. *Hum. Mol. Genet.* **10**, 9–16 (2001).
2. Hedberg-Oldfors, C. *et al.* A new early-onset neuromuscular disorder associated with kyphoscoliosis peptidase (KY) deficiency. *Eur. J. Hum. Genet.* (2016). doi:10.1038/ejhg.2016.98
3. Straussberg, R. *et al.* Kyphoscoliosis peptidase (KY) mutation causes a novel congenital myopathy with core targetoid defects. *Acta Neuropathol. (Berl.)* **132**, 475–478 (2016).
4. Baker, J. *et al.* Identification of a Z-band associated protein complex involving KY, FLNC and IGFN1. *Exp. Cell Res.* **316**, 1856–1870 (2010).
5. Christe, M. *et al.* Transgenic mice with cardiac-specific over-expression of MLK7 have increased mortality when exposed to chronic  $\beta$ -adrenergic stimulation. *J. Mol. Cell. Cardiol.* **37**, 705–715 (2004).
6. Vasli, N. *et al.* Recessive mutations in the kinase ZAK cause a congenital myopathy with fibre type disproportion. *Brain* aww257 (2016). doi:10.1093/brain/aww257
7. Fischman, D. A. Skeletal Muscle & Muscular Dystrophy: A Visual Approach. *Colloq. Ser. Cell Biol. Med.* **1**, 1–56 (2009).
8. Birbrair, A. *et al.* Role of Pericytes in Skeletal Muscle Regeneration and Fat Accumulation. *Stem Cells Dev.* **22**, 2298–2314 (2013).
9. Knöll, R., Buyandelger, B. & Lab, M. The Sarcomeric Z-Disc and Z-Discopathies. *BioMed Res. Int.* **2011**, (2011).

10. Pyle, W. G. & Solaro, R. J. At the Crossroads of Myocardial Signaling The Role of Z-Discs in Intracellular Signaling and Cardiac Function. *Circ. Res.* **94**, 296–305 (2004).
11. Tskhovrebova, L. & Trinick, J. Titin: properties and family relationships. *Nat. Rev. Mol. Cell Biol.* **4**, 679–689 (2003).
12. McNally, E. M. & Pytel, P. Muscle Diseases: The Muscular Dystrophies. *Annu. Rev. Pathol. Mech. Dis.* **2**, 87–109 (2007).
13. Hoffman, E. P., Brown, R. H. & Kunkel, L. M. Dystrophin: The protein product of the duchenne muscular dystrophy locus. *Cell* **51**, 919–928 (1987).
14. Ervasti, J. M. & Campbell, K. P. Membrane organization of the dystrophin-glycoprotein complex. *Cell* **66**, 1121–1131 (1991).
15. Malhotra, S. B. *et al.* Frame-shift deletions in patients with Duchenne and Becker muscular dystrophy. *Science* **242**, 755–759 (1988).
16. Mercuri, E., Sewry, C., Brown, S. C. & Muntoni, F. Congenital muscular dystrophies. *Semin. Pediatr. Neurol.* **9**, 120–131 (2002).
17. Griggs, R. C. & Amato, A. A. *Muscular Dystrophies*. (Elsevier, 2011).
18. Musarò, A. *et al.* Localized Igf-1 transgene expression sustains hypertrophy and regeneration in senescent skeletal muscle. *Nat. Genet.* **27**, 195–200 (2001).
19. Bodine, S. C. *et al.* Akt/mTOR pathway is a crucial regulator of skeletal muscle hypertrophy and can prevent muscle atrophy in vivo. *Nat. Cell Biol.* **3**, 1014–1019 (2001).
20. Pallafacchina, G., Calabria, E., Serrano, A. L., Kalhovde, J. M. & Schiaffino, S. A protein kinase B-dependent and rapamycin-sensitive pathway controls skeletal muscle growth but not fiber type specification. *Proc. Natl. Acad. Sci.* **99**, 9213–9218 (2002).
21. Risson, V. *et al.* Muscle inactivation of mTOR causes metabolic and dystrophin defects leading to severe myopathy. *J. Cell Biol.* **187**, 859–874 (2009).

22. Laplante, M. & Sabatini, D. M. mTOR Signaling in Growth Control and Disease. *Cell* **149**, 274–293 (2012).
23. Mounier, R. *et al.* Antagonistic control of muscle cell size by AMPK and mTORC1. *Cell Cycle* **10**, 2640–2646 (2011).
24. Lee, S.-J. Regulation of Muscle Mass by Myostatin. *Annu. Rev. Cell Dev. Biol.* **20**, 61–86 (2004).
25. Taylor, W. E. *et al.* Myostatin inhibits cell proliferation and protein synthesis in C2C12 muscle cells. *Am. J. Physiol. - Endocrinol. Metab.* **280**, E221–E228 (2001).
26. Han, H. Q., Zhou, X., Mitch, W. E. & Goldberg, A. L. Myostatin/activin pathway antagonism: Molecular basis and therapeutic potential. *Int. J. Biochem. Cell Biol.* **45**, 2333–2347 (2013).
27. Sandri, M. *et al.* Foxo Transcription Factors Induce the Atrophy-Related Ubiquitin Ligase Atrogin-1 and Cause Skeletal Muscle Atrophy. *Cell* **117**, 399–412 (2004).
28. Schiaffino, S., Dyar, K. A., Ciciliot, S., Blaauw, B. & Sandri, M. Mechanisms regulating skeletal muscle growth and atrophy. *FEBS J.* **280**, 4294–4314 (2013).
29. Zhao, J., Brault, J. J., Schild, A. & Goldberg, A. L. Coordinate activation of autophagy and the proteasome pathway by FoxO transcription factor. *Autophagy* **4**, 378–380 (2008).
30. Pickart, C. M. Mechanisms Underlying Ubiquitination. *Annu. Rev. Biochem.* **70**, 503–533 (2001).
31. Lodish, H. *et al.* *Molecular Cell Biology*. (W. H. Freeman, 2000).
32. Bodine, S. C. *et al.* Identification of Ubiquitin Ligases Required for Skeletal Muscle Atrophy. *Science* **294**, 1704–1708 (2001).
33. Eskelinen, E.-L. in (ed. Biology, B.-I. R. of C. and M.) **266**, 207–247 (Academic Press, 2008).
34. Kundu, M. & Thompson, C. B. Autophagy: Basic Principles and Relevance to Disease. *Annu. Rev. Pathol. Mech. Dis.* **3**, 427–455 (2008).

35. Eskelinen, E.-L. & Saftig, P. Autophagy: A lysosomal degradation pathway with a central role in health and disease. *Biochim. Biophys. Acta BBA - Mol. Cell Res.* **1793**, 664–673 (2009).
36. Dice, J. F. Chaperone-Mediated Autophagy. *Autophagy* **3**, 295–299 (2007).
37. Makarova, K. S., Aravind, L. & Koonin, E. V. A superfamily of archaeal, bacterial, and eukaryotic proteins homologous to animal transglutaminases. *Protein Sci.* **8**, 1714–1719 (1999).
38. Anantharaman, V. Peptide-N-glycanases and DNA repair proteins, Xp-C/Rad4, are, respectively, active and inactivated enzymes sharing a common transglutaminase fold. *Hum. Mol. Genet.* **10**, 1627–1630 (2001).
39. Dickinson, A. G. & Meikle, V. H. GENETIC KYPHOSCOLIOSIS IN MICE. *The Lancet* **301**, 1186 (1973).
40. Mason, R. M. & Palfrey, A. J. Intervertebral disc degeneration in adult mice with hereditary kyphoscoliosis. *J. Orthop. Res.* **2**, 333–338 (1984).
41. Bridges, L. R., Coulton, G. R., Howard, G., Moss, J. & Mason, R. M. The neuromuscular basis of hereditary kyphoscoliosis in the mouse. *Muscle Nerve* **15**, 172–179 (1992).
42. Beatham, J. *et al.* Filamin C interacts with the muscular dystrophy KY protein and is abnormally distributed in mouse KY deficient muscle fibres. *Hum. Mol. Genet.* **13**, 2863–2874 (2004).
43. Marechal, G., Coulton, G. R. & Beckers-Bleukx, G. Mechanical power and myosin composition of soleus and extensor digitorum longus muscles of ky mice. *Am. J. Physiol. - Cell Physiol.* **268**, C513–C519 (1995).
44. Ulbricht, A., Arndt, V. & Hohfeld, J. Chaperone-assisted proteostasis is essential for mechanotransduction in mammalian cells. *Commun. Integr. Biol.* **6**, (2013).

45. Mansilla, F. *et al.* Translation elongation factor eEF1A binds to a novel myosin binding protein-C-like protein. *J. Cell. Biochem.* **105**, 847–858 (2008).
46. Chen, J. L. *et al.* Elevated expression of activins promotes muscle wasting and cachexia. *FASEB J.* **28**, 1711–1723 (2014).
47. Chen, J. L. *et al.* Development of Novel Activin-Targeted Therapeutics. *Mol. Ther.* **23**, 434–444 (2015).
48. Rahimov, F. *et al.* Gene expression profiling of skeletal muscles treated with a soluble activin type IIB receptor. *Physiol. Genomics* **43**, 398–407 (2011).
49. Morrison, B. M. *et al.* A soluble activin type IIB receptor improves function in a mouse model of amyotrophic lateral sclerosis. *Exp. Neurol.* **217**, 258–268 (2009).
50. Blanco, G. *et al.* Molecular phenotyping of the mouse ky mutant reveals UCP1 upregulation at the neuromuscular junctions of dystrophic soleus muscle. *Neuromuscul. Disord.* **14**, 217–228 (2004).
51. Bloem, L. J. *et al.* Tissue Distribution and Functional Expression of a cDNA Encoding a Novel Mixed Lineage Kinase. *J. Mol. Cell. Cardiol.* **33**, 1739–1750 (2001).
52. Gallo, K. A. & Johnson, G. L. Mixed-lineage kinase control of JNK and p38 MAPK pathways. *Nat. Rev. Mol. Cell Biol.* **3**, 663–672 (2002).
53. Gotoh, I., Adachi, M. & Nishida, E. Identification and Characterization of a Novel MAP Kinase Kinase Kinase, MLTK. *J. Biol. Chem.* **276**, 4276–4286 (2001).
54. Huang, C.-Y. *et al.* ZAK re-programs atrial natriuretic factor expression and induces hypertrophic growth in H9c2 cardiomyoblast cells. *Biochem. Biophys. Res. Commun.* **324**, 973–980 (2004).
55. Kim, C. A. & Bowie, J. U. SAM domains: uniform structure, diversity of function. *Trends Biochem. Sci.* **28**, 625–628 (2003).

56. Robinson, M. J. & Cobb, M. H. Mitogen-activated protein kinase pathways. *Curr. Opin. Cell Biol.* **9**, 180–186 (1997).
57. Glennon, P. E., Sugden, P. H. & Poole-Wilson, P. A. Cellular mechanisms of cardiac hypertrophy. *Br. Heart J.* **73**, 496–499 (1995).
58. Spielmann, M. *et al.* Exome sequencing and CRISPR/Cas genome editing identify mutations of ZAK as a cause of limb defects in humans and mice. *Genome Res.* (2016). doi:10.1101/gr.199430.115
59. Mao, X., Bravo, I. G., Cheng, H. & Alonso, A. Multiple independent kinase cascades are targeted by hyperosmotic stress but only one activates stress kinase p38. *Exp. Cell Res.* **292**, 304–311 (2004).
60. Takahashi, M. *et al.* Regulation of a mitogen-activated protein kinase kinase kinase, MLTK by PKN. *J. Biochem. (Tokyo)* **133**, 181–187 (2003).
61. Gross, E. A., Callow, M. G., Waldbaum, L., Thomas, S. & Ruggieri, R. MRK, a Mixed Lineage Kinase-related Molecule That Plays a Role in  $\gamma$ -Radiation-induced Cell Cycle Arrest. *J. Biol. Chem.* **277**, 13873–13882 (2002).
62. Tosti, E., Waldbaum, L., Warshaw, G., Gross, E. A. & Ruggieri, R. The Stress Kinase MRK Contributes to Regulation of DNA Damage Checkpoints through a p38 $\gamma$ -independent Pathway. *J. Biol. Chem.* **279**, 47652–47660 (2004).
63. Wang, X. *et al.* Complete Inhibition of Anisomycin and UV Radiation but Not Cytokine Induced JNK and p38 Activation by an Aryl-substituted Dihydropyrrolopyrazole Quinoline and Mixed Lineage Kinase 7 Small Interfering RNA. *J. Biol. Chem.* **280**, 19298–19305 (2005).
64. Jandhyala, D. M., Ahluwalia, A., Obrig, T. & Thorpe, C. M. ZAK: a MAP3Kinase that transduces Shiga toxin- and ricin-induced proinflammatory cytokine expression. *Cell. Microbiol.* **10**, 1468–1477 (2008).

65. Cho, Y.-Y. *et al.* A Novel Role for Mixed-Lineage Kinase-Like Mitogen-Activated Protein Triple Kinase  $\alpha$  in Neoplastic Cell Transformation and Tumor Development. *Cancer Res.* **64**, 3855–3864 (2004).
66. Korkina, O. *et al.* The MLK-related Kinase (MRK) Is a Novel RhoC Effector That Mediates Lysophosphatidic Acid (LPA)-stimulated Tumor Cell Invasion. *J. Biol. Chem.* **288**, 5364–5373 (2013).
67. Rey, C. *et al.* The MAP3K ZAK, a novel modulator of ERK-dependent migration, is upregulated in colorectal cancer. *Oncogene* **35**, 3190–3200 (2016).
68. Liu, J. *et al.* Integrated exome and transcriptome sequencing reveals ZAK isoform usage in gastric cancer. *Nat. Commun.* **5**, (2014).
69. Xu, W.-H. *et al.* Long Non-coding RNA URHC Regulates Cell Proliferation and Apoptosis via ZAK through the ERK/MAPK Signaling Pathway in Hepatocellular Carcinoma. *Int. J. Biol. Sci.* **10**, 664–676 (2014).
70. Yang, J.-J. *et al.* ZAK inhibits human lung cancer cell growth via ERK and JNK activation in an AP-1-dependent manner. *Cancer Sci.* **101**, 1374–1381 (2010).
71. Gluzman, Y. SV40-transformed simian cells support the replication of early SV40 mutants. *Cell* **23**, 175–182 (1981).
72. Yaffe, D. & Saxel, O. Serial passaging and differentiation of myogenic cells isolated from dystrophic mouse muscle. *Nature* **270**, 725–727 (1977).
73. Todaro, G. J. & Green, H. Quantitative Studies of the Growth of Mouse Embryo Cells in Culture and Their Development into Established Lines. *J. Cell Biol.* **17**, 299–313 (1963).
74. Hoetelmans, R. W. M. *et al.* Effects of Acetone, Methanol, or Paraformaldehyde on Cellular Structure, Visualized by Reflection Contrast Microscopy and Transmission and Scanning Electron Microscopy. *Appl. Immunohistochem. Mol. Morphol.* **9**, (2001).

75. Ven, P. F. M. van der *et al.* Differentiation of human skeletal muscle cells in culture: maturation as indicated by titin and desmin striation. *Cell Tissue Res.* **270**, 189–198 (1992).
76. Cooper, G. M. Protein Folding and Processing. *The Cell: A Molecular Approach. 2nd edition.* Available from: [zotero://attachment/1068/](https://doi.org/10.1007/978-1-4020-1068-7) (2000).
77. Yao, T.-P. The Role of Ubiquitin in Autophagy-Dependent Protein Aggregate Processing. *Genes Cancer* **1**, 779–786 (2010).
78. Schubert, U. *et al.* Rapid degradation of a large fraction of newly synthesized proteins by proteasomes. *Nature* **404**, 770–774 (2000).
79. Cyr, D. M., Hohfeld, J. & Patterson, C. Protein quality control: U-box-containing E3 ubiquitin ligases join the fold. *Trends Biochem. Sci.* **27**, 368–375 (2002).
80. Luther, S. A., Tang, H. L., Hyman, P. L., Farr, A. G. & Cyster, J. G. Coexpression of the chemokines ELC and SLC by T zone stromal cells and deletion of the ELC gene in the *plt/plt* mouse. *Proc. Natl. Acad. Sci.* **97**, 12694–12699 (2000).
81. J, P. A. *et al.* Abnormalities in tenectomized muscle fiber repair. *Eur. J. Anat.* **11**, 37–45 (2007).
82. Paulin, D. & Li, Z. Desmin: a major intermediate filament protein essential for the structural integrity and function of muscle. *Exp. Cell Res.* **301**, 1–7 (2004).
83. Tskhovrebova, L. & Trinick, J. Properties of Titin Immunoglobulin and Fibronectin-3 Domains. *J. Biol. Chem.* **279**, 46351–46354 (2004).
84. Makarova, K. S. *et al.* Evolution and classification of the CRISPR–Cas systems. *Nat. Rev. Microbiol.* **9**, 467–477 (2011).
85. Mitchison, T. J. & Cramer, L. P. Actin-Based Cell Motility and Cell Locomotion. *Cell* **84**, 371–379 (1996).

86. Welch, M. D., Mallavarapu, A., Rosenblatt, J. & Mitchison, T. J. Actin dynamics in vivo. *Curr. Opin. Cell Biol.* **9**, 54–61 (1997).
87. Taylor, J. *et al.* Optimization of ectopic gene expression in skeletal muscle through DNA transfer by electroporation. *BMC Biotechnol.* **4**, 11 (2004).
88. Jandhyala, D. M. *et al.* A Novel Zak Knockout Mouse with a Defective Ribotoxic Stress Response. *Toxins* **8**, 259 (2016).
89. Wong, J. *et al.* Small molecule kinase inhibitors block the ZAK-dependent inflammatory effects of doxorubicin. *Cancer Biol. Ther.* **14**, 56–63 (2013).
90. Bruusgaard, J. C., Liestøl, K., Ekmark, M., Kollstad, K. & Gundersen, K. Number and spatial distribution of nuclei in the muscle fibres of normal mice studied in vivo. *J. Physiol.* **551**, 467–478 (2003).
91. Wigston, D. J. & English, A. W. Fiber-type proportions in mammalian soleus muscle during postnatal development. *J. Neurobiol.* **23**, 61–70 (1992).
92. Shi, H. *et al.* Mitogen-activated protein kinase signaling is necessary for the maintenance of skeletal muscle mass. *Am. J. Physiol. - Cell Physiol.* **296**, C1040–C1048 (2009).